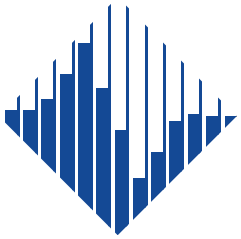

PACIFIC EARTHQUAKE ENGINEERING
RESEARCH CENTER

Probabilistic Seismic Hazard Analysis Code Verification

Christie Hale

Norman Abrahamson

Department of Civil and Environmental Engineering
University of California, Berkeley

Yousef Bozorgnia

Department of Civil and Environmental Engineering
University of California, Los Angeles

PEER Report No. 2018/03
Pacific Earthquake Engineering Research Center
Headquarters at the University of California, Berkeley

July 2018

PEER 2018/03
July 2018

Disclaimer

The opinions, findings, and conclusions or recommendations expressed in this publication are those of the author(s) and do not necessarily reflect the views of the study sponsor(s), the Pacific Earthquake Engineering Research Center, or the Regents of the University of California.

Probabilistic Seismic Hazard Analysis Code Verification

Christie Hale

Norman Abrahamson

Department of Civil and Environmental Engineering
University of California, Berkeley

Yousef Bozorgnia

Department of Civil and Environmental Engineering
University of California, Los Angeles

PEER Report 2018/03
Pacific Earthquake Engineering Research Center
Headquarters at the University of California, Berkeley

July 2018

ABSTRACT

Over the past decade, the use of Probabilistic Seismic Hazard Analysis (PSHA) to assess seismic hazards has expanded, leading to the creation of a number of new PSHA computer codes throughout the industry. Additionally, recent seismic source and ground-motion characterization studies have led to more complex source and ground-motion models, which necessitate implementation in PSHA codes. This project was undertaken to update previous PSHA computer code verification efforts by running an expanded set of verification tests on codes currently in use for PSHA calculations. Following an announcement to the community, fifteen owners of PSHA codes from private consulting companies, academic institutions, risk analysis firms, and government agencies participated in the verification project by running verification tests on their own codes. The project included three sets of tests that increased in complexity from the first test in Set 1 to the last test in Set 3. Over the course of the project the group held ten meetings to discuss and finalize the results. Tests were often re-run several times before the results for all codes were finalized. This report documents the specifications and benchmark answers for the verification tests. Common issues and programming errors are also summarized, along with standard modeling approaches and key discussion points from the meetings. Where differences in modeling approaches lead to differences in reported hazard, those different modeling approaches are described. Through participation in the project, code owners verified the primary functions of their codes as benchmark answers were reached. The PSHA codes developed in the future can be verified by running the tests and comparing the results to the benchmark answers documented in this report.

Note: the scope of this project is PSHA computer code verification. This project does not make recommendations on how to model earthquake scenarios from the specified source-characterization or ground-motion characterization inputs.

ACKNOWLEDGMENTS

The authors would like to acknowledge the generous support of the Pacific Earthquake Engineering Research Center (PEER) with funding from Pacific Gas & Electric Company and swiss*nuclear* The opinions, findings, conclusions or recommendations expressed in this publication are those of the authors and do not necessarily reflect the views of the study sponsors, PEER, or the Regents of the University of California.

The authors are grateful to Mario Gustavo Ordaz Schroeder, Jason Altekruse, Patricia Thomas, Nick Gregor, Gilbert Molas, Trey Apel, Marco Pagani, Graeme Weatherill, Peter Powers, Roland LaForge, Daniel Duggan, Jose Blanco, Manuela Villani, Arash Zandieh, and Valentina Montaldo for their contributions to the project. This work would not have been possible without their participation. The authors greatly appreciate the time and effort from each participant to run the verification tests, examine the results, and their participation in open discussions regarding different modeling approaches.

CONTENTS

LIST OF TABLES

LIST OF FIGURES

1 Introduction

1.1 OBJECTIVE

The objective of the project was to create a set of standardized tests with benchmark answers that can be used to verify the primary functions of Probabilistic Seismic Hazard Analysis (PSHA) codes. Through participation in the project, code owners can verify their code as tests are developed and consensus answers are reached, and codes developed in the future can be verified by comparing test results to the benchmark answers documented in this report.

The project also serves as a platform for community discussion amongst the primary PSHA code developers. Where different modeling approaches were found to result in differences in the reported hazard, the project provided an opportunity for participants to discuss and understand the causes of those differences, and to document the various modeling approaches in this report. Note: this project does not make recommendations on how to model earthquake scenarios from the specified source-characterization or ground-motion characterization inputs.

1.2 REVIEW OF 2010 VERIFICATION PROJECT

In 2001, the Pacific Earthquake Engineering Research Center (PEER) began a project to test and verify PSHA software as part of its goal to improve tools in seismic hazard assessment. This was the first comprehensive, organized, and structured verification of PSHA software. A working group was organized, members tested their own computer codes, and working group meetings were held to discuss and evaluate the test results. Acceptable answers were established either through analytical solutions or as the consensus answer from test results, and the results from eight participating codes were published in a PEER report in 2010 [Thomas 2010].

Two sets of tests were developed to evaluate elements of the PSHA codes. The objective of the Set 1 Tests was to test basic elements of the codes, including how rupture areas were modeled on a fault plane, how recurrence models were used, and how the standard deviations in ground-motion models were incorporated into hazard calculations. Through several iterations, consensus answers for Set 1 were reached, and the results were published in the 2010 PEER report [Thomas 2010]. The purpose of the Set 2 Tests was to test more sophisticated elements of the codes such as the modeling of non-planar faults, multiple seismic sources, and the intraslab regions of subduction zones. The tests for Set 2 were run, but because of the extended duration of the project, the differences between the results were not resolved and only sample results for Set 2 were included in the 2010 PEER report.

1.3 MOTIVATION FOR CURRENT PROJECT

The current verification project aimed to update and build-upon the work completed in the 2010 project. The primary motivation for the current project was to address the unresolved verification of the more complex tests, which reflected more realistic earthquake scenarios, and whose verification was therefore of high importance. The current project was also driven by the expansion of PSHA over the past decade, which has resulted in the creation of a number of new PSHA codes throughout the industry. Since the time of the previous verification project, numerous engineering and risk management firms have developed their own in-house PSHA codes, nearly doubling the number of codes that participated in this verification project compared to the 2010 project. Additionally, recent seismic-source and ground-motion characterization studies have led to more complex source and ground-motion models, which necessitate implementation in the PSHA codes. One example is the 2014 NGA-West2 ground-motion models, which introduced new distance parameters to further describe the geometry of the rupture. Implementation of the NGA-West2 ground-motion models is not just a matter of programming the new equations but also automating the calculation of these new distance values for each possible rupture plane location.

1.4 PARTICIPANTS AND CODES

In August of 2014, the project coordinators began reaching out to potential participants in order to compile a list of codes currently in use for PSHA calculations. To encourage as much participation as possible, a PEER News Alert was sent out to individuals and organizations with a PSHA code to contact PEER and participate in the project. In addition to hazard analysts at various firms with known PSHA codes, participants from the 2010 verification project were also contacted. A list of codes was shown to participants at the kick-off meeting, and additional potential participants were contacted based on feedback from the group regarding the completeness of the list of codes.

Ultimately, the project included fifteen codes from private consulting companies, academic institutions, risk analysis firms, and government agencies. A list of the codes, participating individual, and affiliation are given in Table 1.1. The participant listed is the individual who ran the tests for the code, with the exception of OpenSHA, OpenQuake, and HAZ45, which were run by Christie Hale, with support from the participant listed. Out of the fifteen codes, four codes are composed of the same base code and should not be considered independent. Those four codes are HAZ45, HAZ45b, HAZ38-URS, and THAZ. It was important when examining the results to recognize that these codes were not developed independently; see Section 1.5.1.

Table 1.1 List of codes and participants.

Code	Participant	Affiliation
CRISIS	Mario Gustavo Ordaz Schroeder	Universidad Nacional Autónoma de México
EZ-FRISK	Jason Altekruse	Fugro
FRISK88	Jason Altekruse	Fugro
HAZ38-URS	Patricia Thomas	URS
HAZ45	Norm Abrahamson	Pacific Gas and Elecric Co.
HAZ45b	Nick Gregor	Bechtel
HazMapEQ	Gilbert Molas & Trey Apel	Risk Management Solutions
OpenQuake	Marco Pagani & Graeme Weatherill	Global Earthquake Model
OpenSHA	Peter Powers	U.S. Geological Survey
PROBHAZ	Roland LaForge	Fugro / Nuclear Regulatory Commission
PROSIT	Daniel Duggan	AIR Worldwide
RIZZO-HAZARD	Jose Blanco	RIZZO Associates
SISMIC	Manuela Villani	Arup
THAZ	Arash Zandieh	Lettis Consultants International, Inc.
XCD55, HAZ51, TREE51	Valentina Montaldo	Amec Foster Wheeler

1.5 APPROACH

The first step of the project was to develop the test instructions. The verification tests were designed to test the primary functions of the PSHA codes. When possible, the tests isolate the feature being tested by using a delta function (single value) for other functions that would normally be modeled by a probability density function. This means that some of the tests do not include variability in the magnitude or even variability in the ground motion. Although this simplified modeling was done intentionally for the project, it should not be used outside of the verification test environment.

The project included three sets of tests that increased in complexity from the first test in Set 1 to the last test in Set 3. Test instructions were distributed to participants one set at a time, and participants ran the tests on their own codes. The results were compiled by the authors and redistributed to each participant in a blind feedback loop, meaning that when the participant received the compiled results, only their results were identified and all other results were anonymous. This gave participants an opportunity to identify outliers and fix any errors on their own prior to sharing the results with the group. Figure 1.1 shows an example of the blind feedback loop with the early hazard results for Test 2.2c at Site 6. Only the first round of resubmittals was blind, after which results were distributed to the group with all codes identified. Meetings were held to discuss the results and understand the differences in modeling approaches that led to

differences in reported hazard. Over the course of the project, the group held ten meetings to discuss and finalize the results. Tests were often re-run several times before the results for all codes were finalized. The group sought to finalize the results for a given set of tests before moving on to the next set.

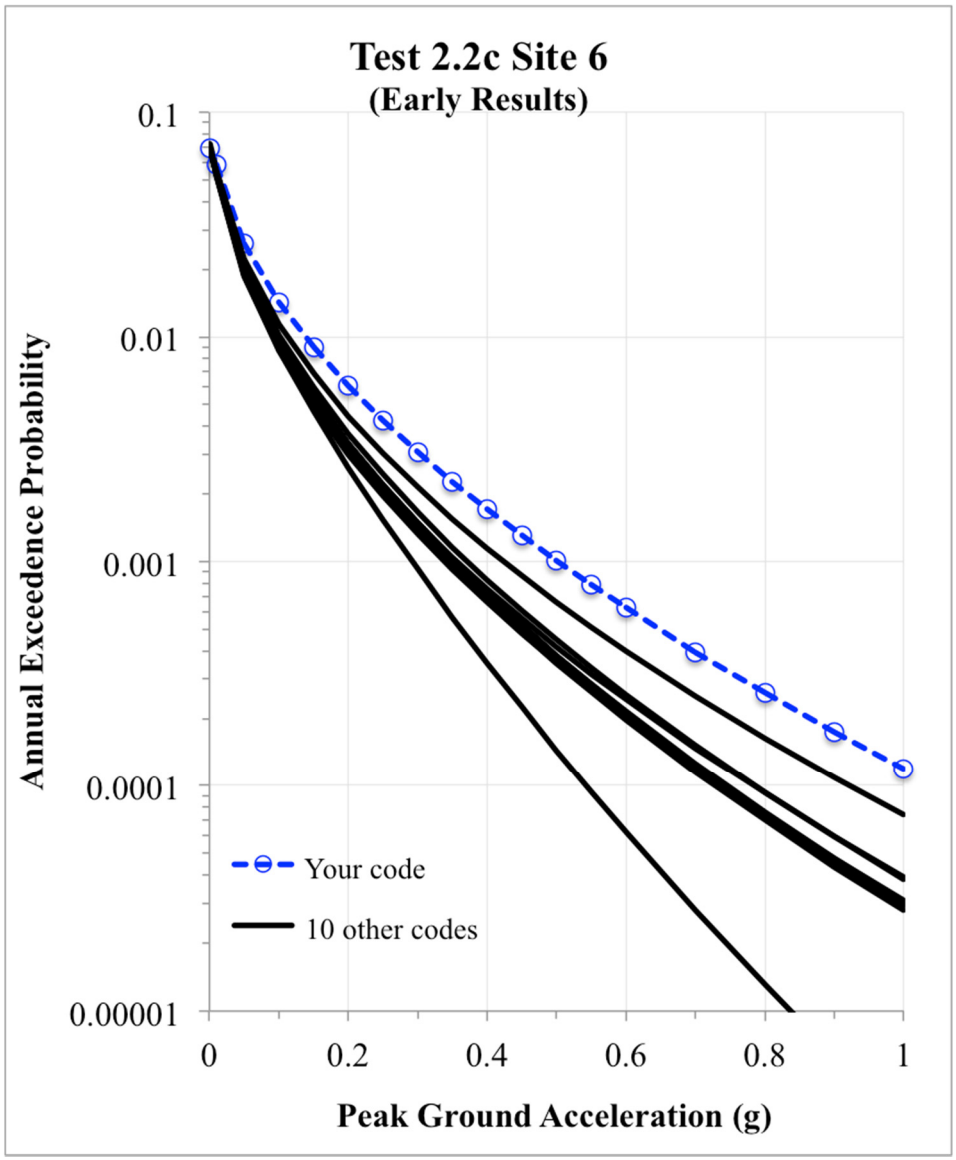

Figure 1.1 **Example of the blind feedback loop, where participants received early results from all codes with only their results identified.**

Throughout the project, there were many changes or modifications to the codes by project participants. The improvements to the codes fall into three general categories: (1) added features; (2) enhancements; and (3) fixes to bugs and programming errors. An example of an added feature is the mixture model for ground-motion distributions (Test 2.5b). At the beginning of the project, only three codes had the capability of modeling the ground-motion distribution with a mixture model; by the end of the project, many codes had added this feature and twelve codes participated in this verification test.

An example of an enhancement is modeling the extreme tails of the ground-motion distribution (Test 2.5a). At the beginning of the project, some codes used normal distribution functions that were accurate up to three or four standard deviations, which is perfectly adequate for the majority of projects. By the end of the project, many codes had implemented normal distribution functions that could calculate probabilities of exceedance for ground motions at six standard deviations. An example of a fix to a bug or programming error is a code that was incorrectly calculating Z_{HYPO} as Z_{TOR}. This type of error may go unnoticed when running a hazard project with multiple ground-motion models because only one of the NGA-West2 ground-motion models uses Z_{HYPO} so the error in the mean hazard is small.

1.5.1 Benchmark Answer and Acceptance Criteria

A benchmark answer was defined for each test and each site. To determine the benchmark answer, an algorithm was developed to search for the five codes whose answers were in best agreement for a given test and site. These codes are referred to as the core codes and can be different from test to test and even from site to site for the same test. A criterion that those five codes be independent was also followed, such that only one code out of those five could be from the HAZ family. The benchmark answer was then computed as the mean of the hazard from the five core codes. When practical, a hand solution was computed by the project coordinator, Christie Hale. For tests with hand solutions, the benchmark answer was compared to the hand solution as a check on the accuracy of the benchmark answer. These comparisons showed that the difference between the hand solution and the benchmark answer was exceptionally small – generally a difference of less than half a percent. This was very encouraging and provided confirmation that the benchmark answer was reliable.

An acceptance criterion of ±5% in hazard from the benchmark answer was applied to the results. Note that all comparisons and acceptance criteria are applied to the reported hazard (i.e., along the y-axis of the hazard curve). Participants were asked to look into results and provide an explanation for results that were more than 5% from the benchmark answer. This typically resulted in the participant discovering that they were not using a small enough discretization step size on one of the parameters, finding an error in their input files, or an error in their code, resulting in the participant submitting revised results. The only code with a prominent feature that caused the hazard results to be significantly different from the group is CRISIS. The CRISIS code models ruptures as ellipses, and this feature causes differences in hazard for many tests compared to the other codes, which model ruptures as rectangles. The CRISIS code submitted an additional set of results where the rupture planes were modeled with rectangles, allowing the results to be directly compared with the other codes. The CRISIS results with elliptical ruptures are provided in the electronic supplement but are not included in the reported ranges and are not discussed in this report.

1.6 ELECTRONIC SUPPLEMENT

The results from all tests are provided as an electronic supplement to this report in Electronic Appendix D. There are three Excel workbooks corresponding to the three sets of tests. Each workbook contains a tab for every test in that set, and within each tab there are tables for every site. The final hazard results from all participating codes are presented in a table; see Figure 1.2, which shows the tabular results from the electronic supplement for Test 1.2 at Site 1. The five core codes for this test are highlighted in yellow, and the mean hazard from the core codes is shown beneath the table and represents the benchmark answer. The percent difference between the core codes and the percent difference between all codes is reported beneath the benchmark answer. The percent difference is calculated as (max-min)/min and reflects the range in the results. The percent difference between the core codes is often less than 1%. With an acceptance criterion of ±5%, the percent difference between all codes can be as high as 10% but is typically much less.

Conditional formatting is used to highlight any results in red that are outside of the ±5% acceptance range, with reference to the benchmark answer. No red-highlighted cells indicates that all codes meet the acceptance criteria. As seen in Figure 1.2, the only results that are highlighted in red are from the CRISIS code where the rupture is modeled as an ellipse. These results should not be viewed as problematic; instead, the red highlighting from the CRISIS-ellipse results shows the difference in hazard due to the shape of the rupture plane. As mentioned previously, the CRISIS results with elliptical ruptures are not included in the reported percent difference between all codes.

Test 1.2 Site 1									
PGA	0.001	0.1	0.2	0.4	0.45	0.5	0.55	0.6	0.7
HAZ38-URS	1.59E-02	1.59E-02	1.59E-02	1.18E-02	8.22E-03	5.33E-03	2.75E-03	4.86E-04	1.00E-20
HAZ45	1.59E-02	1.59E-02	1.59E-02	1.18E-02	8.23E-03	5.33E-03	2.75E-03	4.86E-04	1.00E-20
THAZ	1.59E-02	1.59E-02	1.59E-02	1.17E-02	8.32E-03	5.23E-03	2.62E-03	3.28E-04	1.00E-20
HAZ45b	1.59E-02	1.59E-02	1.59E-02	1.17E-02	8.23E-03	5.17E-03	2.59E-03	3.24E-04	1.00E-20
FRISK88	1.59E-02	1.59E-02	1.59E-02	1.17E-02	8.20E-03	5.20E-03	2.61E-03	3.73E-04	1.00E-20
EZ-FRISK	1.59E-02	1.59E-02	1.59E-02	1.18E-02	8.21E-03	5.24E-03	2.65E-03	3.74E-04	1.00E-20
HazMapEQ	1.59E-02	1.59E-02	1.59E-02	1.17E-02	8.18E-03	5.21E-03	2.63E-03	3.90E-04	1.00E-20
RIZZO-HAZARD	1.59E-02	1.59E-02	1.59E-02	1.17E-02	8.21E-03	5.21E-03	2.65E-03	3.64E-04	1.00E-20
PROSIT	1.59E-02	1.59E-02	1.59E-02	1.17E-02	8.23E-03	5.23E-03	2.63E-03	3.62E-04	1.00E-20
OpenQuake	1.59E-02	1.59E-02	1.59E-02	1.16E-02	8.15E-03	5.28E-03	2.72E-03	4.81E-04	1.00E-20
OpenSHA	1.59E-02	1.59E-02	1.59E-02	1.17E-02	8.21E-03	5.21E-03	2.63E-03	3.90E-04	1.00E-20
SISMIC	1.59E-02	1.59E-02	1.59E-02	1.18E-02	8.31E-03	5.12E-03	2.56E-03	3.21E-04	1.00E-20
PROBHAZ	1.59E-02	1.59E-02	1.59E-02	1.16E-02	8.15E-03	5.28E-03	2.73E-03	4.81E-04	1.00E-20
XCD55, HAZ51, TREE51	1.59E-02	1.59E-02	1.59E-02	1.16E-02	8.15E-03	5.28E-03	2.72E-03	4.84E-04	1.00E-20
CRISIS - rectangle	1.59E-02	1.59E-02	1.59E-02	1.17E-02	8.24E-03	5.25E-03	2.63E-03	3.76E-04	1.00E-20
CRISIS - ellipse	1.59E-02	1.59E-02	1.59E-02	1.36E-02	9.14E-03	5.25E-03	1.73E-03	7.83E-06	1.00E-20
Benchmark	1.59E-02	1.59E-02	1.59E-02	1.17E-02	8.22E-03	5.23E-03	2.64E-03		
% diff 5 core	0.02%	0.02%	0.02%	0.38%	0.36%	0.72%	0.82%		
% diff all	0.14%	0.14%	0.14%	1.39%	2.13%	4.13%	7.31%		

Figure 1.2 **Test 1.2 at Site 1, Example 1: explanation of electronic supplement and tabular results; some PGAs (columns) are hidden for size.**

As shown in Figure 1.2, the very last peak ground acceleration (PGA) that returns a hazard value does not have a benchmark answer and acceptance criteria are not applied. The results are still shown but are struck through. This is because for this test, the results at a PGA of 0.6g are highly sensitive and require an exceptionally small rupture location step size to reach results that are stable. The sensitivity of the results is primary caused by the lack of ground-motion variability, and a hand solution was used to inform the exclusion of these very sensitive PGAs. As seen in Figure 1.2, a dummy zero value of 1E-20 was added at the end of each codes' results so that the graphs clearly show when the hazard results go to zero. This dummy zero value was only needed for tests with no ground-motion variability. Figure 1.3 shows these hazard results for Test 1.2 at Site 1 in graphical form. As seen in Figure 1.3, the results are in such good agreement that the hazard curves for each code plot nearly on top of each other.

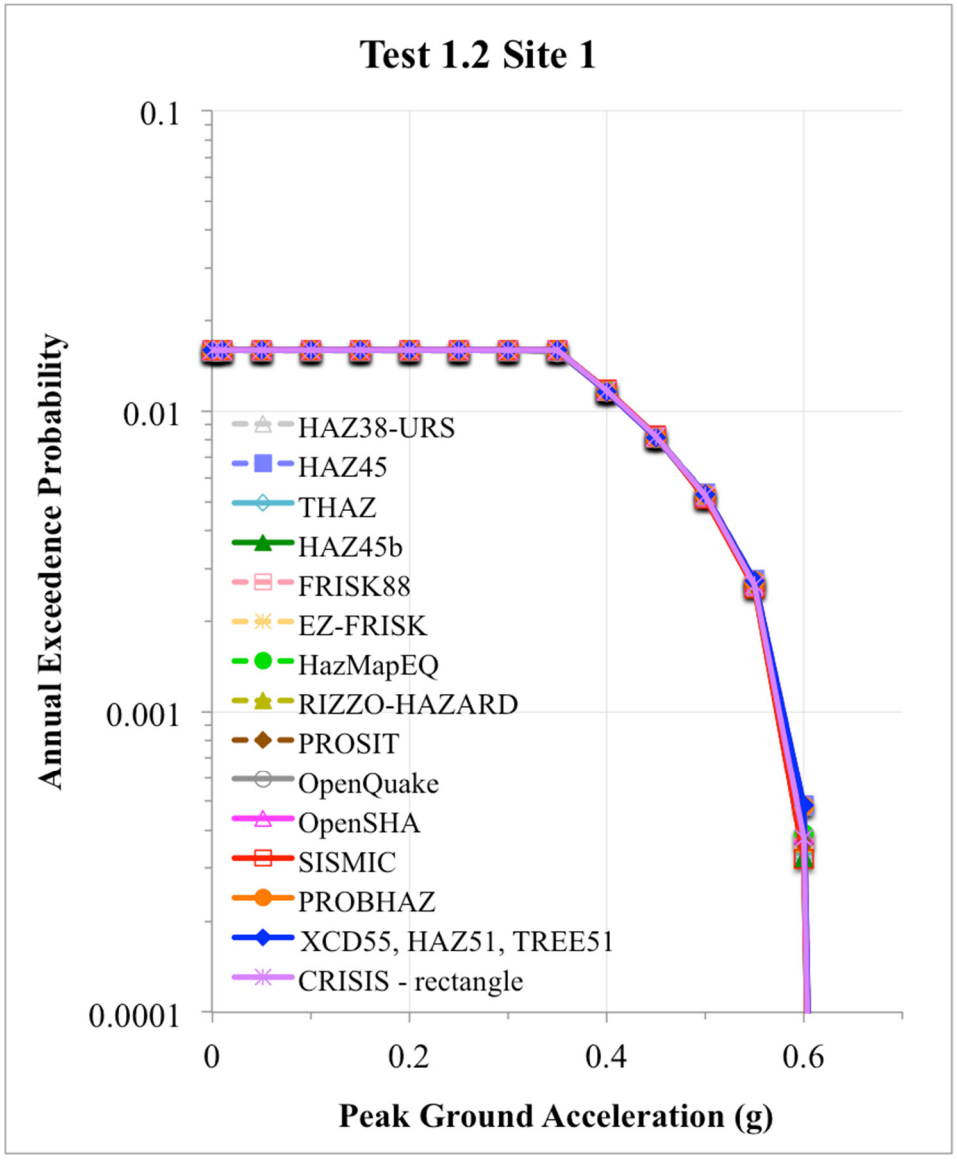

Figure 1.3 **Test 1.2 at Site 1, Example 1: explanation of electronic supplement and graphical results.**

Figure 1.4 shows another example of the tabular results from the electronic supplement, this time for Test 1.8a at Site 1, a test that includes ground-motion variability. Figure 1.5 shows these hazard results for Test 1.8a at Site 1 in graphical form. Note that when ground-motion variability is included, all specified PGAs have a benchmark answer, and a hazard value is reported for all PGAs, including the highest PGA of 1.0*g*.

Test 1.8a Site 1									
PGA	0.001	0.1	0.2	0.3	0.4	0.5	0.6	0.8	1
HAZ38-URS	1.59E-02	1.58E-02	1.47E-02	1.22E-02	9.44E-03	6.99E-03	5.07E-03	2.63E-03	1.37E-03
HAZ45	1.59E-02	1.59E-02	1.47E-02	1.23E-02	9.45E-03	6.99E-03	5.08E-03	2.63E-03	1.38E-03
THAZ	1.59E-02	1.59E-02	1.48E-02	1.23E-02	9.45E-03	7.00E-03	5.08E-03	2.63E-03	1.38E-03
HAZ45b	1.59E-02	1.59E-02	1.47E-02	1.22E-02	9.42E-03	6.96E-03	5.05E-03	2.61E-03	1.36E-03
FRISK88	1.59E-02	1.59E-02	1.47E-02	1.22E-02	9.42E-03	6.97E-03	5.06E-03	2.62E-03	1.37E-03
EZ-FRISK	1.59E-02	1.59E-02	1.47E-02	1.22E-02	9.43E-03	6.98E-03	5.06E-03	2.62E-03	1.37E-03
HazMapEQ	1.59E-02	1.59E-02	1.47E-02	1.22E-02	9.42E-03	6.97E-03	5.06E-03	2.62E-03	1.37E-03
RIZZO-HAZARD	1.59E-02	1.59E-02	1.47E-02	1.22E-02	9.43E-03	6.98E-03	5.06E-03	2.62E-03	1.37E-03
PROSIT	1.59E-02	1.59E-02	1.47E-02	1.22E-02	9.43E-03	6.98E-03	5.06E-03	2.62E-03	1.37E-03
OpenQuake	1.59E-02	1.59E-02	1.47E-02	1.23E-02	9.45E-03	6.99E-03	5.08E-03	2.63E-03	1.38E-03
OpenSHA	1.59E-02	1.59E-02	1.47E-02	1.23E-02	9.45E-03	6.99E-03	5.08E-03	2.63E-03	1.38E-03
SISMIC	1.59E-02	1.59E-02	1.47E-02	1.22E-02	9.43E-03	6.98E-03	5.07E-03	2.63E-03	1.38E-03
PROBHAZ	1.59E-02	1.58E-02	1.47E-02	1.22E-02	9.43E-03	6.98E-03	5.06E-03	2.63E-03	1.37E-03
XCD55, HAZ51, TREE51	1.59E-02	1.59E-02	1.47E-02	1.22E-02	9.43E-03	6.98E-03	5.06E-03	2.62E-03	1.37E-03
CRISIS - rectangle	1.59E-02	1.59E-02	1.47E-02	1.22E-02	9.43E-03	6.98E-03	5.06E-03	2.62E-03	1.37E-03
CRISIS - ellipse	1.59E-02	1.59E-02	1.48E-02	1.24E-02	9.65E-03	7.17E-03	5.20E-03	2.69E-03	1.40E-03
Benchmark	1.59E-02	1.59E-02	1.47E-02	1.22E-02	9.43E-03	6.98E-03	5.06E-03	2.62E-03	1.37E-03
% diff 5 core	0.02%	0.02%	0.02%	0.03%	0.05%	0.06%	0.07%	0.08%	0.10%
% diff all	0.14%	0.14%	0.17%	0.28%	0.39%	0.48%	0.59%	0.86%	1.10%

Figure 1.4 **Test 1.8a at Site 1, Example 2: explanation of electronic supplement and tabular results; some PGAs (columns) are hidden for size.**

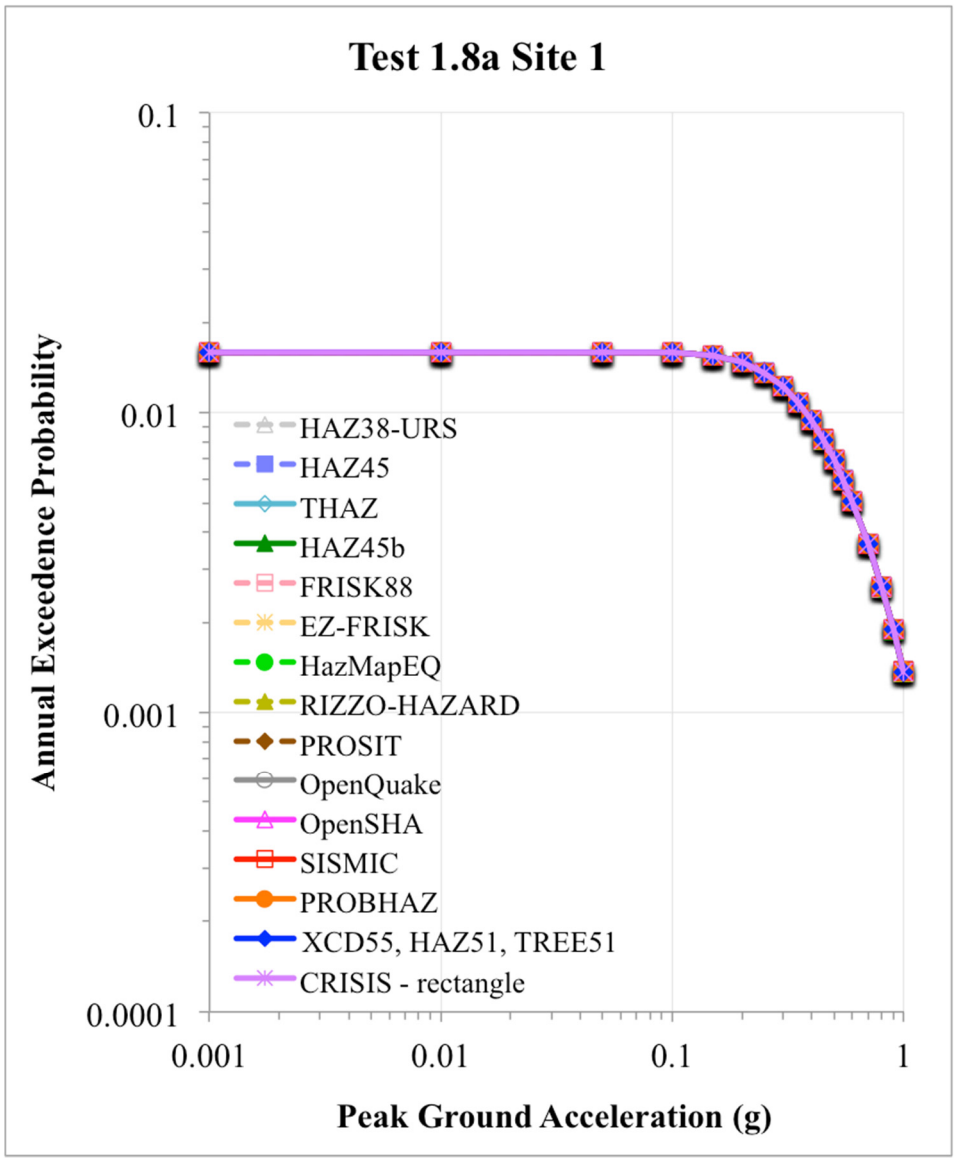

Figure 1.5 **Test 1.8a at Site 1, Example 2: explanation of electronic supplement and graphical results.**

1.7 ORGANIZATION OF REPORT

This report is organized into three main chapters corresponding to the three sets of verification tests. Chapter 2 discusses the tests in Set 1, Chapter 3 discusses the tests in Set 2, and Chapter 4 discusses the tests in Set 3. The chapters are intended to offer enough detail so that someone who did not participate in the project can complete the tests on their own. Common issues and programming errors are summarized along with key discussion points from the meetings. Ground-motion and source-characterization experts may also find the discussions useful in understanding some of the issues that arise when attempting to model earthquake scenarios as specified in hazard input documents.

2 Set 1 Results

2.1 INTRODUCTION

Tests in Set 1 verify basic elements of the codes, including how ruptures are modeled on a fault plane, how magnitude recurrence models are implemented, how area sources are modeled, and how the standard deviation in a ground-motion model is incorporated into the hazard calculations. Table 2.1 presents a short description of each test, and Table 2.2 indicates which codes completed which tests. Test instructions for Set 1 are provided in Appendix A and include test specifications as well as figures of the sources and site locations.

Full hazard results as well as quantitative information about the range in hazard results are provided in the electronic supplement. In Table 2.3, in order to offer remarks about the overall agreement between codes, the range in hazard results between the five core codes and the range in hazard results between all codes are reported as being less than a given percentage for each test. For example, if Table 2.3 reports a range of less than 4%, then the range in results across all PGAs and for all sites within that test is less than 4%. In this way, 4% represents a maximum range in results for that test, not an average.

Table 2.1 Set 1 tests and descriptions.

Test	Description
1.1	Rate calculation
1.2	Rupture location variability
1.3	Rupture area variability
1.4	Dipping fault
1.5	Truncated exponential magnitude pdf
1.6	Truncated normal magnitude pdf
1.7	Youngs and Coppersmith magnitude pdf
1.8a	Ground-motion variability, untruncated
1.8b	Ground-motion variability, truncate 2σ
1.8c	Ground-motion variability, truncate 3σ
1.10	Areal zone with point sources, single depth
1.11	Areal zone with point sources, depth range

Table 2.2 Set 1 tests completed by each code.

Test	1.1	1.2	1.3	1.4	1.5	1.6	1.7	1.8a	1.8b	1.8c	1.10	1.11
HAZ38-URS	✓	✓		✓	✓	✓	✓	✓	✓	✓		
HAZ45	✓	✓	✓	✓	✓	✓	✓	✓	✓	✓	✓	✓
THAZ	✓	✓	✓	✓	✓	✓	✓	✓	✓	✓	✓	✓
HAZ45b	✓	✓	✓	✓	✓	✓	✓	✓	✓	✓	✓	✓
FRISK88	✓	✓			✓		✓	✓	✓	✓	✓	✓
EZ-FRISK	✓	✓		✓	✓	✓	✓	✓	✓	✓		
HazMapEQ	✓	✓	✓	✓	✓	✓	✓	✓	✓	✓	✓	✓
RIZZO-HAZARD	✓	✓	✓	✓	✓	✓	✓	✓	✓	✓	✓	✓
PROSIT	✓	✓	✓	✓	✓	✓	✓	✓	✓	✓	✓	✓
OpenQuake	✓	✓		✓	✓	✓	✓	✓	✓	✓	✓	✓
OpenSHA	✓	✓	✓	✓	✓	✓	✓	✓	✓	✓	✓	✓
SISMIC	✓	✓	✓	✓	✓	✓	✓	✓	✓	✓	✓	✓
PROBHAZ	✓	✓	✓	✓	✓	✓	✓	✓	✓	✓	✓	✓
XCD55, HAZ51, TREE51	✓	✓	✓	✓	✓	✓	✓	✓	✓	✓	✓	✓
CRISIS	✓	✓		✓	✓	✓	✓	✓	✓	✓	✓	✓

Table 2.3 Set 1 tests: range in hazard results.

	Range in results for core codes						Range in results for all codes				
Test	<1%	<2%	<3%	<4%	<5%		<2%	<4%	<6%	<8%	<10%
1.1	✓						✓				
1.2	✓									✓	
1.3				✓						✓	
1.4		✓								✓	
1.5		✓							✓		
1.6		✓							✓		
1.7			✓							✓	
1.8a	✓									✓	
1.8b			✓					✓			
1.8c	✓									✓	
1.10			✓						✓		
1.11				✓						✓	

The sections below summarize the discussions and findings from the tests in Set 1, with a focus on the range in hazard results and differences in approaches discovered through the verification tests. For a complete set of hazard results and plots, the reader is referred to the electronic supplement in Appendix D.

2.2 TEST 1.1

2.2.1 Purpose

Test 1.1 is a single magnitude event on a strike–slip fault, which produces a rupture plane that fills the entire fault plane. With no ground-motion variability, the test requires the code to calculate the fault activity rate, the closest distance to the rupture, and the median ground motion. The test also requires the code to convert the rate of exceedance to a probability of exceedance using the standard assumption of Poissonian earthquake occurrences.

2.2.2 Discussion and Results

Due to the lack of variability in the distance and ground-motion calculations, the hazard curve at each site is a horizontal line at the fault activity rate until the median PGA is reached, after which the hazard becomes zero. The fault activity rate for this test is 0.0028528 events/yr, and the Poissonian probability of exceedance is 0.0028487 per year. Some participants noted that their code does not perform the calculation of rate given the slip rate within the code. Instead, these codes require the rate of earthquakes greater than M_{min} as an input, or the total moment accumulated by the slip of the fault as an input. For these codes, the test is more an indication of whether or not the individual running the code can calculate the required input correctly. Additionally, some codes do not convert the rate of exceedance to Poisson probability within the code and instead perform this step post-processing.

Test 1.1 also tests the ability of the code to restrict the rupture area to the fault area. The precise rupture area and rupture width calculated from the magnitude-dimension scaling relationships are 316.23 km^2 and 12.57 km, respectively. The stipulation that ruptures are not allowed to exceed the defined fault boundary means that the rupture area must be limited to 300 km^2, and the width must be limited to 12 km. This is accomplished by limiting the rupture width to the fault width, and then increasing the rupture length until the maximum length is reached. In this way, the rupture area is conserved at the expense of aspect ratio, and the fault boundary is maintained at the expense of rupture area. Though the restricted rupture area is less than the original rupture area calculated for the M = 6.5 event, the magnitude is not downgraded to reflect this new rupture. The original M = 6.5 value is carried through to the ground-motion model calculations. Discussion amongst participants confirmed that all codes follow this approach, and results for Test 1.1 showed good agreement in the calculated rate.

As shown in Table 2.3, the range in hazard results between the five core codes is less than 1%, and the range in hazard results between all codes is less than 2%. This small difference in results is a reflection of the differences in the calculated rate, and may be due to small differences in the conversion of fault and site longitude and latitude coordinates to distances, differences in

the numerical precision of the calculations, and differences in the number of significant digits reported by each code.

2.3 TEST 1.2

2.3.1 Purpose

Test 1.2 is a single magnitude event, which produces a rupture plane smaller than the fault plane. With a rupture plane that does not fill the entire fault, the test requires the code to move the rupture around the fault plane and address the aleatory variability in the location of the rupture.

2.3.2 Discussion and Results

There are slight differences in approaches in terms of how each code models a rupture smaller than the fault plane. Some codes create a rupture plane, which is incrementally moved along the strike of the fault and down the dip of the fault by a specified step size. This approach is illustrated in Figure 2.1, using the fault plane and rupture plane dimensions for this test. This approach often allows for the step sizes along strike and down dip to be different, in which case each can be optimized such that the rupture plane fits evenly into the available space either along strike or down dip, leaving no gap at the end of the discretization. Although the figure uses a relatively large step size of 1.0 km for illustrative purposes, a step size of 0.05 km was utilized by most codes in order to meet the acceptance criteria over the range of PGAs.

Another approach is to turn the fault plane into a mesh or grid, and then keep track of the cells that make up the dimensions of the rupture plane. This approach, as illustrated in Figure 2.2, does not maintain the exact rupture plane dimensions, as the rupture area must equal a multiple of whole cell areas. Although codes utilizing the gridded fault approach lose some accuracy, this approach has other advantages when modeling more complex fault geometries. The majority of codes using this approach require the grid cells to be squares, in which case the discretization along strike and down dip must be the same. This difference between the specified rupture area and dimensions, and the modeled rupture plane area and dimensions, leads to slight differences in the distance parameter calculations. A smaller grid cell discretization reduces the impact of these differences. Again, although Figure 2.2 uses a relatively large grid cell size for illustrative purposes, a grid cell with length and width of 0.05 km was utilized by most codes in order to meet the acceptance criteria over the range of PGAs.

As shown in Table 2.3, the range in hazard results between the five core codes is less than 1%, and the range in hazard results between all codes is less than 8%. The difference in results can be attributed to the difference in step size used by each code, and the differences in approaches of modeling a rupture plane smaller than the fault, which leads to slight differences in the distance calculations, in addition to the differences described in Test 1.1.

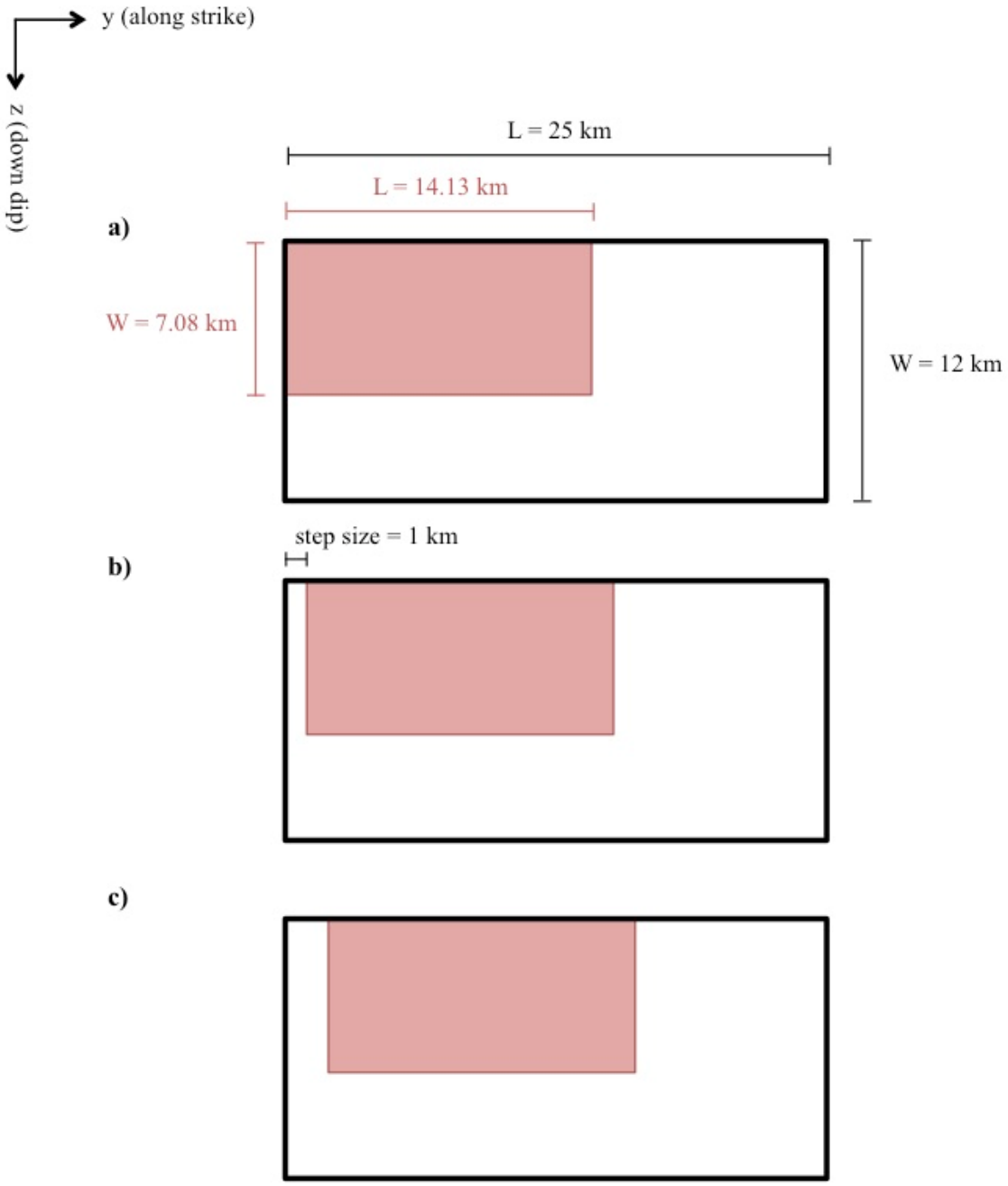

Figure 2.1 **Rupture plane modeled as a polygon which is incrementally moved along strike from (a) first rupture location, to (b) second rupture location, to (c) third rupture location, etc.**

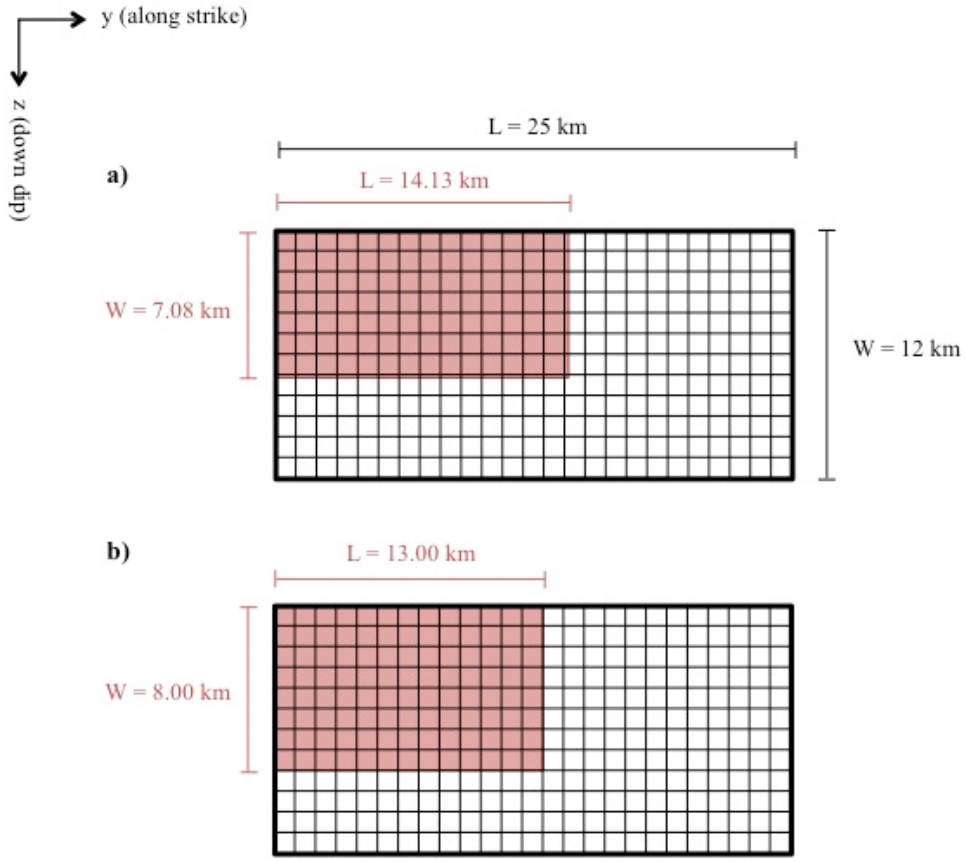

Figure 2.2 **Gridded fault plane approach with (a) precise rupture plane dimensions, which cannot be modeled by the gridded fault, and (b) adjusted rupture plane dimensions.**

2.4 TEST 1.3

2.4.1 Purpose

Test 1.3 is a single magnitude event, which is identical to Test 1.2 but with variability of the rupture plane area. With rupture area variability, the test requires the code to calculate a range of rupture planes and associated probabilities from the magnitude-area relationship.

2.4.2 Discussion and Results

The original instructions from the 2010 Verification Project specified three separate equations for rupture area, width, and length based on magnitude. Each of these equations had an associated standard deviation. Participants ran the test with these instructions and found that the test could not be implemented as described. With the rupture dimension relationships all based on magnitude, the equations could produce an area, width, and length that were not internally consistent. Absent any specifications about the correlation between the rupture dimensions, participants took a

number of different approaches when initially running this test. Some participants only varied the rupture area, others calculated rupture areas and widths from the equations provided without imposing any restrictions, others applied the area and width equations with a fully correlated epsilon, and others used all three equations with a fully correlated epsilon. In addition, the initial instructions did not specify a truncation level for the rupture dimension relationships, so in theory the rupture dimensions could approach zero on the low end and infinity on the high end. Due to the differences in approaches taken, initial results showed poor agreement.

Revised instructions specified variability in the rupture area only, with sigma truncated at two standard deviations on both the low and high end. One rupture width and length are defined per rupture area, using the specified aspect ratio of 2. For codes that are not programmed to calculate rupture width and length from an aspect ratio, the width could be calculated using the magnitude-width scaling relationship with a sigma of 0.125 and a full correlation between area and width variability. For example, if a rupture area at one standard deviation is calculated from the magnitude-area scaling relationship, a rupture width, also at one standard deviation, would be calculated from the magnitude-width scaling relationship. Both the aspect ratio approach and the fully correlated area and width approach yield the same width. The decision to vary only the rupture area was made to simplify the test, but also because variability in the rupture area has a bigger impact on the hazard than variability in the rupture width. Discussion amongst participants confirmed that for projects, if variability in the rupture dimensions is included, it is typically only applied to the rupture area.

Revised results showed much better agreement between codes. Figure 2.3 provides a side-by-side comparison of early results using the original instructions and final results using the revised instructions for Site 1. The improved agreement can be attributed to the simplified instructions, as well as participants decreasing their step sizes and increasing the number of rupture areas modeled for the final submittal in order to reach more stable results. The time interval between the initial results and final results was about one year, so some of the improved agreement is due to the fact that codes were modified after working through some of the later tests, which allowed participants to rerun this test with their improved code. Again, this test intentionally does not include ground-motion variability, so the results are sensitive to the step sizes utilized by each code. This sensitivity was explored by running a series of hand calculations, which confirmed that results were highly sensitive to the rupture location step size and number of rupture areas modeled, particularly at the higher PGA test values. Satisfactory results were generally achieved by using a rupture location step size of 0.05 km and at least 25 rupture areas.

As shown in Table 2.3, the range in hazard results between the five core codes is less than 4%, and the range in hazard results between all codes is less than 8%. The difference in results can be attributed to the difference in step size used by each code, and the difference in the number of rupture planes generated, in addition to previously described differences in approaches.

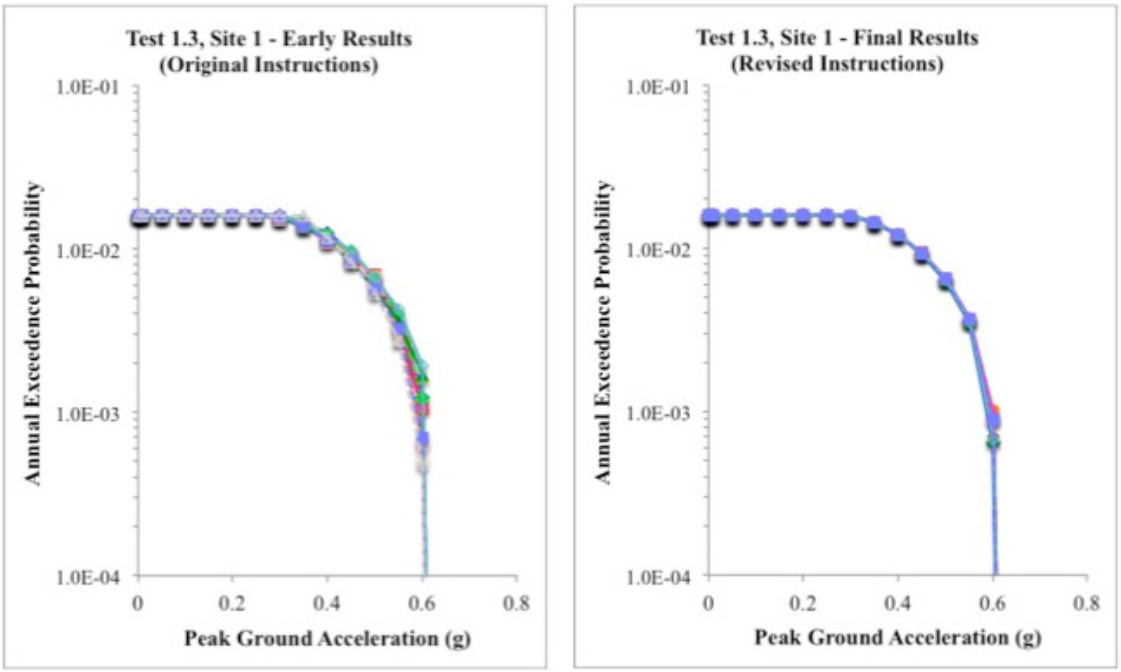

Figure 2.3 Test 1.3, Site 1: comparison of early results and final results.

2.5 TEST 1.4

2.5.1 Purpose

Test 1.4 is a single magnitude event, similar to Test 1.2, but on a reverse fault that dips 60° west and is buried at a depth of 1 km. This test requires the code to calculate distance metrics for a more complicated geometry and correctly pass on the fault mechanism to the ground-motion model.

2.5.2 Discussion and Results

All other tests involving fault sources in Set 1 utilize a purely strike–slip fault (dip = 90°). When a fault is modeled as purely strike–slip, the closest distance to the rupture plane, R_{RUP}, is always the distance from the site to the top of the rupture plane. In contrast, for sites on the hanging wall of dipping faults, the closest distance to the rupture plane can be the distance to the top of the rupture, the bottom of the rupture, or a point in between where a line from the site to the rupture forms a 90° angle. Figure 2.4 illustrates these various R_{RUP} distances in plane view for the seven sites in Test 1.4, with the more complicated geometry of a buried dipping fault.

Because this test does not include ground-motion variability, and many of the sites are very near the fault, the results are quite sensitive to any inaccuracies in the R_{RUP} distance values. Initial results indicated that the distance calculation functions for some codes were not precise enough at these short distances to meet the acceptance criteria. Discussion amongst participants led to the understanding that some codes are not typically used for site-specific hazard calculations or have only been used on projects where the relevant sources were far from the site. These codes utilized

simplified distance calculation functions that met the needs of their users but didn't have the level of precision required by this test. Participants for these codes modified their distance calculation functions in order to correctly calculate R_{RUP} for sites at short distances. Additionally, a hand solution was utilized by participants to troubleshoot results with outliers, and coding errors or bugs were identified in some codes and fixed.

As shown in Table 2.3, the range in hazard results between the five core codes is less than 2%, and the range in hazard results between all codes is less than 8%. Similar to Test 1.2, the difference in results can be attributed to the difference in step size used by each code, and the differences in approaches of modeling a rupture plane smaller than the fault, which leads to slight differences in the distance calculations.

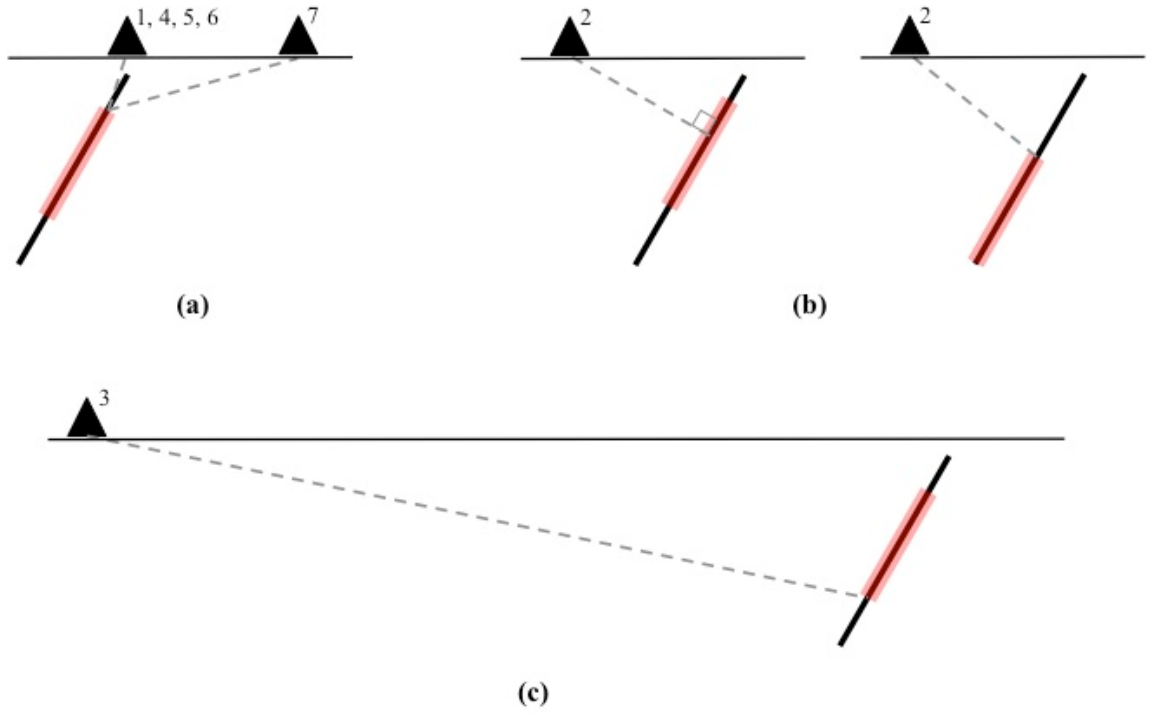

Figure 2.4 **Test 1.4: possible R_{RUP} distances in plane view for (a) sites directly above the fault trace or on the footwall; (b) sites close to the fault on the hanging wall; and (c) sites far from the fault on the hanging wall.**

2.6 TEST 1.5

2.6.1 Purpose

Test 1.5 uses the same strike–slip fault from Test 1.2 but replaces the single magnitude event with a truncated exponential magnitude density function; see Figure 2.5(a). With variability in the magnitude of the earthquake on the fault, the test requires the code to calculate the probability of each magnitude, the corresponding rupture plane dimensions, and the fault activity rate from a range of magnitudes.

2.6.2 Discussion and Results

A number of small differences in the codes were discovered relative to Test 1.5, all of which resulted in small or negligible differences in results, but are discussed briefly here for completeness. One difference is that a few codes do not allow for the slip rate as a direct input. For instance, when running this test on OpenSHA, the user must calculate the fault area and then use the specified slip rate to calculate the total moment accumulated on the fault, which is then input into the hazard code. For this test, that total moment rate is 1.8E16 Nm/yr. When running this test on OpenQuake, the user must calculate the fault area and then use the slip rate to balance the moment on the fault in order to calculate the rate of earthquakes above a magnitude of zero. That rate is then used to calculate the *a*-value, which is input into the hazard code. For this test, the rate of earthquakes greater than magnitude zero is 1347 earthquakes/yr and the associated *a*-value is 3.129.

Discussion also revealed differences in codes related to the discretization of the magnitude density function. Because the truncated exponential relationship has an analytical solution, the majority of codes solve the magnitude density function analytically; however, a few codes calculate the probability of each magnitude numerically. The analytical approach requires calculating the probability of the magnitude by solving the integral from the upper and lower bounds of the discretized magnitude range, while the numerical approach requires solving the equation for the center value of the discretization only and then multiplying by the discretization step size. Satisfactory results were generally achieved by using a magnitude step size of 0.05 and a rupture location step size of 0.1 km, although many of the core codes used smaller discretization values.

As shown in Table 2.3, the range in hazard results between the five core codes is less than 2%, and the range in hazard results between all codes is less than 6%. This difference between all codes is reduced from previous tests due to the added variability in the magnitude of the earthquakes, which tends to smooth through other differences in codes amplified in previous tests. The differences in results can be attributed to the differences in step size used by each code and slight differences in the truncated exponential magnitude recurrence calculations, in addition to previously described differences in approaches.

2.7 TEST 1.6

2.7.1 Purpose

Test 1.6 is similar to Test 1.5 but uses a truncated normal magnitude density function, representative of a purely characteristic earthquake. An illustration of the truncated normal magnitude density function is provided in Figure 2.5(b). This test similarly requires the code to calculate the probability of each magnitude, the corresponding rupture plane dimensions, and the fault activity rate from a range of magnitudes.

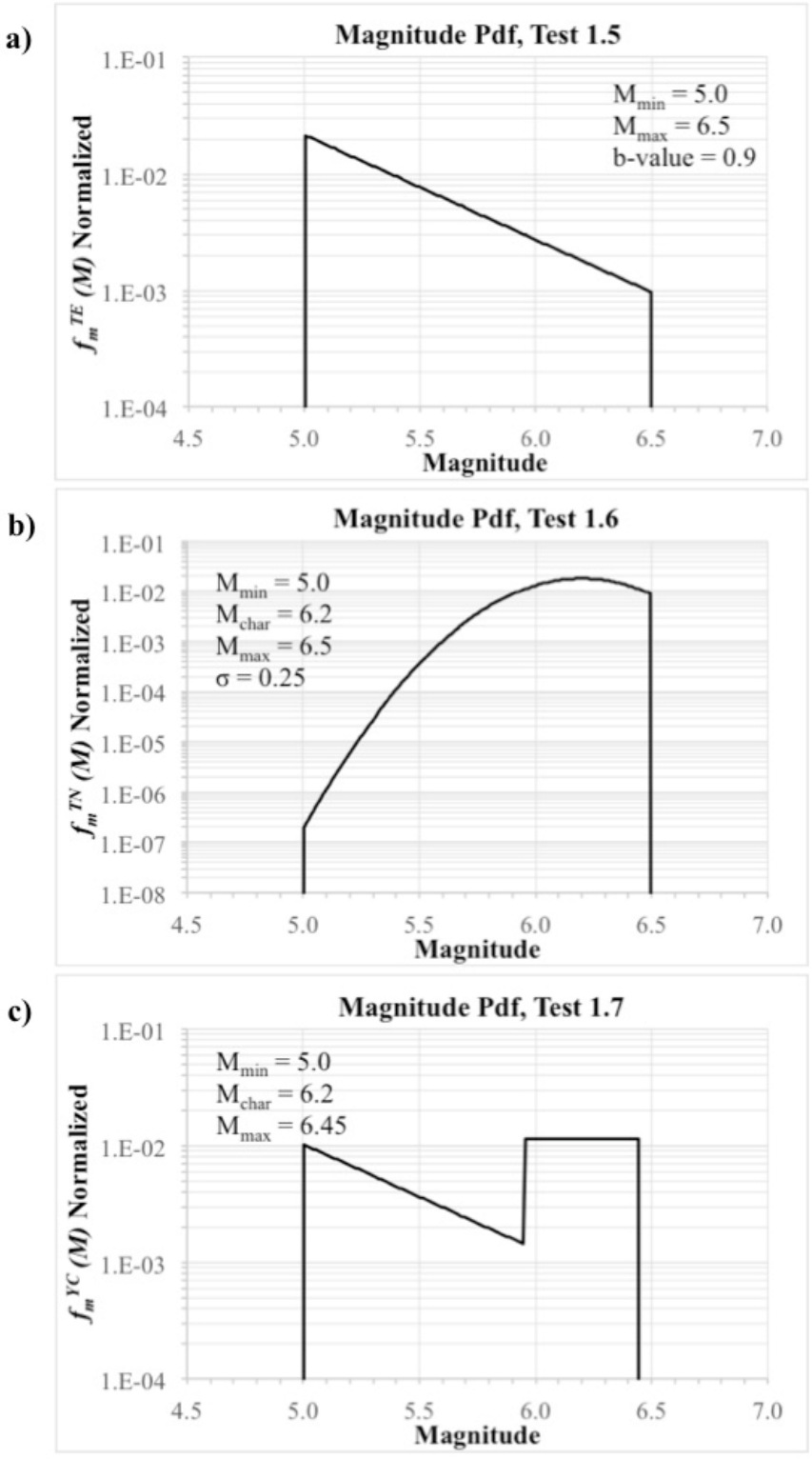

Figure 2.5 **Tests 1.5, 1.6, and 1.7: magnitude probability density functions.**

2.7.2 Discussion and Results

The magnitude density function for this test specifies a normal distribution with a fairly severe truncation at the high end. This severe truncation tended to highlight any inaccuracies in a code's magnitude recurrence function for the truncated normal magnitude distribution model. A hand solution with incremental occurrence rates was utilized by participants to troubleshoot results with outliers, and coding errors or bugs were identified in some codes and fixed. Additionally, four codes do not have built-in functions for modeling a normal magnitude distribution and instead rely on the modeler to perform moment balancing and magnitude probability calculations outside of the code. For these codes, the test is more an indication of whether or not the individual running the code can balance the moment and calculate the magnitude probabilities correctly.

As shown in Table 2.3, the range in hazard results between the five core codes is less than 2%, and the range in hazard results between all codes is less than 6%. The difference in results can be attributed to the difference in step size used by each code and slight differences or inaccuracies in the truncated normal magnitude recurrence calculations, in addition to previously described differences in approaches.

2.8 TEST 1.7

2.8.1 Purpose

Test 1.7 is similar to Tests 1.5 and 1.6, but uses a Youngs and Coppersmith [1985] characteristic magnitude density function; see Figure 2.5(c). This test similarly requires the code to calculate the probability of each magnitude, the corresponding rupture plane dimensions, and the fault activity rate from a range of magnitudes.

2.8.2 Discussion and Results

Initial results for Test 1.7 showed strong agreement between codes and few revisions were necessary to obtain the final test results. The Youngs and Coppersmith [1985] relationship is a composite model consisting of an exponential portion and a constant probability (boxcar) portion, and the majority of codes solve the magnitude density function analytically. Note that four codes do not have fully automated functions for modeling the Youngs and Coppersmith magnitude density function and require the user to perform some calculations manually outside of the code.

As shown in Table 2.3, the range in hazard results between the five core codes is less than 3%, and the range in hazard results between all codes is less than 8%. The difference in results can be attributed to the difference in step size used by each code and slight differences or inaccuracies in the Youngs and Coppersmith magnitude recurrence calculations, in addition to previously described differences in approaches.

2.9 TEST 1.8

2.9.1 Purpose

Test 1.8 is a single magnitude event, identical to Test 1.2, but with the inclusion of ground-motion variability. This test requires the code to calculate the probability of exceeding the PGA test value using the standard assumption of a log-normal distribution for ground-motion variability.

2.9.2 Discussion and Results

Test 1.8 includes three sub-tests with different truncation levels of the ground motion. Test 1.8a specifies no truncation, Test 1.8b specifies a truncation level of 2 standard deviations, and Test 1.8c specifies a truncation level of 3 standard deviations. These are the first tests that included the variability in the ground motion, moving toward more realistic hazard results and a percentage difference that better reflects the numerical differences between codes.

Results for Test 1.8a showed exceptional agreement between codes; however, the results did indicate a larger range in hazard results between all codes at Site 3 for the highest test PGAs. The reason for the increase at Site 3 is that the site is 50 km away from the fault, causing the probabilities of exceeding the test PGAs to be associated with high epsilon values. For instance, at a PGA of 0.45*g*, the mean epsilon needed to exceed the test value is approximately 5 standard deviations. The larger percent difference is therefore likely caused by a few codes whose normal distribution functions cannot precisely calculate probabilities at these high epsilons. The larger percent difference may also be caused by participants who specified a truncation level that they thought was high enough to be equivalent to running sigma untruncated, say, four standard deviations, but is too low for the highest test PGAs. Differences in normal distribution functions are specifically tested in Test 2.5a and discussed in Section 3.6 of this report. For this test, PGAs beyond 0.45*g* were excluded from the acceptance criteria. Note that the core codes still show exceptional agreement at Site 3 up to a PGA of 0.45*g* despite the high epsilon values.

While results for Test 1.8a were in very good agreement, initial results for Test 1.8b showed a small but clear division between two groups of codes. Discussion amongst participants led to the understanding that when truncating the ground-motion distribution, one group of codes truncates and renormalizes the ground motion on both the low and high end, and one group of codes truncates and renormalizes the ground motion on the high end only. Out of the fifteen codes, four codes were initially truncating on both ends, while eleven codes were truncating on the high end only. Though the difference in results based on these approaches was relatively small, the group discussed the merits of each approach and sought to recommend one approach for consistency in practice.

The group consensus is that the truncation should be performed on both ends of the distribution. The reason for truncating on both sides is to reflect a statistical deviation from a log-normal distribution, recognizing that the deviation we see in practice is actually a higher probability of rare ground motions rather than fewer, as a truncation would imply, but the deviation applies to both sides. The basis provided by many participants for truncating on the high end only was to place an upper bound on earthquake ground motions due to physical limits. However, this physical limit in truncation is more closely tied to a limit on the amount of shaking that the earth

can transmit, for instance 8.0*g*, rather than a statistical limit defined by a number of standard deviations. Importantly, many participants noted that in practice, they no longer truncate ground motions, or they apply a high truncation level, say, four standard deviations.

The difference in truncation approaches can only be seen in the results for Test 1.8b, where sigma is truncated at two standard deviations. The group recommendation meant that eleven codes should be modified to truncate on both ends; however, participants were not required to rerun this test due to the small impact on hazard results and the time limits of the project. Instead, the results were split into two groups, and a benchmark answer for each approach is reported in the electronic supplement. Two participants did modify their code and rerun the test, bringing the total number of codes with truncation on both ends up to six. The results for Test 1.8c do not show a difference between the two truncation approaches, as a truncation level of three standard deviations is high enough that it has no impact for this specific test. Therefore, the results for Test 1.8c were not split.

As shown in Table 2.3, for Test 1.8a, the range in hazard results between the five core codes is less than 1%, and the range in hazard results between all codes is less than 8%. For Test 1.8b, the results have been split into two groups based on whether the code truncates on both ends or the high end only. Five codes are still used to define the benchmark answer for both groups. The range in hazard results between the five core codes is less than 3%, and the range in hazard results for all codes is less than 4% for both groups. For Test 1.8c, the range in hazard results between the five core codes is less than 1%, and the range in hazard results between all codes is less than 8%. The difference in results can be attributed to the normal distribution function implemented by each code, in addition to previously described differences in approaches.

2.10 TEST 1.10

2.10.1 Purpose

Test 1.10 is an area source zone with a truncated exponential magnitude density function. The area boundary is a circle, and point sources are fixed at a constant depth of 5 km. For codes that model an area source zone by creating a grid of point sources, the recommended point source spacing is 0.5 km on the horizontal plane. This test requires the code to model an area source zone, calculating distance metrics and probabilities for point sources. Ground-motion variability is included.

2.10.2 Discussion and Results

The original instructions from the 2010 Verification Project recommended a point source spacing of 1 km on the horizontal plane and did not include variability in the ground motion. Initial results for this test showed reasonable agreement between codes, but hazard results were not close enough to declare a clear benchmark answer or apply the strict ±5% acceptance criteria at all sites. Through discussion and a number of sensitivity studies, the group gained an understanding for the differences, ultimately leading to modifying the test instructions.

Similar to Test 1.5, one difference concerned the inputs required by each code to calculate rate. The test instructions specify a source activity rate of N (M > 5) = 0.0395; however, some codes require different input parameters. For this test, the rate of earthquakes greater than magnitude zero is 1308 earthquakes/yr, and the associated a-value for the Gutenberg-Richter

relationship is 3.116. Inaccuracies or errors in these calculations led to differences in the rate calculated by some codes. Also, while the instructions recommended a point source spacing of 1 km, some codes define the spacing in longitude and latitude degrees, and participants of those codes were initially using a degree spacing that turned out to be much larger than 1 km. Another difference is that while many codes treat all point sources separately, several codes group point sources that are at similar distances from the site, and then use a representative distance to carry through the ground-motion calculations. Codes that performed this simplification generally had to specify narrow grouping criteria such that the distances were more precise. Additionally, one code, FRISK88, does not model area source zones with a grid of point sources and instead uses the swinging arc approach, where the area source zone is discretized into arcs, and the area of each arc is used to partition the activity rate. Finally, a series of diagnostic tests related to this source zone led to some participants modifying their code to implement a more precise conversion of latitude and longitude coordinates to kilometers.

Even with the above issues resolved, results were not in close enough agreement to define a benchmark answer, particularly at Site 3, which is located at the edge of the source boundary. Discussion amongst participants led to the theory that this site may be more sensitive to the particular grid orientation that a code creates. Because Site 3 only has point sources on one side, two codes may both create a grid of point sources with 1-km spacing, but one code may place the closest point directly on top of the site and the other may place the closest point 0.99 kilometers from the site.

A sensitivity study was performed by varying the starting point of the grid in increments of 0.1 km, which confirmed that the hazard results were sensitive to the specific grid orientation. Figure 2.6 shows the results of this sensitivity study, plotting the hazard results from each of the 100 possible grid orientations. A high sensitivity to the specific starting point of the grid indicates that the 1-km grid spacing is not small enough to produce stable results. For a code that utilizes the swinging arc approach, this means that an arc spacing of 1 km is likely not small enough to produce stable results. Note that this sensitivity was greatly amplified because the test was initially being run with no ground-motion variability.

It’s important to mention that the exact grid spacing of 1 km and where a code starts the grid is not really the issue. The grid of points is being used to model a zone of seismicity with a continuous distribution, allowing the earthquake to occur anywhere within that zone. For this test, when the site is at the center of the circle (Site 1), a grid spacing of 1 km produces results that are relatively stable because there are point sources on all sides of the site. Stable results indicate that the point source spacing being utilized is correctly modeling the intended continuous distribution; however, for Site 3, there are only point sources on one side of the site, so the results become more sensitive to the spacing. Therefore, a smaller spacing should be used to correctly model the continuous distribution for sites at the edges of area source zones.

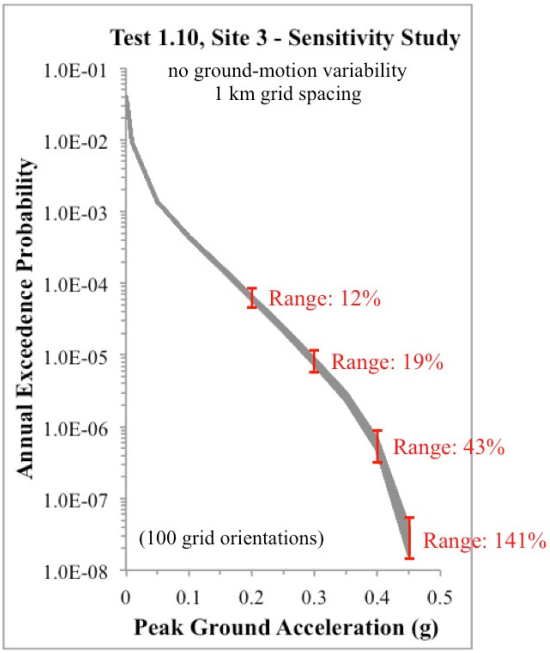

Figure 2.6 **Results from sensitivity conducted using HAZ45 code with 1-km grid spacing and no ground-motion variability. The sensitivity study shows the difference in hazard when the starting point of the grid is shifted in increments of 0.1 km to run all possible grid orientations.**

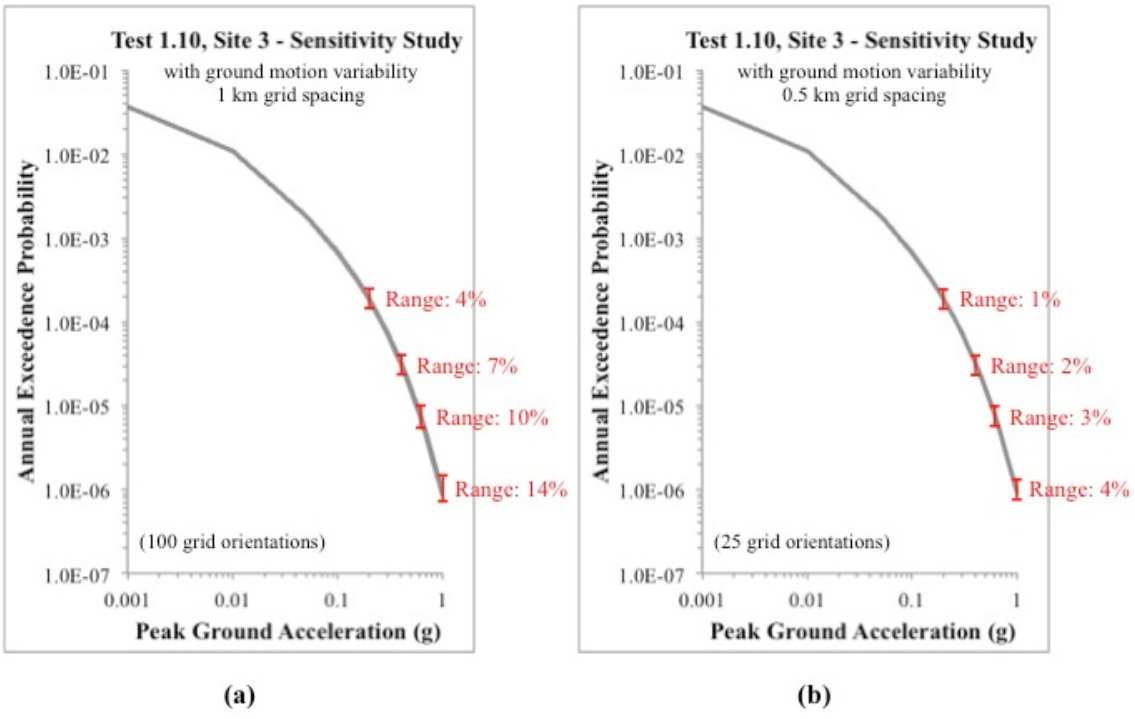

Figure 2.7 **Results from sensitivity conducted using HAZ45 code with (a) 1-km grid spacing, and (b) 0.5-km grid spacing. Each sensitivity study shows the difference in hazard when the starting point of the grid is shifted in increments of 0.1 km to run all possible grid orientations.**

Revised instructions recommended a point source spacing of 0.5 km and included ground-motion variability with sigma untruncated. These two modifications produced much more stable results and allow a code to reach acceptable answers without extensive run times for the test. Figure 2.7 shows the results for the same sensitivity study performed previously, but with ground-motion variability included. To illustrate the stability in hazard results gained by reducing the point source spacing to 0.5 km, results are shown for a point source spacing of 1 km as well as 0.5 km. The revised results showed much better agreement between codes, even out to the highest PGA of 1.0*g*, where the hazard results are very low and beyond the typical range of interest for most engineering projects. For instance, at Site 1, which is in the center of the area source, the benchmark hazard at a PGA of 1.0*g* is 1.91E-6, which corresponds to a return period greater than 500,000 years.

As shown in Table 2.3, the range in hazard results between the five core codes is less than 3%, and the range in hazard results between all codes is less than 6%. The difference in results can be attributed to differences in how a code models an area source zone, including differences in latitude and longitude conversions, and differences in locations of point sources, in addition to previously described differences in approaches.

2.11 TEST1.11

2.11.1 Purpose

Test 1.11 is an area source zone, identical to Test 1.10, but with added variability in the depth of the point sources. This test similarly requires the code to model an area source zone, calculating distance metrics and probabilities for point sources. Ground-motion variability is included.

2.11.2 Discussion and Results

Instructions for this test were also revised to achieve more stable results, recommending a point source spacing of 0.5 km on the horizontal plane and the inclusion of ground-motion variability. Again, stable results indicate that we are correctly modeling the intended continuous distribution, which reflects the assumption that an earthquake can occur anywhere within the area source zone.

Initial results and discussions revealed two main differences between codes related to the distribution of point sources with depth. First, because the instructions did not make a recommendation regarding the discretization of the depth range, participants specified different numbers of point sources to discretize the depth. Second, some codes include the boundaries of the seismogenic zone when discretizing the depth range, while others place the point sources in the center of the specified depth discretization increment. These different modeling approaches are illustrated in Figure 2.8 for a depth discretization step size of 1 km. At the time of this test, the group was not able to reach a consensus on which of these two modeling approaches was best. Because the majority of the codes were including the boundaries of the seismogenic zone in the depth discretization, and given the possible run-time issues for some codes if a very fine discretization was used, the recommendation was made for everyone to include the boundaries of the seismogenic zone in their depth discretization and use a step size of 1 km for the depth range.

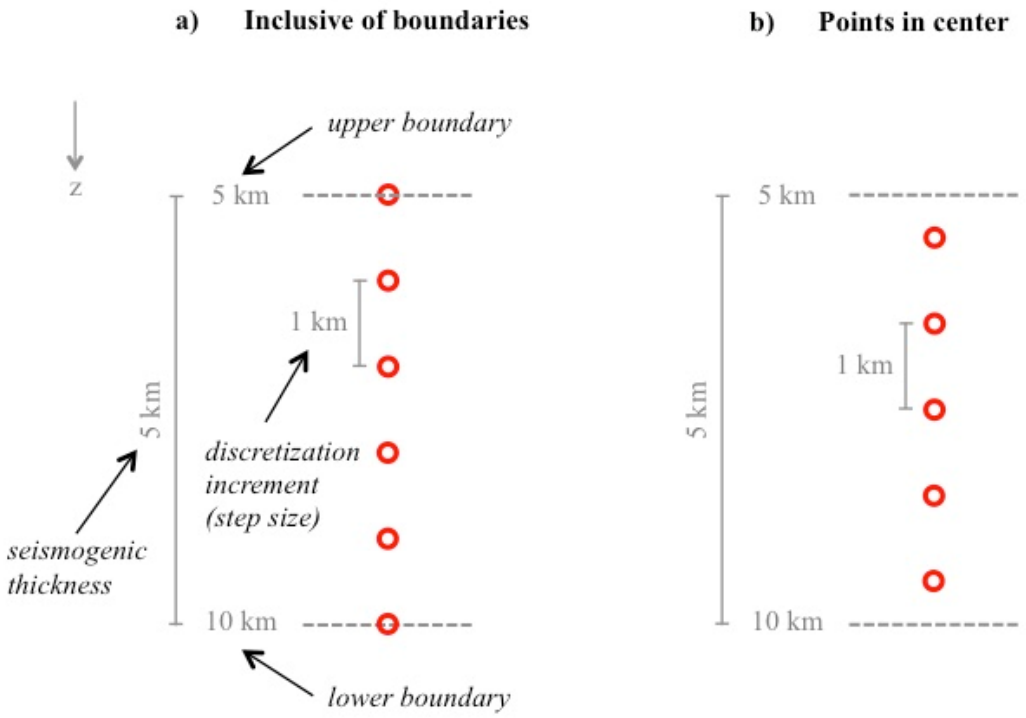

Figure 2.8 **Test 1.11: different modeling approaches for the depth distribution of point sources in an area source zone.**

A sensitivity study indicated that the difference in hazard between using the 1-km-depth discretization and a much smaller depth discretization of 0.05 km was about 3% at the highest test PGA. Obviously, this recommendation produces relatively stable hazard results. Ten codes used the recommended 1-km-depth step size, while two codes used significantly smaller depth step sizes, resulting in more stable hazard results. The results from the two codes that used the finer discretization are about 3% lower than the results from the other ten codes at the highest test PGA, confirming the results from the sensitivity study.

As shown in Table 2.3, the range in hazard results between the five core codes is less than 4%, and the range in hazard results between all codes is less than 8%. The difference in results can be attributed to differences in the distribution of point sources with depth, in addition to previously described differences in approaches.

After the results for this test were finalized, the group revisited the issue of whether the seismogenic zone boundaries should be included in the discretization of point sources with depth, or if the point sources should be placed in the center of the discretization increment. A sensitivity study was performed where both approaches were modeled, and the depth step size was varied. The best modeling approach should be the one that produces results closest to the stable results while using a larger depth step size. When the seismogenic zone boundaries are included, the difference in hazard between using the 1-km-depth step size and a 0.05-km-depth step size was about 3% at the highest test PGA. When the point sources are placed in the center of the discretization increment, the difference in hazard between using the 1-km-depth discretization and a 0.05-km-depth discretization is less than 0.25%. This sensitivity study was performed using the Sadigh et al. [1997] ground-motion model as Test 1.11 specified, but the process was repeated

with some of the NGA-West2 ground-motion models that have a depth dependent term; the results were the same.

The sensitivity study concluded that the best approach is to place point sources in the center of the discretization increment. In hindsight, the group should have recommended that point sources always be placed in the center of the discretization increment rather than including the boundaries of the seismogenic zone. The instructions should have recommended a point source spacing of 1 km for the depth distribution; this results in very stable hazard values when the point sources are placed in the center of the discretization increment.

3 Set 2 Results

3.1 INTRODUCTION

Tests in Set 2 verify more sophisticated elements of the codes, including modeling multiple seismic sources and providing deaggregation information, implementing the more complex NGA-West2 ground-motion models, and calculating probabilities of exceedance for ground-motion distributions described by a mixture-model. Table 3.1 presents a short description of each test, and Table 3.2 indicates which codes completed which tests. Test instructions for Set 2 are provided in Appendix B, and include test specifications as well as figures of the sources and site locations. Test results for Set 2 are provided as an electronic supplement in Appendix D. Similar to Set 1, the range in hazard results between the five core codes and the range in hazard results between all codes are reported as being less than a given percentage for each test in Table 3.3.

Table 3.1 Set 2 tests and descriptions.

Test	Description
2.1	Multiple sources
2.1 Avg	Deaggregation averages
2.1 Tables	Deaggregation percentages
2.2a	Abrahamson Silva and Kamai [2014]
2.2b	Boore Stewart Seyhan Atkinson [2014]
2.2c	Campbell and Bozorgnia [2014]
2.2d	Chiou and Youngs [2014]
2.3a	Hanging Wall, ASK14
2.3b	Hanging Wall, BSSA14
2.3c	Hanging Wall, CB14
2.3d	Hanging Wall, CY14
2.4a	Uniform hypocenter distribution
2.4b	Triangular hypocenter distribution
2.5a	Upper tails, ground-motion distribution
2.5b	Mixture model, ground-motion distribution

Table 3.2 Set 2 tests completed by each code.

Test	2.1	2.1 Avg	2.1 Tables	2.2a-d	2.3a-d	2.4a	2.4b	2.5a	2.5b
HAZ38-URS	✓	✓	✓	✓	✓				
HAZ45	✓	✓	✓	✓	✓	✓	✓	✓	✓
THAZ	✓	✓	✓	✓	✓	✓	✓	✓	✓
HAZ45b	✓	✓	✓	✓	✓	✓	✓	✓	✓
FRISK88									
EZ-FRISK									
HazMapEQ	✓	✓	✓	✓	✓	✓	✓	✓	✓
RIZZO-HAZARD	✓	✓	✓	✓	✓	✓	✓	✓	✓
PROSIT	✓	✓	✓	✓	✓	✓	✓	✓	✓
OpenQuake	✓	✓	✓	✓	✓	✓	✓	✓	✓
OpenSHA				✓	✓	✓	✓	✓	✓
SISMIC	✓	✓	✓	✓	✓	✓		✓	✓
PROBHAZ	✓	✓	✓	✓	✓	✓	✓	✓	✓
XCD55, HAZ51, TREE51	✓	✓	✓	✓	✓	✓	✓	✓	✓
CRISIS	✓		✓	✓	✓	✓		✓	✓

Table 3.3 Set 2 tests: range in hazard results.

	Range in results for core codes						Range in results for all codes				
Test	**<1%**	**<2%**	**<3%**	**<4%**	**<5%**		**<2%**	**<4%**	**<6%**	**<8%**	**<10%**
2.1			✓							✓	
2.2a			✓						✓		
2.2b		✓							✓		
2.2c				✓						✓	
2.2d			✓						✓		
2.3a					✓				✓		
2.3b		✓									✓
2.3c		✓								✓	
2.3d		✓								✓	
2.4a	✓								✓		
2.4b	✓									✓	
2.5a	✓										✓
2.5b	✓							✓			

3.2 TEST 2.1

3.2.1 Purpose

Test 2.1 includes an area source zone, similar to Test 1.11, and two fault sources. The test requires the code to calculate and sum the hazard for multiple sources and perform a deaggregation on the magnitude, distance, and epsilon values. Ground-motion variability is included.

3.2.2 Discussion and Results

Initial hazard results indicated that a couple of codes were incorrectly converting the rate of exceedance to Poisson probability for each source and then summing the Poisson probabilities. Those codes were revised to correctly sum the rates of exceedance from all sources and then convert the total rate of exceedance to Poisson probability. The area source specifications are essentially the same as Test 1.11, but because the site is in the middle of the area source, results are stable with a point source spacing of 1 km on the horizontal plane. As with Test 1.11, the difference in the number of point sources used to model the depth of the area source is primarily responsible for the difference in hazard results at the higher PGAs where the hazard from the area source is driving the total hazard.

As shown in Table 3.3, the range in hazard results between the five core codes is less than 3%, and the range in hazard results between all codes is less than 8%. The difference in results can be attributed to differences in the distribution of point sources with depth for the area source, in addition to previously described differences in approaches.

Participants were also asked to provide deaggregation information at three different PGAs. Two of the PGAs were specified directly, while a third problem asked for deaggregation information for the PGA corresponding to an annual probability of exceedance of 0.001. Deaggregation results included two parts. The first part asked participants to report the mean magnitude, distance, and ε^* (epsilon star) values at each of the three PGAs. The second part specified magnitude, distance, and epsilon bins, and asked participants to report the percent contribution to the total hazard for each bin, again at each of the three PGAs. More information on the deaggregation specifications can be found in the instructions for this test in Appendix B.

One difference related to the deaggregation had to do with how participants arrived at the deaggregation values for the case where the annual probability of exceedance was specified rather than the PGA directly. This applies to both the mean deaggregation values and the deaggregation bins. Some participants used log–linear interpolation between hazard results and deaggregation values to obtain the deaggregation results corresponding to the specified hazard level. Other participants used log–log interpolation between hazard results to obtain the associated PGA, and then reran their code with that PGA as a test value in order to have the code provide the deaggregation information directly. This difference did not cause a large range in deaggregation results; however, the agreement between the interpolation and the results from rerunning the hazard analysis depends on the particular problem at hand. If PGA test values are spaced farther apart, or if the mean magnitude, distance, or epsilon* values plotted against the log of the hazard does not exhibit a linear relationship for the hazard level of interest, interpolation may not provide deaggregation results as accurately.

Another difference related to the deaggregation concerns how the codes deaggregate on epsilon. One method is to assign the entire marginal hazard contribution for a given scenario to the epsilon bin corresponding to the test spectral acceleration value. For example, for a given earthquake scenario, if the median PGA from the ground-motion model is 0.5*g*, the standard deviation is 0.7 natural log units, and the specified test PGA = 0.25*g*. Then the epsilon corresponding to the test PGA is -1, and the entire probability of exceedance for that scenario would be assigned to the bin containing $\varepsilon = -1$. In this first method, the epsilon is typically referred to as epsilon*.

A second method is to assign the proportional contribution of the probability of exceedance for a given scenario to the full range of epsilons that satisfy the exceedance of the test value. In the above example, this would entail dividing the probability of exceedance for a given scenario into the epsilon bins above $\varepsilon = -1$, with the appropriate contribution based on the probability density function used for the ground-motion distribution. For a more detailed explanation of these two methods, the reader is referred to the explanation on page 508 of Bazzurro and Cornell [1999]. Per Bazzurro, both methods are perfectly legitimate—they simply correspond to different specifications—but when the results are reported it should be made clear which method was used. The binned deaggregation results for epsilon (or epsilon*) were split into two groups based on these methods.

An acceptance criteria of ±2% was used for the deaggregation results. As an example, if the benchmark answer for the mean magnitude was 6.02, acceptable answers ranged from 5.90 to 6.14. For the deaggregation tables, if the contribution to the total hazard for the distance bin from 40–60 km was 33%, acceptable answers ranged from 31% to 35%. All participating codes were well within this acceptance criteria. Complete deaggregation results and comparisons between codes can be found in the electronic supplement Appendix D.

3.3 TEST 2.2

3.3.1 Purpose

Test 2.2 uses a strike-slip fault, which produces a range of earthquake magnitudes from a truncated exponential magnitude density function. The test includes multiple sub-tests for each of the four NGA-West2 ground-motion models tested. The test requires the code to calculate the median and standard deviation from the more complicated NGA-West2 ground-motion models, including distance parameters R_{JB}, Z_{TOR}, and Z_{HYP}, which were not required in previous tests.

3.3.2 Discussion and Results

Test 2.2 includes four sub-tests with different NGA-West2 ground-motion models. Test 2.2a specifies the ASK14 model, Test 2.2b specifies the BSSA14 model, Test 2.2c specifies the CB14 model, and Test 2.2d specifies the CY14 model. I14 was not tested because it did not require a code to program any new predictor variables. This test was designed to require the code to go through all of the magnitude breakpoints in the NGA-West2 ground-motion models, which is why a truncated exponential magnitude density function from $M_{min} = 5$ to $M_{max} = 7$ was specified. An

85-km-long fault was used to accommodate a rupture plane for the high end of the magnitude range.

At the beginning of the project, many of the codes had not yet implemented the NGA-West2 ground-motion models, and initial results indicated programming errors for many codes. Discussion amongst participants highlighted a few particularly tricky aspects of the NGA-West2 ground-motion models, which are summarized here for the benefit of the reader:

- ASK14: The depth to a shear wave velocity of 1.0 km/sec, $Z_{1.0}$, should be in kilometers. There is a typo in ASK14 in the list of parameters, which incorrectly shows $Z_{1.0}$ with units of meters.
- ASK14, BSSA14, and CY14: Both ASK14 and BSSA14 require $Z_{1.0}$ in kilometers, while CY14 requires $Z_{1.0}$ in meters. This means that a code will likely have to convert the units for the $Z_{1.0}$ input within one of the ground-motion model subroutines, depending on the units the code's input file requires.
- BSSA14: The electronic supplement provides coefficient values out to four decimal points, however most applications that open the file will only show the values out to three decimal places with the default view. Some participants used the coefficients with three decimal places in error, rather than the correct coefficients with four decimal places.
- BSSA14: For other NGA-West2 ground-motion models, the shortest period is T = 0.01 sec, and the coefficients for T = 0.01 sec should be used for PGA. However, BSSA14 provides coefficients for both T = 0.01 sec and PGA. Some participants used the T = 0.01 sec coefficients in error rather than the PGA coefficients.
- CB14: When calculating rock PGA, A_{1100}, the code should use the depth to a shear wave velocity of 2.5 km/sec, $Z_{2.5}$, calculated from equation 33 or 34 in CB14.
- CY14: The centered depth to the top of the rupture plane, ΔZ_{TOR}, must be calculated for every rupture plane by calculating the depth to the top of the rupture plane, Z_{TOR}, and the mean depth to the top of the plane E [Z_{TOR}], calculated from equation 4 or 5 in CY14.

Through a series of revisions, programming errors were fixed and results converged to a consensus answer. Although this test did help many participants identify errors in their codes, it did not provide a complete validation of the NGA-West2 ground-motion models. Testing all periods, site locations, and site conditions is beyond the scope of the project, and participants were encouraged to perform their own full validation by creating validation tables from the PEER NGA-West2 Excel spreadsheet.

As shown in Table 3.3, the range in hazard results between the five core codes is less than 4%, and the range in hazard results between all codes is less than 8%. The ranges for Site 6 drive these maximum reported ranges up and are due to Site 6's location off the end of the fault, which causes the results to be more sensitive to the rupture location step size. The difference in results can be attributed to differences in step sizes used by each code, in addition to previously described differences in approaches.

3.4 TEST 2.3

3.4.1 Purpose

Test 2.3 is a single, large magnitude event on a reverse fault that dips 45° west and is buried to a depth of 1 km. The test includes multiple sub-tests for each of the four NGA-West2 ground-motion models tested. This test requires the code to calculate the hanging-wall terms of the NGA-West2 ground-motion models, including new distance parameters R_X and R_{Y0}. The test does not include ground-motion variability.

3.4.2 Discussion and Results

Similar to Test 2.2, Test 2.3a specifies the ASK14 model, Test 2.3b the BSSA14 model, Test 2.3c the CB14 model, and Test 2.3d the CY14 model. The single M 7 event produces a large rupture, which is always passing in front of the sites located at the midpoint of the fault along the strike. Due to this lack of variability in the distance and ground-motion calculations, the hazard curves at Sites 1–5 are a horizontal line at the fault activity rate until the median PGA is reached, after which the hazard becomes zero. Site 6 is located off the end of the fault, so variability in the distance calculations is included as the rupture moves from the north end of the fault to the south end of the fault. The hazard curves for Site 6 exhibit some curvature due to the variability in the location of the rupture on the fault.

Initial results indicated some programming errors in the hanging-wall terms of the ground-motion models. Programming of the ASK14 hanging-wall model proved the most challenging for participants. The ASK14 hanging-wall model provides two options for calculating $T5$, a taper used for scaling off the end of the rupture. The first option is to calculate $T5$ based on R_{Y0}, a new distance parameter introduced in ASK14. This is the preferred method for calculating $T5$. The second option is to calculate $T5$ based on R_{JB}. This alternative option was offered so that codes that did not have the capability to compute R_{Y0} could still use the ASK14 ground-motion model. For Sites 1–3, the hazard results from the two ASK14 options are the same, but for Sites 4–6, the results from the two options are different. Seven codes implemented the preferred $T5$ taper, while six codes implemented the alternative option. Results for Sites 4–6 were split based on which option was used. Programming errors in the hanging-wall models were identified and fixed through discussions and the use of a hand solution. An error in the PEER NGA-West2 Excel file related to the R_{Y0} term in ASK14 was also discovered and fixed.

As shown in Table 3.3, the range in hazard results between the five core codes is less than 5%, and the range in hazard results between all codes is less than 10%. At Sites 1–5 the ranges are less than 1% and are simply a difference in the reported rate. Again, the reported ranges for Site 6 are due to Site 6's location off the end of the fault. The difference in results can be attributed to differences in step size used by each code, in addition to previously described differences in approaches.

3.5 TEST 2.4

3.5.1 Purpose

Test 2.4 is a single magnitude event on a strike slip fault with an increased fault width of 30 km. The test specifies a triangular distribution of hypocenter locations down dip, requiring the code to calculate rupture location probabilities for a distribution other than the typical uniform distribution. The test does not include ground-motion variability.

3.5.2 Discussion and Results

Test 2.4a specifies the typical uniform distribution of hypocenters down dip, while Test 2.4b specifies a triangular distribution. The purpose of Test 2.4a was to have a comparison for the triangular distribution in Test 2.4b. A further explanation of the triangular distribution of hypocenter locations is provided in the instructions for this test; see Appendix B. The use of non-uniform hypocenter distributions is relatively new in PSHA, and the majority of codes that ran this test added this feature to their code as a result of the verification project. From a practical standpoint, the actual moving around of ruptures on the fault doesn't change, but the probability assigned to each rupture location with depth is different and is based on the location of the hypocenter for that rupture. Some discussions about how to implement the new distribution took place prior to running the test, which resulted in a uniform approach across codes. Initial results showed strong agreement between codes.

As shown in Table 3.3, the range in hazard results between the five core codes is less than 1%, and the range in hazard results between all codes is less than 8%. The ranges in results for Test 2.4a and Test 2.4b are very similar, indicating that the difference in results did not increase significantly with the introduction of the triangular depth distribution. The difference in results can be attributed to slight differences in the modeling of a triangular depth distribution, in addition to previously described differences in approaches.

3.6 TEST 2.5

3.6.1 Purpose

Test 2.5 is a single magnitude event on a strike-slip fault, with PGA test values up to 7.0*g*. With the site 15 km away from the fault and high PGA test values, the code is required to calculate probabilities of exceedance for high epsilon values on the extreme tails of the ground-motion distribution.

3.6.2 Discussion and Results

Test 2.5a specifies the standard lognormal distribution and was designed to test how far out on the tails of the ground-motion distribution a code could reliably compute probabilities of exceedance. The hazard results at the highest PGA test value of 7.0*g* correspond to a mean epsilon of about 6. Despite the much higher epsilon values associated with the hazard results for this test, the range in

hazard results between the five core codes is still exceptionally small and about the same as it was in Test 1.8a. The benchmark answer was also checked against a hand solution, and the two agreed very well. The hand solution utilized the normal distribution function built into Excel, which was also checked against the normal distribution function built into *R* code, and the two were found to be in strong agreement.

Test 2.5b specifies a mixture model of two lognormal distributions. Use of a mixture model distribution, similar to the one specified for Test 2.5b, is gaining recognition for projects with long return periods, as residuals have shown a deviation from the standard lognormal distribution, with higher probabilities of ground motions on the tails of the distribution. Appendix B provides instructions for this test and additional explanation of the mixture model. The majority of codes that ran this test added this feature to their code through the verification project.

As shown in Table 3.3, the range in hazard results between the five core codes is less than 1%, and the range in hazard results between all codes is less than 10%. Note that the range in hazard results between all codes is closer to 3% at a PGA of 1.5*g*, which is still associated with a high epsilon of about 4. The electronic supplement indicates that one code does not meet the acceptance criteria for Test 2.5a at the highest PGA of 7.0*g*, reporting results that are just under the -5% acceptance criteria. This outlier is not significant, as the hazard results at an epsilon of 6 correspond to such long return periods that they have no practical use; they are only reported here to determine when the normal distribution functions start to break down. The difference in results can be attributed to the different normal distribution functions implemented by each code, in addition to previously described differences in approaches.

4 Set 3 Results

4.1 INTRODUCTION

Tests in Set 3 build on the complexities of the tests in the previous two sets and verify more challenging elements of the codes. The tests in Set 3 include modeling a bending fault, calculating the mean hazard and fractiles from a logic tree, modeling the intraslab region of a subduction zone, and modeling an area source with finite ruptures. Table 4.1 presents a short description of each test, and Table 4.2 indicates which codes completed which tests. Test instructions for Set 3 are provided in Appendix C, and include test specifications as well as figures of the sources and site locations. Test results for Set 3 are provided as an electronic supplement in Appendix D.

Unlike the tests in Set 1 and Set 2, the tests in Set 3 do not have benchmark answers and acceptance criteria. For the majority of tests in Set 3, there are multiple modeling approaches currently used by the codes. Specifying the best approach is beyond the scope of this project. Separate workshops with seismic-source characterization, ground-motion characterization, and hazard analysts are needed to validate the methods and develop consensus recommendations. The results are therefore split into groups based on the different approaches, and the project's role was to reach agreement within each group. The participants also worked to understand why one modeling approach would lead to higher or lower hazard than another approach, and these observations are documented in this chapter. For quantitative information regarding the ranges in hazard between the codes and across different approaches, the reader is referred to the electronic supplement in Appendix D.

Table 4.1 Set 3 tests and descriptions.

Test	Description
3.1a	Bending fault, dipping east
3.1b	Bending fault, dipping west
3.2	Logic tree, percentiles
3.3	Intraslab zone
3.4	Areal zone, finite ruptures

Table 4.2 Set 3 Tests completed by each code.

Test	3.1a	3.1b	3.2	3.3	3.4
HAZ38-URS					
HAZ45	✓	✓	✓	✓	✓
THAZ	✓	✓	✓	✓	✓
HAZ45b					
FRISK88					
EZ-FRISK					
HazMapEQ	✓	✓	✓	✓	✓
RIZZO-HAZARD	✓	✓	✓	✓	✓
PROSIT					
OpenQuake	✓	✓	✓	✓	✓
OpenSHA	✓	✓			
SISMIC	✓	✓	✓	✓	✓
PROBHAZ	✓	✓	✓	✓	✓
XCD55, HAZ51, TREE51	✓	✓	✓	✓	✓
CRISIS	✓	✓	✓	✓	✓

4.2 TEST 3.1

4.2.1 Purpose

Test 3.1 is a single magnitude event on a dipping fault whose trace bends along strike. The test requires the code to model the geometry and calculate distance metrics for a bending fault with strike variation along the fault length. Ground-motion variability is included.

4.2.2 Discussion and Results

The fault for Test 3.1 is 60 km long and made up of four segments that create a bending fault. Here the term "segment" is meant to imply a section of the fault that has a different strike than the neighboring section, not that the fault is segmented with points that stop the rupture. The large magnitude 6.75 event creates a rupture that takes up the entire width of the fault, so the rupture is only moved along strike. The test includes two sub-tests with the fault dipping in different directions. Test 3.1a specifies an east-dipping fault, while Test 3.1b specifies a west-dipping fault. The test specifies use of the CY14 ground-motion model, which includes a hanging-wall term that utilizes the R_X distance parameter.

There are two aspects to a bending fault that are modeled differently by the codes. The first is the fault geometry. When a dipping fault bends along the strike, gaps or overlaps are formed where the fault segments meet at the bend if the dip direction is maintained orthogonal to strike.

These gaps or overlaps must be resolved by the code so that a rupture can be moved uniformly around a continuous fault. One group of codes addresses these areas by filling in gaps and removing overlaps. The other group of codes projects the bottom points of the fault trace along an average strike and then connects those points at depth to form the bottom of the fault.

This second approach was suggested during the first verification project by Mark Stirling and is sometimes referred to as the Stirling approach. Although the Stirling approach offers a consistent method for handling fault traces with severe bends, it violates the standard assumption that the dip direction is orthogonal to the local strike for each segment. The different approaches for modeling the fault geometry result in different fault areas and can also result in different R_{RUP} and R_{JB} distances, both of which cause differences in the hazard results. These two geometry approaches are illustrated in Figure 4.1 for the east-dipping fault and Figure 4.2 for the west-dipping fault. The fault areas for each approach are also provided in Figures 4.1 and 4.2.

The second aspect to modeling a bending fault is the calculation of R_X. For a straight rupture, R_X is simply the horizontal distance from the site to the top of rupture trace measured perpendicular to strike. For a bending rupture, the calculation of R_X becomes more complicated because the perpendicular distance changes as the rupture bends, creating as many R_X values as there are bending segments of the rupture. The issue is that only one R_X value can be used in the GMPE. Again, there are two different methods utilized by the codes to calculate R_X for a bending fault.

One approach is to calculate R_X for the rupture segment that is closest to the site. This approach is straightforward and follows the logic that the segment closest to the site contributes most to the hanging-wall effect. Note that this is not necessarily the minimum R_X; it is the R_X for the segment that produces the minimum rupture distance, R_{RUP}. Another approach is to calculate a local R_X for each rupture segment and then use a weighted-average of those local R_X values to produce a single global R_X. The weights for the local R_X distances are based on the distance from each segment to the site, with the weights being highest for segments closest to the site. This approach was developed by Spudich and Chiou [2015] and is part of the generalized coordinate system (GC2). The GC2 approach is more involved from a calculation perspective, but offers a solution for incorporating the hanging-wall effect for all rupture segments. The GC2 methodology was also used in the development of the NGA-West2 ground-motion models and thus provides consistency in terms of how those distance measures were derived from data. Nine out of the ten codes participating in this test use one of these two R_X approaches. The tenth code, OpenSHA, uses an approach where R_X is calculated for the rupture segment closest to the site if the site is located along the strike, and R_X is calculated from an average strike if the site is off the end of the rupture.

The results were split into groups based on the different geometry and R_X approaches. Three codes use the Stirling approach and GC2, five codes use the Stirling approach and R_X to the closest segment, and three codes project the segments orthogonal to strike and use R_X to the closest segment. Ten codes participated in this verification test, but RIZZO-HAZARD has the capability to model the fault geometry using both approaches, resulting in eleven hazard results for each site. The OpenSHA results were grouped with codes that calculate R_X to the closest segment for Sites 1, 3, and 4, and grouped with codes that calculate R_X using GC2 for Site 2 because GC2 produces R_X values that are similar to those from an average strike method when the site is off the end of the rupture.

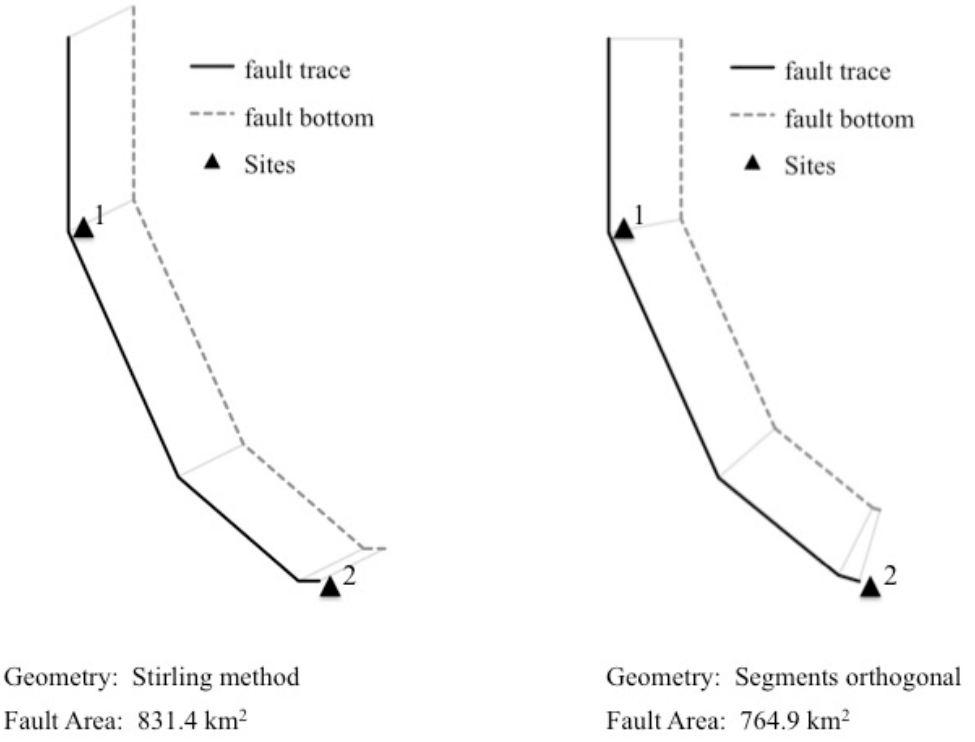

Figure 4.1 **Test 3.1a (east dipping): fault trace and projection of bottom of fault for different geometry approaches.**

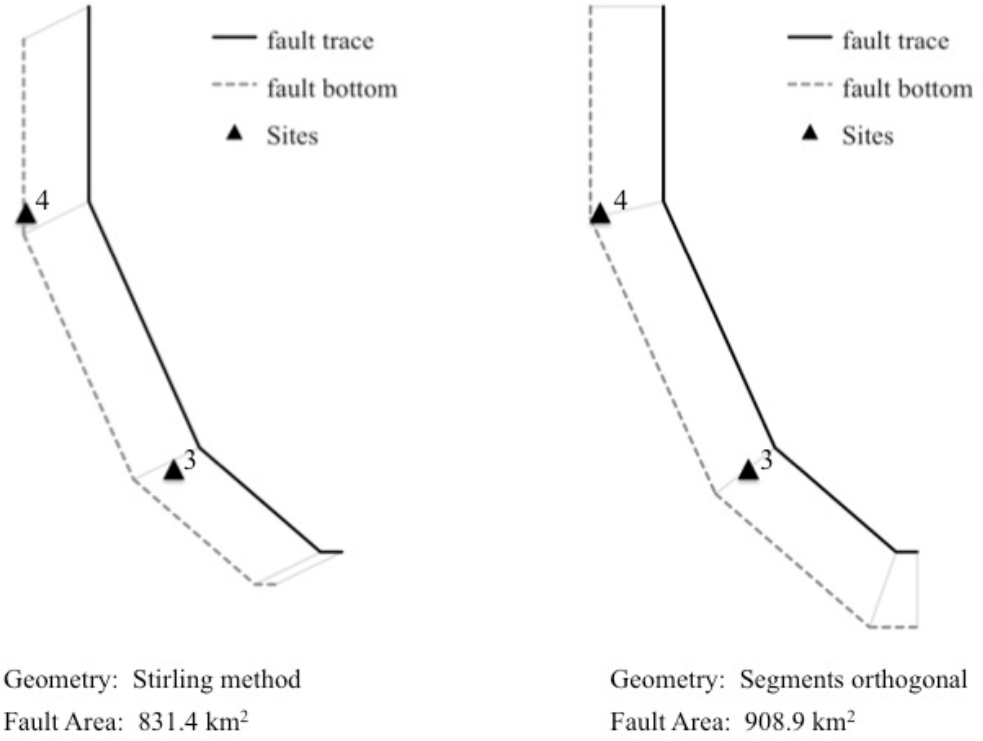

Figure 4.2 **Test 3.1b (west dipping): fault trace and projection of bottom of fault for different geometry approaches.**

Site 1 is located 1.5 km east of the trace of the fault on the hanging wall at the intersection of two segments, such that an overlap forms if the segments are projected orthogonal to strike. The results for Site 1 show strong agreement between codes utilizing the same approaches, with a maximum difference in hazard results of 1 or 2% within each group. The approach used to calculate R_X has a negligible effect on the hazard results for this site, as both the closest R_X approach and GC2 approach yield similar R_X distance values when the site is close to the trace of the rupture. The different approaches used to model the fault geometry result in a 9% difference in the fault area but don't appear to result in drastically different distance values (i.e., R_{RUP} and R_{JB}). A comparison of the results across all approaches shows that the difference in hazard is approximately 9% at all test values. This means that the difference in fault area, which is carried through to the rate calculation, is responsible for the majority of the difference in results from all approaches.

Site 2 was intentionally placed off the southern end of the fault trace to highlight differences in the approaches used to calculate R_X. The severe bend at the southern end of the fault caused problems for multiple codes, and led to the identification of errors in many codes. For codes that project the segments orthogonal to strike, the original coordinates of the fault trace were problematic because the very southern bend of the fault overlaps entirely with the third segment when projected orthogonal to strike. Participants with codes that use this geometry method noted that their code would flag this geometry as unphysical, and they would adjust the coordinates of the fault trace slightly to resolve the issue. For the three codes that model the geometry by projecting segments orthogonal to strike, the following revised coordinates were used for Test 3.1a (east dipping fault, Sites 1 and 2):

From south to north:

-0.45236 -64.78365

-0.44700 -64.80164

-0.36564 -64.90498

-0.16188 -65.00000

0.00000 -65.00000

Codes utilizing the Stirling method used the original coordinates specified in the instructions. Some of the errors that were identified and fixed included a misunderstanding of the implementation of the Stirling method, errors in the calculation of R_X (particularly off the end of the fault), and errors related to the code's ability to correctly identify when the site is on the hanging wall and when the site is on the footwall. The final results for Site 2 show fair agreement between codes utilizing the Stirling method and GC2, with a maximum difference in hazard results of 4% within the group. The results for Site 2 show strong agreement between codes utilizing the Stirling method and closest R_X, with a maximum difference in hazard results of 1.5% within the group. A comparison of the results between these two groups shows that the maximum difference in hazard results is about 17%, which can be attributed to the different R_X approaches. When the rupture is located at the very southern end of the fault, the GC2 approach produces a positive R_X distance with the site on the hanging wall, while the closest-segment approach produces a negative R_X distance with the site on the footwall. As expected, this difference results in higher hazard results from codes utilizing the GC2 approach. The results for Site 2 show decent agreement

between codes that project the segments orthogonal to strike and use the closest R_X method, with a maximum difference in hazard results of about 8%. A comparison across all approaches is not meaningful here as the coordinates of the fault are not the same and greatly impact the results for this site.

Site 3 is located about 3 km west of the trace of the fault on the hanging wall at the intersection of two segments, such that a gap forms if the segments are projected orthogonal to strike. The results for Site 3 show fair agreement between codes utilizing the same approaches, with a maximum difference in hazard results of 2 to 5% within each group. A comparison of the results across all approaches shows the difference in hazard ranges from about 9% at the lower PGAs to about 13% at the highest PGA. The different approaches used to model the fault geometry again account for this 9% difference due to differences in the fault area.

Site 4 is located about 5 km west of the trace of the fault, on the hanging wall at the intersection of two segments, such that a gap forms if the segments are projected orthogonal to strike. The results for Site 4 show good agreement between codes utilizing the same approaches, with a maximum difference in hazard results of about 1 to 3% within each group. A comparison of the results across all approaches shows the difference in hazard ranges from about 9% at the lower PGAs to about 6% at the highest PGA. The fault area accounts for the 9% difference; differences in the calculated distances are likely narrowing the difference at the higher PGAs by working in the opposite direction.

4.3 TEST 3.2

4.3.1 Purpose

Test 3.2 uses a strike–slip fault, similar to Test 2.2, but includes epistemic uncertainty in the source and ground-motion characterization. The test requires the code to calculate the mean hazard from a logic tree and provide the hazard at the 10th, 50th (median), and 90th percentiles. Ground-motion variability is included.

4.3.2 Discussion and Results

Test 3.2 includes a logic tree that specifies three slip rates, two magnitude recurrence relationships, three maximum magnitudes, and two ground-motion models. There is no correlation between branches on the logic tree, resulting in thirty-six possible alternative hazard curves.

Some of the maximum magnitudes specified in this test produce rupture areas larger than the defined fault area. Although this is not the first test where this scenario occurs, the difference between the largest rupture area and the defined fault area was generally small for previous tests, so results within the acceptance criteria could still be obtained without following the common practice of restricting the rupture to the fault area. In this test, the difference is large, and initial hazard results indicated that some codes were not restricting large ruptures to the fault boundaries. These codes were modified and revised results showed better agreement between all codes.

Initial results for the mean hazard showed a division between two groups of codes at the lower PGA test values. Discussion amongst participants led to the understanding that the majority

of the codes were not converting rates of exceedance to Poisson probability correctly when epistemic uncertainty is included. To compute the Poisson probability from a logic tree correctly, the code must first calculate the unweighted rates of exceedance from each branch of the logic tree. These unweighted rates of exceedance must then be converted to Poisson probabilities. The Poisson probabilities are then weighted, and those results are summed. Initially, only two codes were following this scheme and reporting the mean hazard correctly as Poisson probabilities. The remaining seven codes were summing up the weighted rates of exceedance and converting to a Poisson probability at the end: this is not correct. This error is largest at the lower PGA test values—where the hazard results are relatively high—and diminishes as the PGA test values increase. The maximum difference due to this error is about 9% at the first PGA test value of 0.001*g*.

Although the instructions ask participants to report results as Poisson probabilities, many participants noted that their codes output is reported as annual frequencies of exceedance, and this is what they always report for projects. These participants were converting results to Poisson probabilities as a post-processing step to be consistent with the instructions; however, when epistemic uncertainty is included, it is not possible to convert the mean hazard to a Poisson probability, as described above. Because the users of these codes have no practical use for modifying their codes to compute Poisson probabilities, these participants were given the option of reporting results for the mean hazard as annual frequency of exceedance, and the results were split into two groups. The results for all other tests, including the fractiles results for this test, are still reported as Poisson probabilities to be consistent with the initial instructions. The range in mean hazard results between the codes in each group is less than 1%.

Participants were asked to report the hazard at the 10th, 50th (median), and 90th percentiles. These are commonly referred to as fractiles. Codes participating in this test compute the fractiles using two different approaches. The first approach is to interpolate between the cumulative weight and the hazard to obtain the hazard at the fractile of interest. The majority of codes using this approach are using linear–linear interpolation, but the interpolation should be linear on the cumulative weights and log on the hazard. The second approach does not use interpolation but reports the hazard at the first cumulative weight exceeding the fractile of interest. Due to the simplicity of this test, and the very small logic tree, there can be large jumps between cumulative weights, causing relatively large differences in the reported fractile when comparing the two methods. The jumps in cumulative weight are shown in Figure 4.3, where the cumulative weights are plotted against the hazard for one PGA. In this plot, there are thirty-six markers, one for each of the thirty-six possible combinations from the logic tree. When looking at a particular fractile, for instance the 10th percentile (0.1 on the *y*-axis), a cumulative weight does not fall there, so some codes would interpolate between the two closest fractiles, and some codes would report the first point exceeding 0.1. The difference in fractile hazard results at the 10^{th} percentile is 29%, as shown on Figure 4.3, and is the maximum difference in results for this test. A typical project contains multiple sources and thousands of combinations from the logic tree; therefore, large jumps between cumulative weights do not exist. For these reasons, on a typical project, the difference in reported fractiles based on whether a code interpolates or reports the first value exceeding is expected to be negligible.

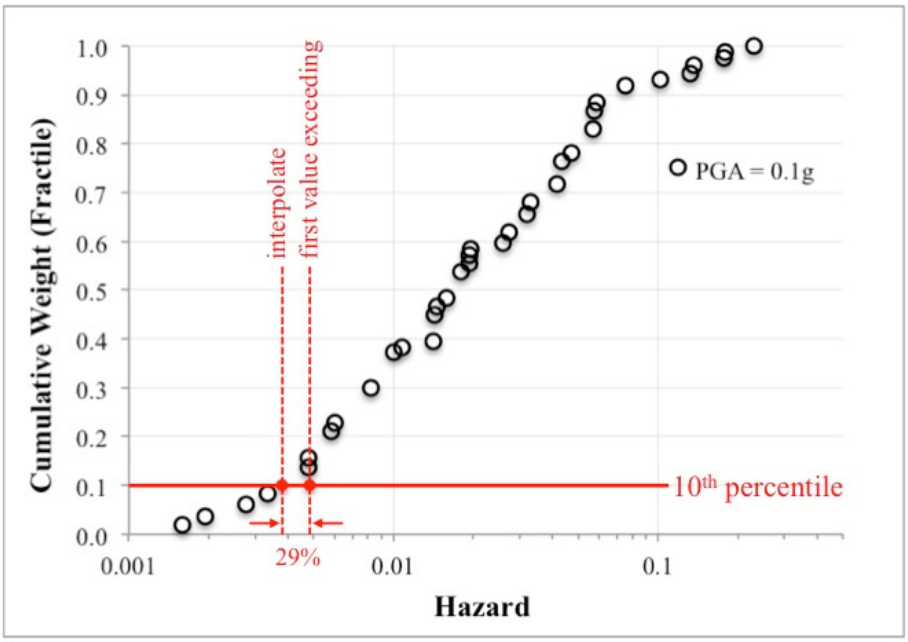

Figure 4.3 Test 3.2: cumulative weights versus hazard for one PGA.

The fractile results were split into groups based on the two different approaches, with five codes using interpolation and four codes reporting the first value exceeding. The range in fractile hazard results between the codes in each group is less than 2%. When comparing the results across these two groups, the maximum difference is about 29% and can be attributed to the different fractile approaches.

4.4 TEST 3.3

4.4.1 Purpose

Test 3.3 is an intraslab region of a subduction zone, consisting of a 12.5-km-thick slab with a dip of 30° in the shallower portion and 45° in the deeper portion. The test requires the code to generate ruptures in a three-dimensional volume, calculate distance metrics from those ruptures, and correctly pass on the source-type parameter to the ground-motion model. The Zhao et al. [2006] ground-motion model is specified, and ground-motion variability is included.

4.4.2 Discussion and Results

The approaches used to model intraslab sources vary greatly across the codes and can even vary from one analyst to the next using the same code. The central issue is how to model a rupture that occurs within the slab. The codes generally have a couple of different built-in source types that are used to model ruptures for different sources. For example, one source type might be used for faults,

where the user can define the boundary of the fault as a plane, and then the code generates a rupture on that plane, which is moved around to all possible locations. A different source type might be used for areal sources, where the user can define the boundary of the areal zone as a polygon and specify the seismogenic thickness of the zone, and then the code generates point sources within that volume. Because a majority of the codes do not have a specific source type for intraslab sources, one of the built-in source types is used to model the slab.

Each code contains nuances and variations in its approach to model the ruptures from the specified intraslab zone. The discussion here will focus on the four main approaches, which are illustrated in Figure 4.4 with a side view of the entire slab looking north. Approach (a) models the intraslab as an areal zone and fills it with point sources. This is typically accomplished by using staircasing blocks of areal zones to approximate the slab shape; see Figure 4.4(a). Approach (b) ignores the thickness of the slab and models only the top of the slab or the middle of the slab as a dip-varying fault, similar to a listric fault. Ruptures with finite dimensions are then moved around the dip-varying fault; see Figure 4.4(b). Approach (c) involves filling the slab with pseudo faults that approximate the slab shape; see Figure 4.4(c). The faults are merely a mechanism to establish boundaries so that ruptures can be created and moved around. Approach (d) is similar to approach (a) where staircasing blocks of areal zones are used to approximate the slab shape; only finite ruptures are used instead of point sources. This approach is similar to the virtual-fault method used in typical areal zones. This is accomplished by filling the slab volume with point sources, which represent the hypocenter, and then expanding those hypocenter points into finite ruptures; see Figure 4.4(d).

Specific inputs for each of these four approaches were provided to the participants so that hazard results from codes using the same approach would not be dissimilar due to differences in how the participant divided the slab into faults or stairsteps. For approaches (c) and (d), the participants needed to know what dip to use for the ruptures. Although this level of detail is not often specified in the source characterization, the participants were instructed to use a dip of 35° relative to the slab corresponding to an absolute dip of 65° in the shallower slab section and 80° in the deeper slab section. The relative dip of 35° came from looking at some of the preliminary finite rupture data for the ongoing PEER NGA-Subduction project.

An example **M**6.5 rupture for each of the four approaches is shown in Figure 4.5 with a view of a vertical slice of the slab looking west. The hypocenter location and shortest distance to the rupture, R_{RUP}, are shown for each approach. As illustrated in Figure 4.5, approach (a) models the ruptures as point sources while the other three approaches model the rupture as a plane with finite dimensions. Figure 4.5 also illustrates the different treatment of the boundaries by the approaches using finite ruptures. In approach (c), the slab defines the boundaries of the ruptures, and no rupture is allowed to leak out of the slab. In approach (d), the slab defines the boundaries of the hypocenters, and ruptures are allowed to leak out laterally, i.e., ruptures associated with hypocenters located at the southern and northern ends of the slab will leak out of the slab to the south and north.

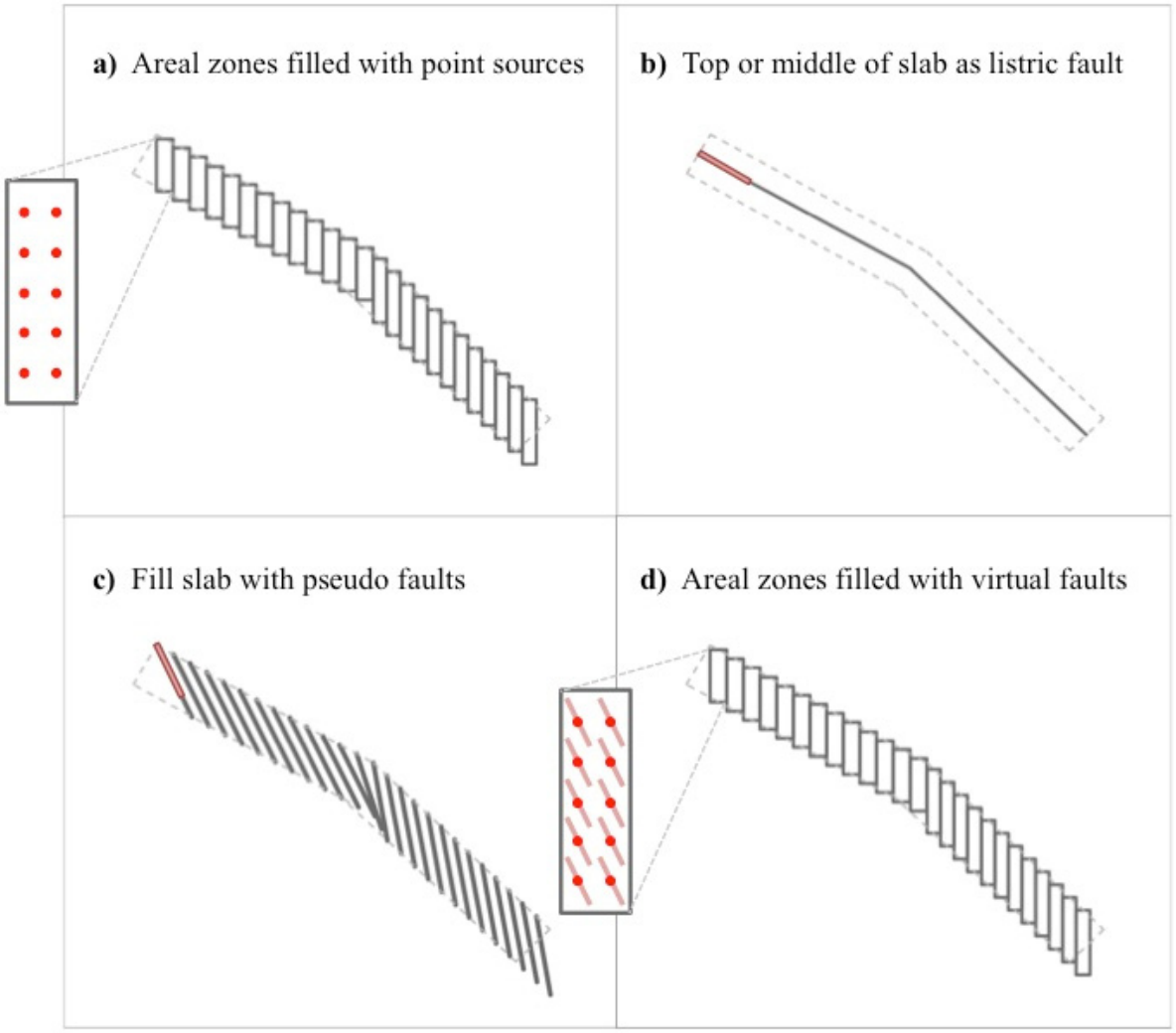

Figure 4.4 **Test 3.3 looking north: different approaches for modeling intraslab region.**

To explain why these modeling approaches lead to differences in reported hazard, Figure 4.6 compares approaches (a) and (c) with the same example **M**6.5 rupture, and in addition to R_{RUP}, shows the hypocenter depth, Z_{HYP}. As shown in the figure, the point source in approach (a) is associated with a larger R_{RUP} distance, which leads to lower median ground motions and thus lower hazard. Additionally, the point source in approach (a) is associated with a smaller Z_{HYP} depth, which also leads to lower median ground motions and thus lower hazard. Though this effect from Z_{HYP} may seem counterintuitive to some, deeper ruptures are associated with higher ground motions; therefore, a smaller Z_{HYP} leads to lower median ground motions. Note that the difference in hazard from Z_{HYP} is specific to the instructions for this verification test where the hypocenter is constrained to the center of the rupture plane. Had the instructions specified randomizing the hypocenter location on the rupture plane, there would be no difference in Z_{HYP} between approaches (a) and (c).

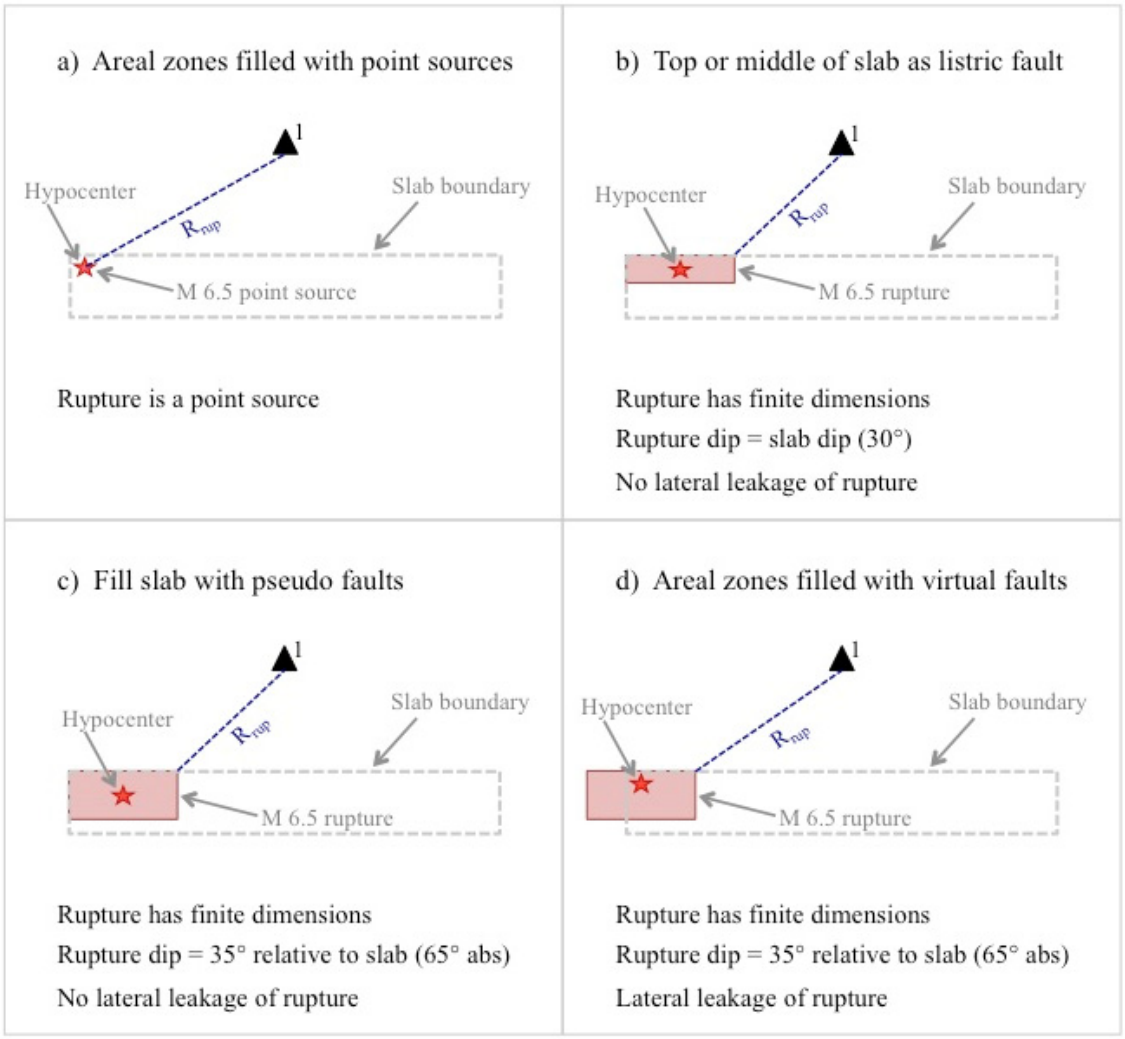

Figure 4.5 Test 3.3 looking west at a vertical slice: different approaches for modeling intraslab region.

Figure 4.7 shows the hazard results for Test 3.3 at Site 1 for codes utilizing one of the four main approaches. The results are grouped by approach, and there is good agreement between codes utilizing the same approach. As expected, the point sources in approach (a) lead to significantly lower hazard results than the approaches utilizing finite ruptures. Note that although the point source approach has obvious shortcomings in terms of being able to model the real dimensions of a rupture, it cannot be reasonably eliminated as a viable approach and is the most consistent with current ground-motion models. The majority of current intraslab ground-motion models, including Zhao et al. [2006], were predominantly derived from data using hypocentral distance, not R_{RUP}. The Zhao et al. [2006] publication states, "Source distance x is the shortest distance to the rupture zone for earthquakes with available fault models, and hypocentral distance for the other events."

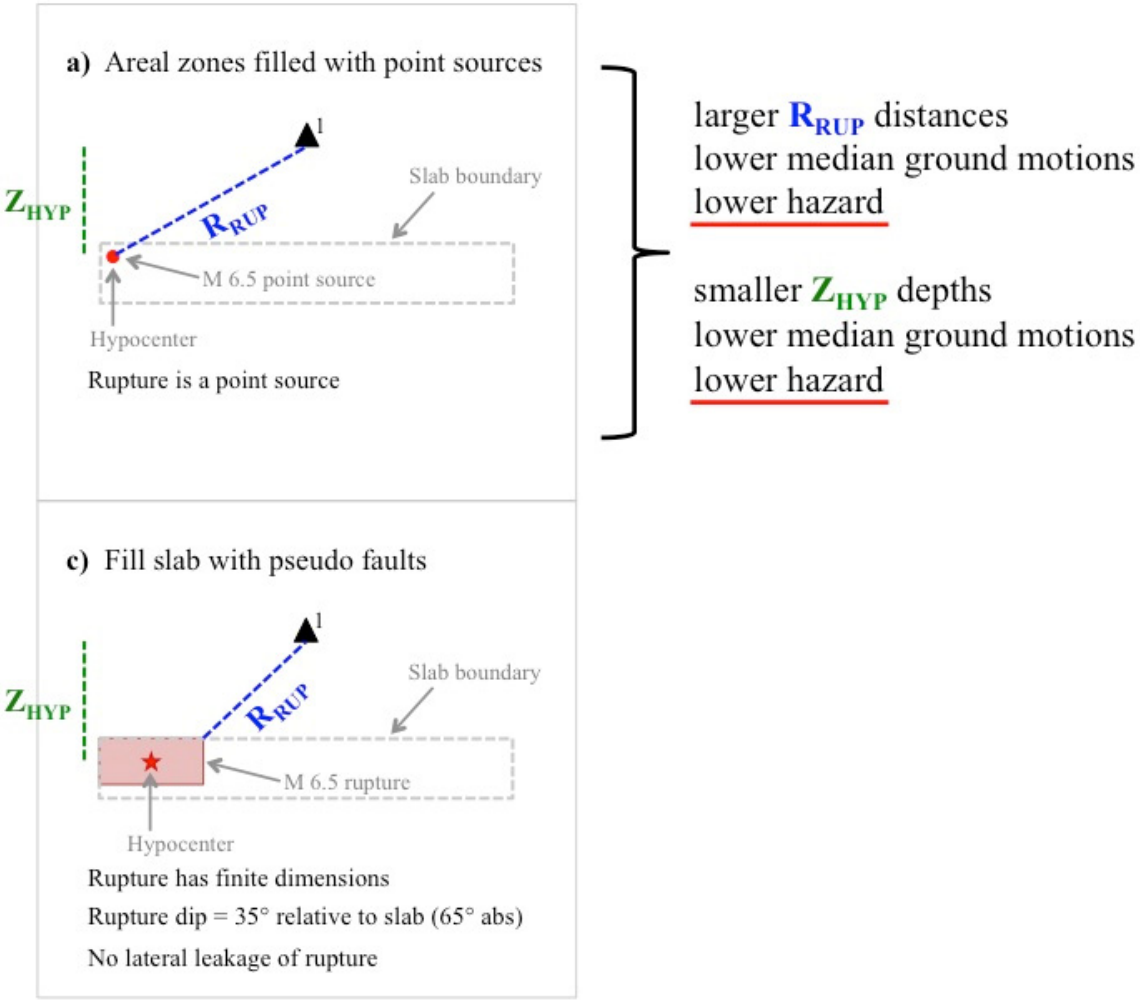

Figure 4.6 **Test 3.3: comparison of two approaches for modeling ruptures in an intraslab zone and their impact on hazard.**

Overall, the differences in hazard are well-understood and primarily due to different modeling approaches for generating ruptures within a dipping slab volume. The results show good agreement between codes utilizing the same approaches, with differences in hazard results generally less than 5% within each group. The differences in hazard are large when the results are compared across all approaches. For the industry to move forward with a consistent approach requires: (1) additional seismic source characterization work in terms of understanding how finite ruptures occur within the slab; (2) additional ground-motion characterization work in terms of developing a model consistent with these observed ruptures and utilizes appropriate distance measures to describe the ruptures, as opposed to current models that rely heavily on hypocentral distance; and (3) more detailed specifications in hazard input documents including preferred dip of ruptures and whether the slab volume represents the limits of hypocenters or the limits of ruptures. For expanded studies on modeling intraslab earthquakes in PSHA, the reader is referred to LaForge and Hale [2017] and Weatherill et al. [2017].

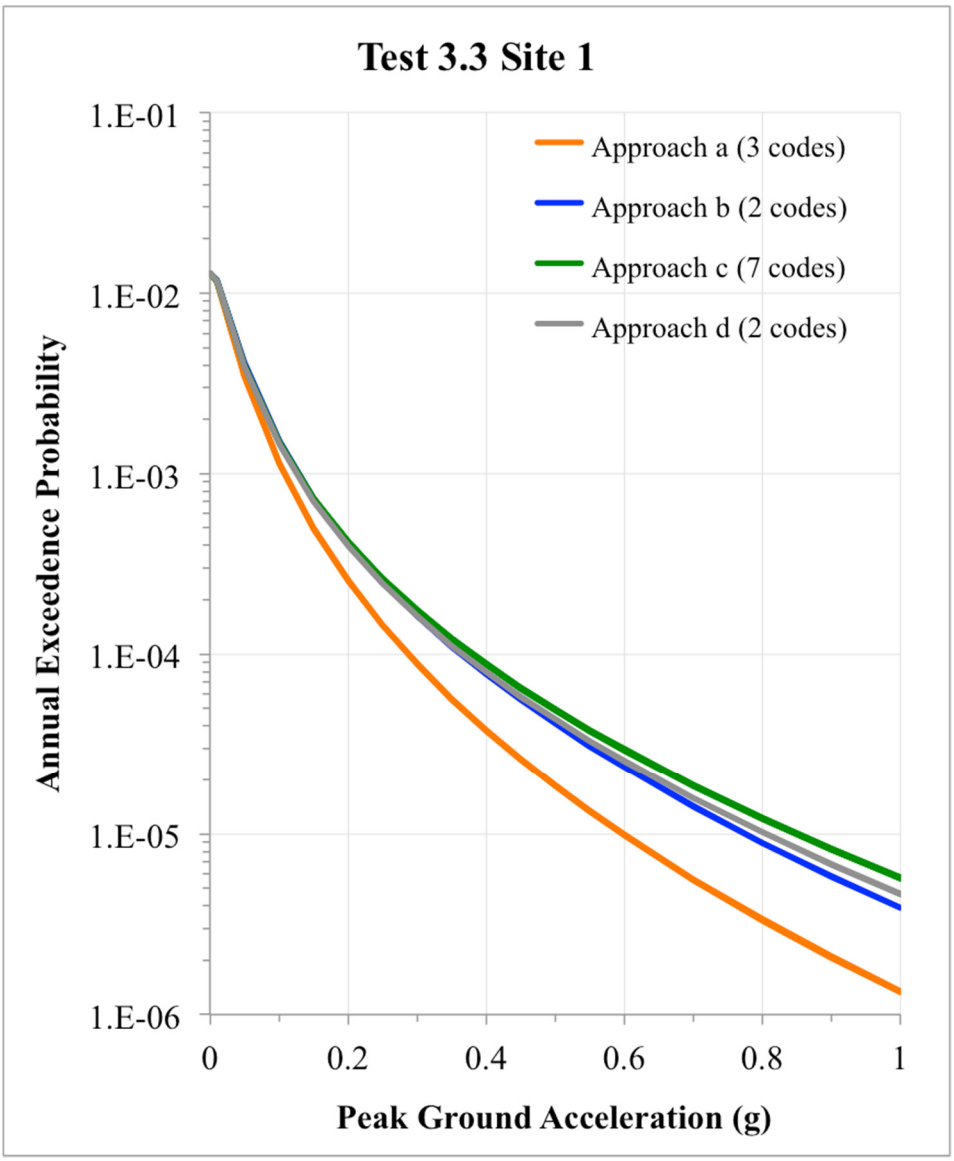

Figure 4.7 **Test 3.3: comparison of hazard results when different approaches are used to model the ruptures for the intraslab zone.**

4.5 TEST 3.4

4.5.1 Purpose

Test 3.4 is an area source zone, similar to Test 1.11, but with an increased depth range from 5 to 25 km. Rather than modeling earthquakes as point sources, the test requires the code to use virtual ruptures to account for the rupture dimensions. The Chiou and Youngs [2014] ground-motion model is specified, and ground-motion variability is included.

4.5.2 Discussion and Results

This test adds significant complexity to the area source zone used in previous tests by specifying additional information related to the characteristics of future earthquakes. Faulting styles were specified as 60% strike-slip with a dip of 90°, 20% normal with a dip of 60°, and 20% reverse with a dip of 30°. The approaches used to model areal zones with virtual faults vary across the codes. The central issue is whether the seismogenic zone represents the boundaries of the ruptures or the boundaries of the hypocenters. This level of detail is not typically provided to the hazard analysts, and the participants interpret the boundaries in different ways, resulting in four main approaches, as described below.

Each code contains nuances and variations in its approach to model the ruptures in the areal source zone. The discussion here will focus on the four main approaches, which are illustrated in Figure 4.8. Approach (a) assumes that the seismogenic zone is based on hypocenter data, and thus the top and bottom boundaries define the hypocenter locations. Ruptures are allowed to go above the top boundary and below the bottom boundary if necessary. This approach is illustrated in Figure 4.8(a), where the limits of the seismogenic zone are shown along with two example **M**6 ruptures. Approach (b) also interprets the boundaries of the seismogenic zone as defining the hypocenter locations, but it does not allow the rupture to go above the upper boundary. This approach is illustrated in Figure 4.8(b). Approach (c) assumes that the boundaries define the rupture limits, and no part of the rupture is allowed to go above the top boundary or below the bottom boundary, as illustrated in Figure 4.8(c). This approach is similar to how ruptures are modeled on a fault source and results in a narrower depth range for the hypocenters, particularly for large ruptures. Approach (d) assumes that the seismogenic zone boundaries define the top of ruptures, as illustrated in Figure 4.8(d). In all of these approaches, the areal zone polygon is treated as a leaky boundary for ruptures such that hypocenters are constrained within the areal zone polygon, but rupture planes are allowed to leak out laterally if necessary.

To explain why these modeling approaches lead to differences in the reported hazard, Figure 4.9 compares approaches (a) and (d) with the same example **M**6 ruptures, along with the closest distance to the rupture, R_{RUP}, and the depth to the top of rupture, Z_{TOR}. As shown in the figure, the shallower ruptures in approach (a) are associated with smaller Z_{TOR} distances, which lead to lower median ground motions and thus lower hazard. At the same time, the shallower ruptures in approach (a) are associated with smaller R_{RUP} distances, which lead to higher median ground motions and thus higher hazard. These competing effects require a more critical interpretation of the hazard curves.

Figure 4.10 shows the hazard results for Test 3.4 at Site 1 located in the middle of the areal zone for codes utilizing one of the four main approaches. The results are grouped by approach, and there is good agreement between codes utilizing the same approach. The impact from Z_{TOR} can be seen at the portion of the hazard curve corresponding to low intensity values, where all rupture scenarios contribute to the hazard. As expected, here, the shallower ruptures in approach (a) lead to lower hazard results. The impact from R_{RUP} can be seen at the portion of the hazard curve corresponding to high intensity values, where close-in rupture scenarios dominate the hazard. As expected, here, the shallower ruptures in approach (a) lead to higher hazard results.

Overall, the differences in hazard are well-understood and primarily due to different interpretations of the seismogenic zone boundaries. The results show good agreement between

codes utilizing the same approaches, with differences in hazard results generally less than 5% within each group. The differences in hazard are large when the results are compared across all approaches. For the industry to move forward with a consistent approach requires: (1) additional studies of the bounds of the hypocenters and the ruptures, especially for the larger magnitude events where data is limited; and (2) more detailed specifications in hazard input documents regarding the treatment of the seismogenic zone boundaries, as well as specifications for the ruptures including faulting styles, dip, and strike.

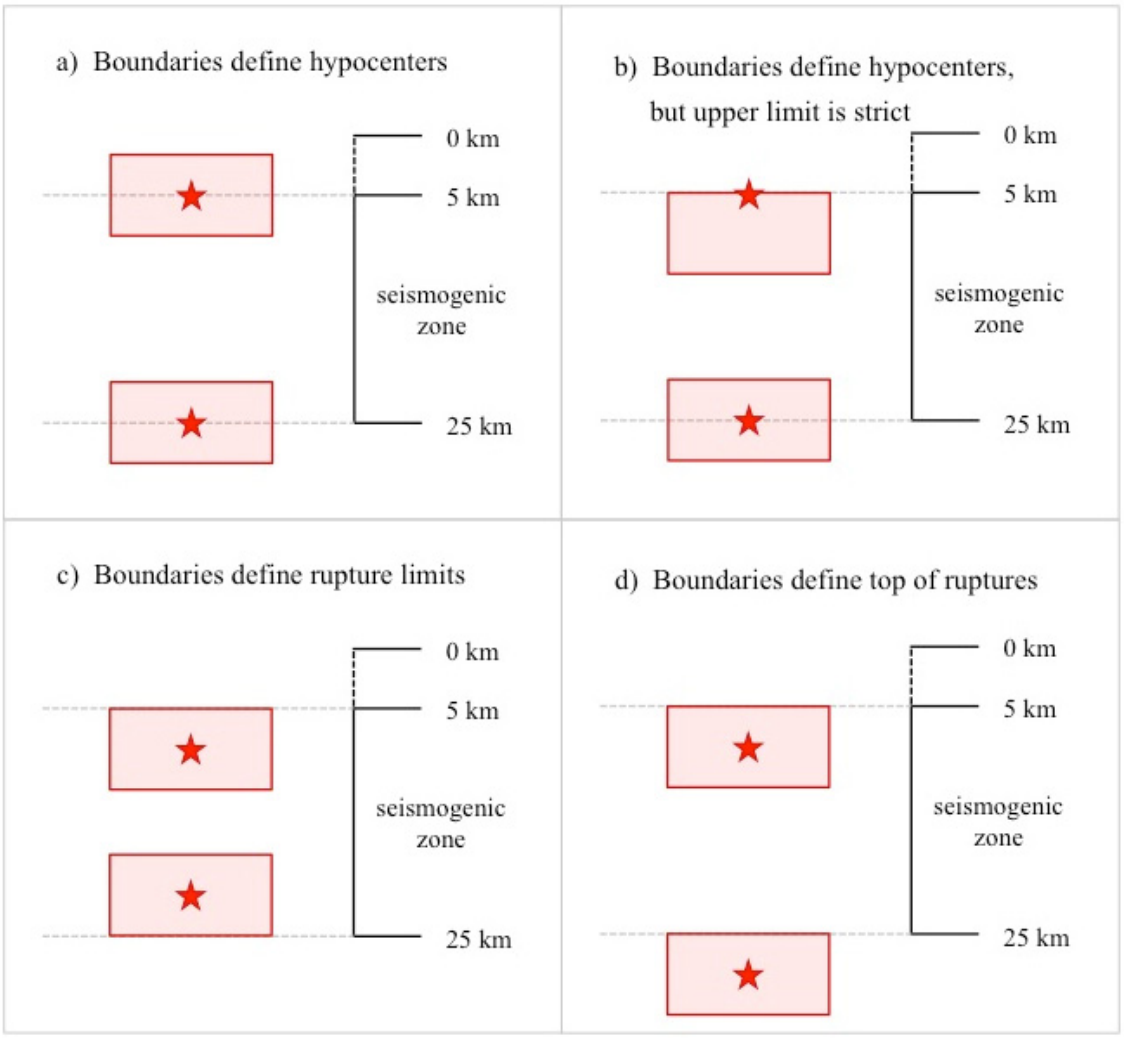

Figure 4.8 **Test 3.4: different approaches for modeling an area source zone with virtual faults.**

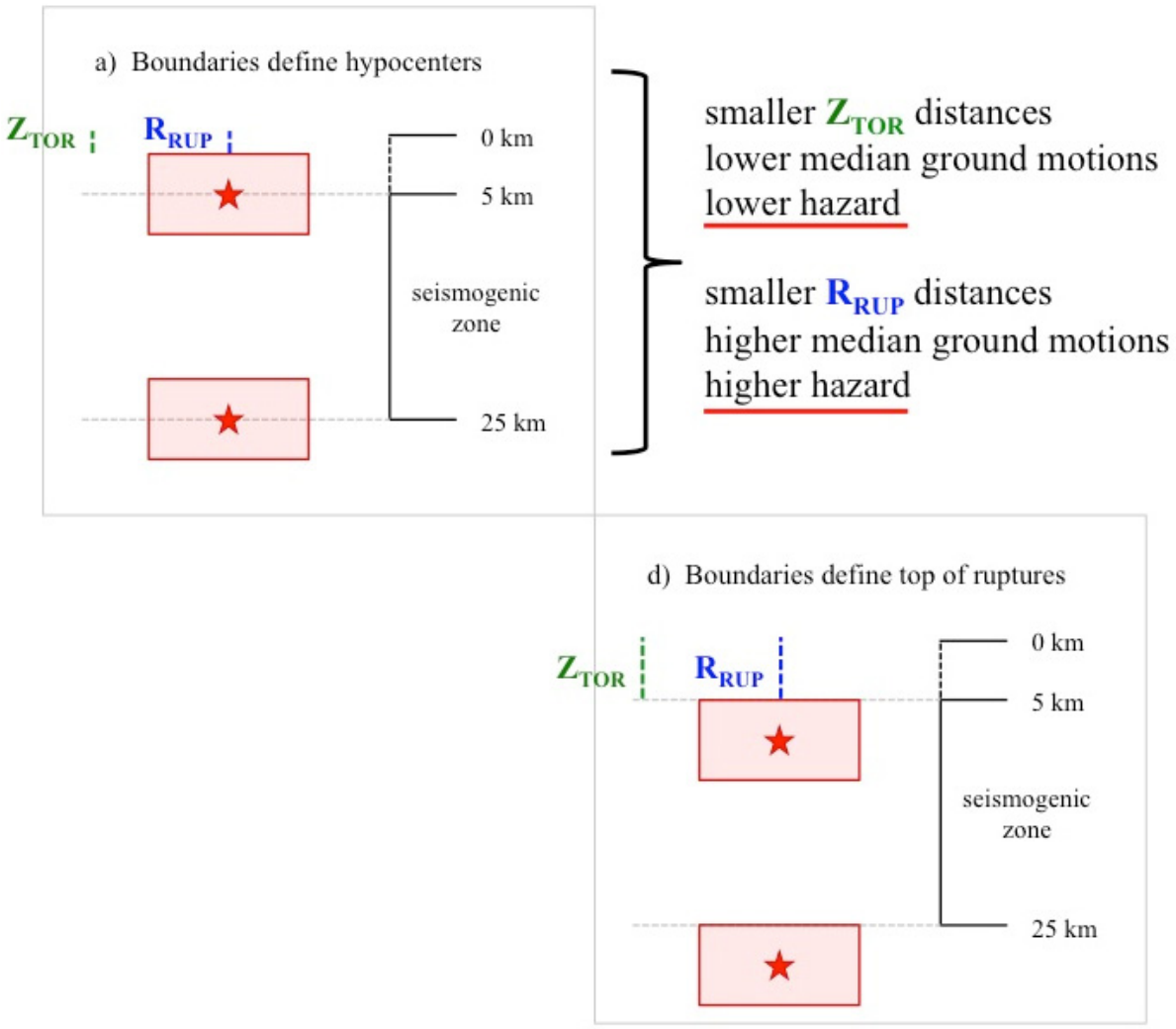

Figure 4.9 **Test 3.4: comparison of two approaches for modeling ruptures in an areal zone and their impact on hazard.**

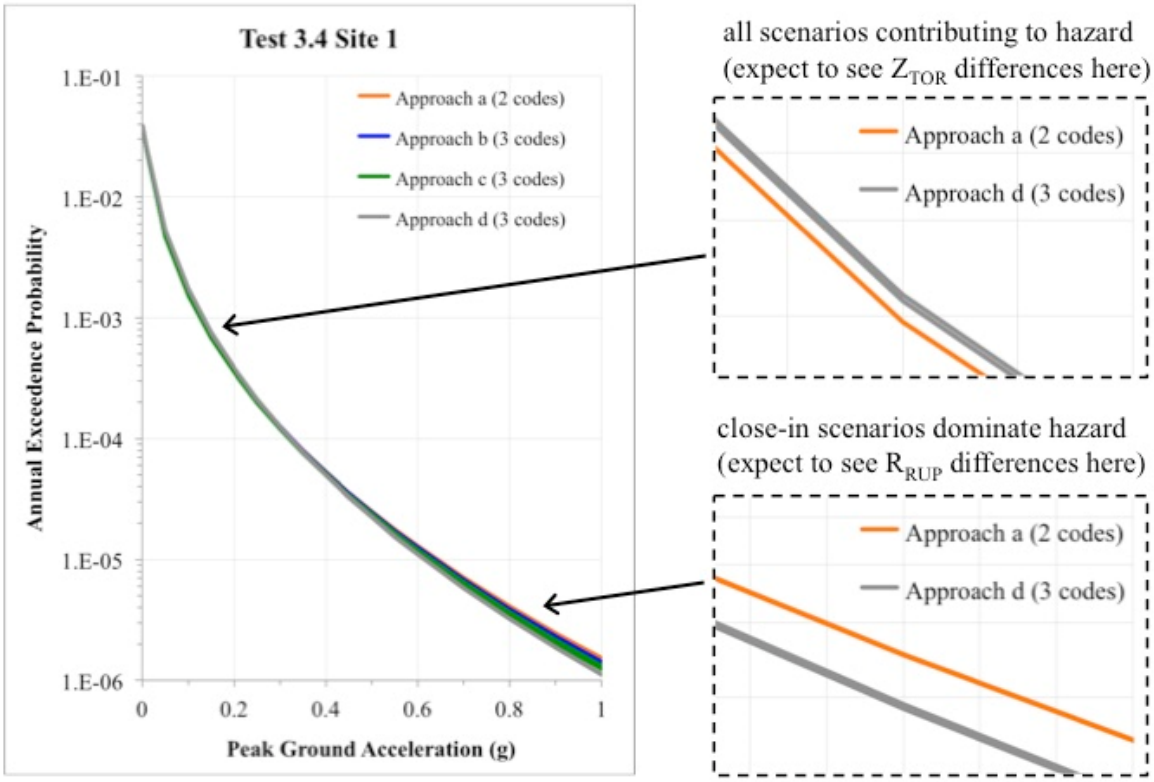

Figure 4.10 **Test 3.4: comparison of hazard results when different approaches are used to model the ruptures for the areal zone.**

5 Conclusions

5.1 SUMMARY AND CONCLUSIONS

The objective of the project was to create a set of tests with benchmark results that can be used to verify the primary functions of PSHA codes. Three sets of verification tests were developed during this project, and participants ran the tests on their own PSHA codes. A major accomplishment of the project is the close agreement in the final hazard results for the verification tests in Set 1 and Set 2. The reported benchmark answers are robust, and the narrow range in results from all codes indicates consistency across the practice for the fundamental PSHA code functions verified by these tests. The Set 1 and Set 2 final hazard results from all participating codes along with benchmark answers are available through the electronic supplement in Appendix D.

Though not as close as the results for Set 1 and 2, the final hazard results for the verification tests in Set 3 are also in good agreement when the hazard analysts use the same modeling approaches. Another key accomplishment of the project was the identification and understanding of several outstanding issues for source modeling approaches that led to significant differences in reported hazard for the tests in Set 3. The Set 3 final hazard results from all participating codes are also available through the electronic supplement in Appendix D.

As a result of the project, many PSHA codes were modified to correct programming errors, enhance existing functions, and add capabilities for more advanced source and ground-motion modeling. These improvements to the PSHA codes are a significant accomplishment of the project and benefit the earthquake engineering community by increasing consistency and improving the tools used in seismic hazard studies.

5.2 FUTURE WORK

With the goal of improving the tools used in seismic hazard analysis in mind, future verification efforts should aim at including all codes in use at the time, and expansion of the use of verification tests to include more functions of PSHA codes used in practice. One important topic for future verification tests is the incorporation of directivity models in PSHA codes. Future verification efforts should also include tests to verify implementation of additional magnitude density functions, such as the WAACY model [Wooddell et al. 2014] and event sets such as UCERF3 [Field et al. 2013]. Verification tests should be developed for ground-motion models that introduce new distance measures, such as the NGA-Subduction models currently under development. It will also be important to develop a verification test for the NGA-East ground-motion models, which

include median estimates published as look-up tables and site amplification estimates published as equations. It would be beneficial to develop a test requiring the codes to calculate hazard for multiple periods and include relevant specifications like period-dependent logic tree weights on the median ground-motion models (as in NGA-East). Finally, the authors recommend that future verification efforts include tests for sources with more complex geometries such as listric faults and non-continuous ruptures. These proposed future test topics offer a starting point and can be undertaken in the next verification project, pending necessary funding.

REFERENCES

Abrahamson N.A., Silva W.J., Kamai R. (2014). Summary of the ASK14 ground motion relation for active crustal regions, *Earthq. Spectra*, 30(3): 1025–1055.

Bazzurro P., Cornell C.A. (1999). Disaggregation of seismic hazard, *Bull. Seismol. Society Am.*, 89(2): 501–520.

Boore D.M., Stewart J.P., Seyhan E., Atkinson G.M. (2014). NGA-West2 equations for predicting PGA, PGV, and 5% damped PSA for shallow crustal earthquakes, *Earthq. Spectra*, 30(3): 1057–1085.

Campbell K.W., Bozorgnia Y. (2014). NGA-West2 ground motion model for the average horizontal components of PGA, PGV, and 5% damped linear acceleration response spectra, *Earthq. Spectra*, 30(3): 1087–1115.

Chiou B.S.-J., Youngs R.R. (2014). Update of the Chiou and Youngs NGA model for the average horizontal component of peak ground motion and response spectra, *Earthq. Spectra*, 30(3): 1117–1153.

Field E.H., Biasi G.P., Bird P., Dawson T.E., Felzer K.R., Jackson D.D., Johnson K.M., Jordan T.H., Madden C., Michael A.J., Milner K.R., Page M.T., Parsons T., Powers P.M., Shaw B.E., Thatcher W.R., Weldon R.J., II, Zeng, Y. (2013). Uniform California earthquake rupture forecast, version 3 (UCERF3)—The time-independent model: *U.S. Geological Survey Open-File Report 2013-1165*, 97 p., *California Geological Survey Special Report 228*, and *Southern California Earthquake Center Publication 1792*.

LaForge R., Hale C. (2017). Slab models for PSHA, *Seismol. Res. Lett.,* 87(2b): 672. Presented at 2017 Annual meeting of the Seismological Society of America.

Sadigh K., Chang C.–Y., Egan J.A., Makdisi F., Youngs R.R. (1997). Attenuation relationships for shallow crustal earthquakes based on California strong motion data, *Seismol. Res. Lett.*, 68(1): 180–189.

Spudich P., Chiou B. (2015). Strike-parallel and strike-normal coordinate system around geometrically complicated rupture traces—Use by NGA-West2 and further improvements, *U.S. Geological Survey, USGS Open-File Report 2015-1028*, Menlo Park, CA, 20 pgs.

Thomas P., Wong I., Abrahamson N. (2010). Verification of probabilistic seismic hazard analysis computer programs, *PEER Report No. 2010/106*, Pacific Earthquake Engineering Research Center, University of California, Berkeley, CA.

Weatherill G.A., Pagani M., Garcia J. (2017). Modelling in-slab subduction earthquakes in PSHA: current practice and challenges for the future, *Proceedings of the 16th World Conference on Earthquake Engineering*, Paper No. 1935, Santiago, Chile.

Wooddell K.E., Abrahamson N.A., Acevedo-Cabrera A.L., Youngs R.R. (2014). Hazard implementation of simplified seismic source characterization allowing for linked faults, *Seismol. Res. Lett.*, 85(2): 471.

Youngs R.R., Coppersmith K.J. (1985). Implications of fault slip rates and earthquake recurrence models to probabilistic seismic hazard estimates. *Bull. Seismol. Soc. Am.,* 75: 939–964.

Zhao J.X., Zhang J., Asano A., Ohno Y., Oouchi T., Takahashi T., Ogawa H., Irikura K., Thio H.K., Somerville P.G., Fukushima Y., Fukushima Y. (2006). Attenuation relations of strong ground motion in Japan using site classification based on predominant period, *Bull. Seismol. Society Am.*, 96(3): 898–913.

APPENDIX A SET 1 INSTRUCTIONS

GENERAL INSTRUCTIONS

- Provide mean hazard results (probability of exceedance) for peak horizontal acceleration (PGA) defined at 0.001, 0.01, 0.05, 0.1, 0.15, 0.2, 0.25, 0.3, 0.35, 0.4, 0.45, 0.5, 0.55, 0.6, 0.7, 0.8, 0.9, and 1.0g.
- Assume a Poisson model when converting rates to annual probabilities of exceedance
- Use 16.05 (not 16.1) in the equation logMo = 16.05 + 1.5M
- Use μ = 3×1011 dyne/cm2
- Use a magnitude integration step size small enough to define the specified magnitude density function. The bin size for magnitude integration should be defined such that Mmin is at the lower edge of a bin, not in the center (i.e., if your magnitude step size is 0.01, one magnitude bin should be from M 5.0 to 5.01)
- When integrating over the magnitude density function, integrate from zero (not M_{min})
- Use uniform slip with tapered edges. Down dip and along-strike integration step size should be small enough to produce uniform rupture location. Do not allow rupture off the ends of the fault.
- Maintain the aspect ratio defined until maximum width is reached, then increase length (conservation of area at the expense of aspect ratio)
- Sigma = 0 for the ground-motion model implies that the sigma in the relationship is artificially set to zero, not that the sigma is truncated
- Rupture dimension relationships:

  $$\text{Log (A)} = M - 4 \quad \text{(A.1)}$$

  $$\text{Log (W)} = 0.5*M - 2.15 \quad \text{(A.2)}$$

  $$\text{Log (L)} = 0.5*M - 1.85 \quad \text{(A.3)}$$

  The above equations are equivalent to an aspect ratio of 2

- You should be using as small a step size as feasible/necessary to produce stable results. This may be much smaller than you normally use on projects.

- For cases where you are asked to truncate the ground-motion sigma (Tests 1.8b and 1.8c), you should be renormalizing the pdf so that the probabilities for ground motion sum to 1.

Table A.1 Set 1 test instructions.

Name	Description	Source	Mag-density function	Ground-motion model	Rupture dimension relationship
Test 1.1	Rate calculation	Fault 1 Strike slip 90° Slip rate = 2 mm/yr	Delta Function at M 6.5	Sadigh et al (1997), rock $\sigma = 0$	Eq. A1, A2, A3 $\sigma_A = 0$, $\sigma_W = 0$, $\sigma_L = 0$
Test 1.2	Rupture location variability	Fault 1 Strike slip 90° Slip rate = 2 mm/yr	Delta Function at M 6.0	Sadigh et al (1997), rock $\sigma = 0$	Eq. A1, A2, A3 $\sigma_A = 0$, $\sigma_W = 0$, $\sigma_L = 0$
Test 1.3	Rupture area variability	Fault 1 Strike slip 90° Slip rate = 2 mm/yr	Delta Function at M 6.0	Sadigh et al (1997), rock σ = 0	Eq. A1, $\sigma_A = 0.25$ truncate 2σ Aspect Ratio = 2
Test 1.4	Dipping fault	Fault 2 Reverse 60° Slip rate = 2 mm/yr	Delta Function at M 6.0	Sadigh et al (1997), rock $\sigma = 0$	Eq. A1, A2, A3 $\sigma_A = 0$, $\sigma_W = 0$, $\sigma_L = 0$
Test 1.5	Truncated exponential magnitude pdf	Fault 1 Strike slip 90° Slip rate = 2 mm/yr	Truncated exponential *b*-value = 0.9 $M_{min} = 5$ $M_{max} = 6.5$	Sadigh et al. (1997), rock $\sigma = 0$	Eq. A1, A2, A3 $\sigma_A = 0$, $\sigma_W = 0$, $\sigma_L = 0$
Test 1.6	Truncated normal magnitude pdf	Fault 1 Strike slip 90° Slip rate = 2 mm/yr	Truncated normal $M_{min} = 5$ $M_{char} = 6.2$ $M_{max} = 6.5$ $\sigma = 0.25$	Sadigh et al. [1997], rock $\sigma = 0$	Eq. A1, A2, A3 $\sigma_A = 0$, $\sigma_W = 0$, $\sigma_L = 0$
Test 1.7	Youngs and Coppersmith magnitude pdf	Fault 1 Strike slip 90° Slip rate = 2 mm/yr	Y&C *b*-value = 0.9 $M_{min} = 5$ $M_{char} = 6.2$ $M_{max} = 6.45$	Sadigh et al (1997), rock σ = 0	Eq. A1, A2, A3 $\sigma_A = 0$, $\sigma_W = 0$, $\sigma_L = 0$
Test 1.8a	Ground-motion variability, untruncated	Fault 1 Strike slip 90° Slip rate = 2 mm/yr	Delta Function at M 6.0	Sadigh et al. [1997], rock σ untruncated	Eq. A1, A2, A3 $\sigma_A = 0$, $\sigma_W = 0$, $\sigma_L = 0$
Test 1.8b	Ground-motion variability, truncate 2σ	Fault 1 Strike slip 90° Slip rate = 2 mm/yr	Delta Function at M 6.0	Sadigh et al. [1997], rock, truncate 2σ	Eq. A1, A2, A3 $\sigma_A = 0$, $\sigma_W = 0$, $\sigma_L = 0$
Test 1.8c	Ground-motion variability, truncate 3σ	Fault 1 Strike slip 90° Slip rate = 2 mm/yr	Delta Function at M 6.0	Sadigh et al. [1997], rock truncate 3σ	Eq. A1, A2, A3 $\sigma_A = 0$, $\sigma_W = 0$, $\sigma_L = 0$
~~Test 1.9~~					
Test 1.10	Areal zone with point sources, single depth	Area 1 $N(M \geq 5) = 0.0395$	Truncated exponential *b*-value = 0.9 $M_{min} = 5$ $M_{max} = 6.5$	Sadigh et al [1997], rock σ untruncated	Point sources with recommended grid spacing of 0.5 km to simulate uniform distribution

Table A.1 Set 1 Test Instructions (continued).

Name	Description	Source	Mag-Density Function	Ground-Motion Model	Rupture Dimension Relationship
Test 1.11	Areal zone with point sources, depth range	Area 1 $N(M \geq 5) = 0.0395$	Truncated exponential b-value = 0.9 $M_{min} = 5$ $M_{max} = 6.5$	Sadigh et al. [1997], rock, σ untruncated	Point sources with recommended grid spacing of 0.5 km to simulate uniform distribution. For the depth distribution use 1 km spacing, inclusive of 5 and 10 km.
~~Test 1.12~~					

Table A.2 Tests 1.1 – 1.8: coordinates for Fault 1 and Fault 2.

Latitude	Longitude	Comment
38.00000	-122.000	South end of fault
38.22480	-122.000	North end of fault

Table A.3 Tests 1.1 – 1.8: coordinates for Sites 1–7.

Site	Latitude	Longitude	Comment
1	38.113	-122.000	On fault, at midpoint along strike
2	38.113	-122.114	10 km west of fault, at midpoint along strike
3	38.111	-122.570	50 km west of fault, at midpoint along strike
4	38.000	-122.000	On fault, at southern end
5	37.910	-122.000	10 km south of fault along strike
6	38.2248	-122.000	On fault, at northern end
7	38.113	-121.886	10 km east of fault, at midpoint along strike

Table A.4 Tests 1.10 and 1.11: coordinates for Area 1.

Point	Latitude	Longitude
1	38.901	-122.000
2	38.899	-121.920
3	38.892	-121.840
4	38.881	-121.760
5	38.866	-121.682
6	38.846	-121.606
7	38.822	-121.532
8	38.794	-121.460
9	38.762	-121.390
10	38.727	-121.324
11	38.688	-121.261
12	38.645	-121.202
13	38.600	-121.147
14	38.551	-121.096
15	38.500	-121.050
16	38.446	-121.008
17	38.390	-120.971
18	38.333	-120.940
19	38.273	-120.913
20	38.213	-120.892
21	38.151	-120.876
22	38.089	-120.866
23	38.026	-120.862
24	37.963	-120.863
25	37.900	-120.869
26	37.838	-120.881
27	37.777	-120.899
28	37.717	-120.921
29	37.658	-120.949
30	37.601	-120.982
31	37.545	-121.020
32	37.492	-121.063

Point	Latitude	Longitude
33	37.442	-121.110
34	37.394	-121.161
35	37.349	-121.216
36	37.308	-121.275
37	37.269	-121.337
38	37.234	-121.403
39	37.203	-121.471
40	37.176	-121.542
41	37.153	-121.615
42	37.133	-121.690
43	37.118	-121.766
44	37.108	-121.843
45	37.101	-121.922
46	37.099	-122.000
47	37.101	-122.078
48	37.108	-122.157
49	37.118	-122.234
50	37.133	-122.310
51	37.153	-122.385
52	37.176	-122.458
53	37.203	-122.529
54	37.234	-122.597
55	37.269	-122.663
56	37.308	-122.725
57	37.349	-122.784
58	37.394	-122.839
59	37.442	-122.890
60	37.492	-122.937
61	37.545	-122.980
62	37.601	-123.018
63	37.658	-123.051
64	37.717	-123.079

Table A.4 Tests 1.10 and 1.11: coordinates for Area 1 (continued).

Point	Latitude	Longitude
65	37.777	-123.101
66	37.838	-123.119
67	37.900	-123.131
68	37.963	-123.137
69	38.026	-123.138
70	38.089	-123.134
71	38.151	-123.124
72	38.213	-123.108
73	38.273	-123.087
74	38.333	-123.060
75	38.390	-123.029
76	38.446	-122.992
77	38.500	-122.950
78	38.551	-122.904
79	38.600	-122.853
80	38.645	-122.798
81	38.688	-122.739
82	38.727	-122.676
83	38.762	-122.610
84	38.794	-122.540
85	38.822	-122.468
86	38.846	-122.394
87	38.866	-122.318
88	38.881	-122.240
89	38.892	-122.160
90	38.899	-122.080

Table A.5 Tests 1.10 and 1.11: coordinates for Sites 1–4.

Site	Latitude	Longitude	Comment
1	38.000	-122.000	At center of area
2	37.550	-122.000	50 km from center (radially)
3	37.099	-122.000	On area boundary
4	36.874	-122.000	25 km from boundary

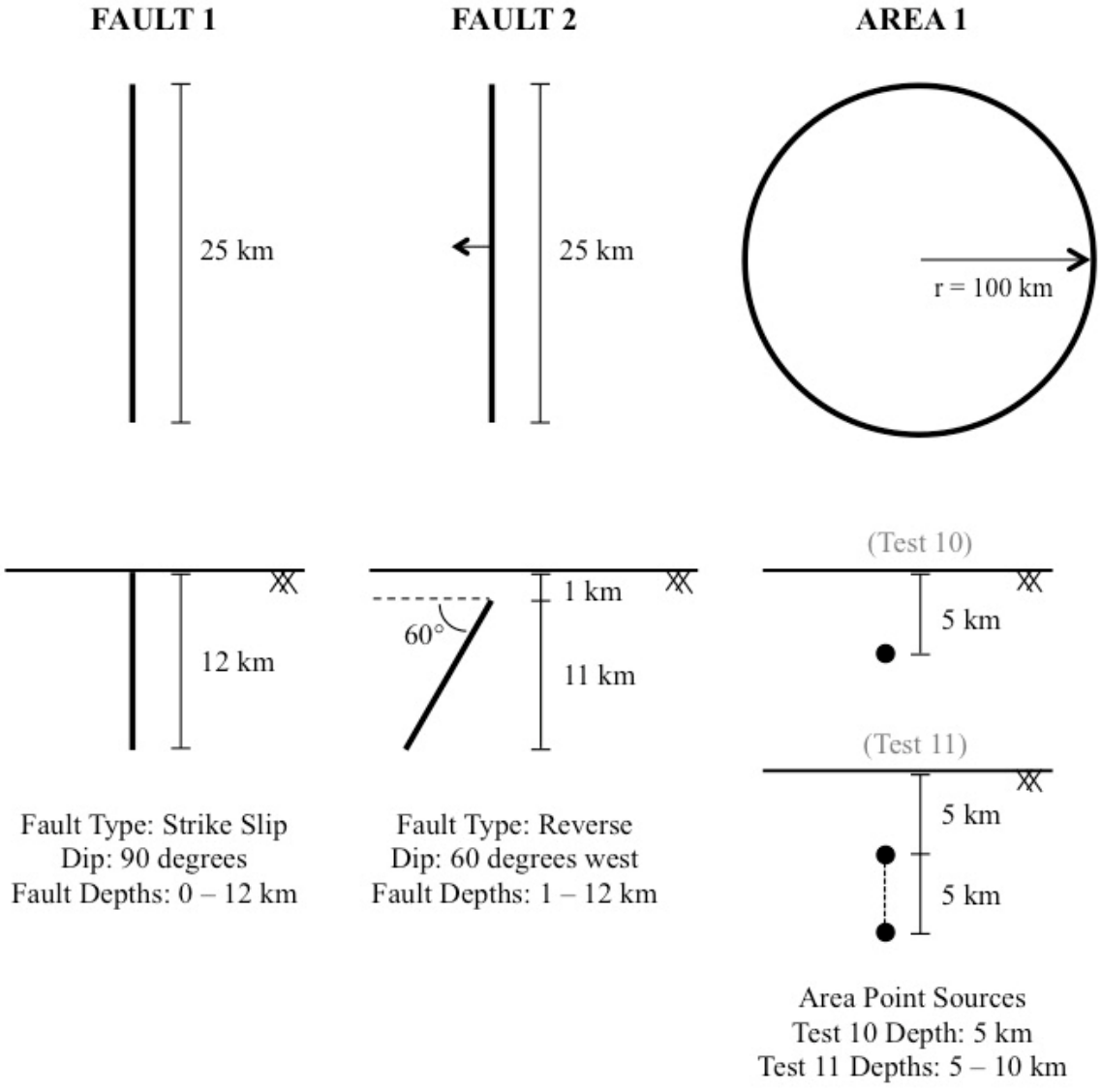

Figure A.1 Illustrations and dimensions of sources for Set 1 tests.

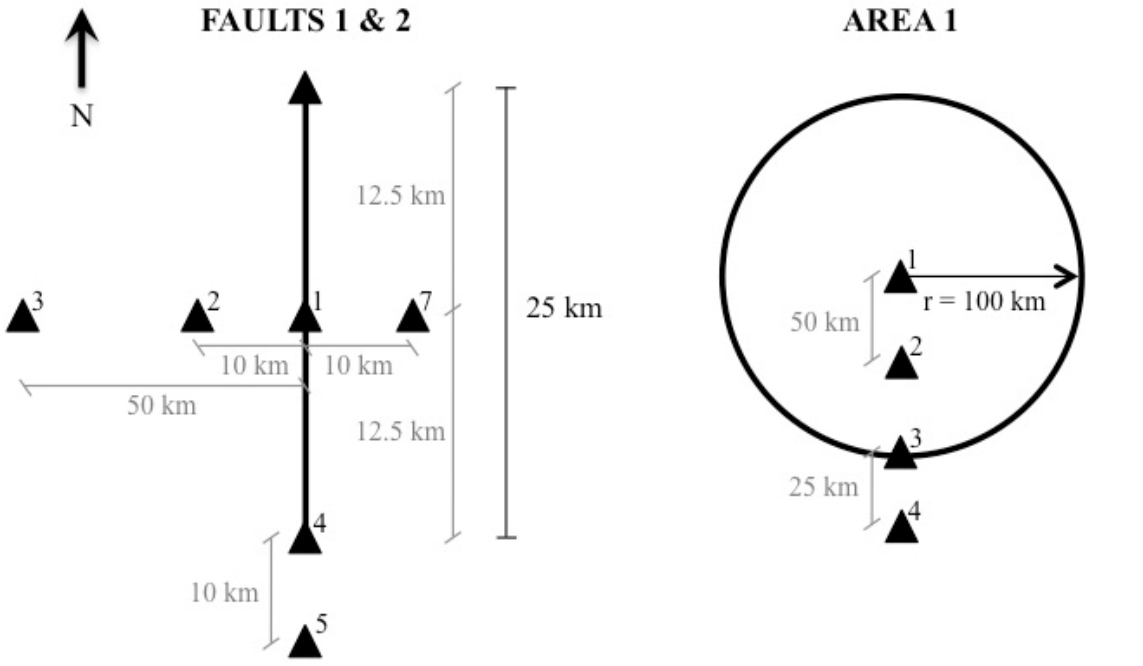

Site 1: On fault, at midpoint along strike
Site 2: 10 km west of fault, at midpoint along strike
Site 3: 50 km west of fault, at midpoint along strike
Site 4: On fault, at southern end
Site 5: 10 km south of fault along strike
Site 6: On fault, northern end
Site 7: 10 km east of fault, at midpoint along strike

Site 1: At center of area
Site 2: 50 km from center (radially)
Site 3: On area boundary
Site 4: 25 km from boundary

Figure A.2 Illustrations and dimensions of sites for Set 1 tests.

APPENDIX B SET 2 INSTRUCTIONS

General instructions are the same as Set 1.

TEST 2.1 INSTRUCTIONS

Description: Calculate the hazard for Site 1 shown in Figure B.1 due to Area 2, Fault B, and Fault C. See Tables B.1–B.4 for source and site coordinates.

Area 2

Geometry: circle with r = 100 km, seismogenic zone is from 5–10 km

Rupture dimension relationships: use point sources with recommended grid spacing of 1 km to simulate uniform distribution, for depth distribution use 1 km spacing inclusive of 5 and 10 km

Activity: $N(\mathbf{M} \geq 5) = 0.0395$ eq/yr

Mag-Density Function: truncated exponential, b-value = 0.9, M_{min} = 5, M_{max} = 6.5

Fault B

Geometry: length 85 km, fault plane depths 0–12 km, strike-slip, dip 90°

Activity: slip rate 2 mm/yr

Mag-Density Function: Y&C, b-value = 0.9, M_{min} = 5, M_{char} = 6.75, M_{max} = 7

Fault C

Geometry: length 50 km, fault plane depths 0–12 km, strike-slip, dip 90°

Activity: slip rate 1 mm/yr

Mag-Density Function: Y&C, b-value = 0.9, M_{min} = 5, M_{char} = 6.5, M_{max} = 6.75

Rupture dimension relationships for Fault B and Fault C

Log (A) = M – 4 $\quad \sigma_A = 0$

Log (W) = 0.5*M – 2.15 $\quad \sigma_W = 0$

Log (L) = 0.5*M – 1.85 $\quad \sigma_L = 0$

The above equations are equivalent to an aspect ratio of 2

Uniform distribution along strike and down dip

Ground-motion model for all sources: Sadigh et al. [1997], rock, σ untruncated

Deaggregation: Provide deaggregation results for the following three PGA values at Site 1:

PGA 0.05*g*

The PGA corresponding to a hazard of 0.001

PGA 0.35*g*

Tables: Provide a table for each PGA with distance (R_{RUP}), magnitude, and epsilon* bins. Distance bins should each be 20 km, starting at 0 km and ending at 100 km, with an extra bin for > 100 km. Magnitude bins should each be 0.1 M, starting at M 5.0 and ending at M 7.0. Epsilon* bins should be defined as <-1, -1 to 0, 0 to 1, 1 to 2, >2. This results in 6 distance bins, 20 magnitude bins, and 5 epsilon* bins. See Table B.5 for the expected deaggregation tables.

Means: Provide the mean M, R_{RUP}, and ε* for each PGA at Site 1. A more detailed explanation on epsilon* and deaggregation mean values follows the tables and figures for this test.

Table B.1 Test 2.1: coordinates for Fault B.

Latitude	Longitude	Comment
0.44966	-65.38222	West end of fault
0.44966	-64.61778	East end of fault

Table B.2 Test 2.1: coordinates for Fault C.

Latitude	Longitude	Comment
-0.22483	-65.22484	West end of fault
-0.22483	-64.77516	East end of fault

Table B.3 Test 2.1: coordinates for Site 1.

Site	Latitude	Longitude	Comment
1	0.00000	-65.00000	In center of area source

Table B.4 Test 2.1: coordinates for Area 2.

Point	Latitude	Longitude
0	0.8993	-65.0000
1	0.8971	-64.9373
2	0.8906	-64.8748
3	0.8797	-64.8130
4	0.8645	-64.7521
5	0.8451	-64.6924
6	0.8216	-64.6342
7	0.7940	-64.5778
8	0.7627	-64.5234
9	0.7276	-64.4714
10	0.6899	-64.4219
11	0.6469	-64.3753
12	0.6017	-64.3316
13	0.5537	-64.2913
14	0.5029	-64.2544
15	0.4496	-64.2211
16	0.3942	-64.1917
17	0.3369	-64.1662
18	0.2779	-64.1447
19	0.2176	-64.1274
20	0.1562	-64.1143
21	0.0940	-64.1056
22	0.0314	-64.1012
23	-0.0314	-64.1012
24	-0.0940	-64.1056
25	-0.1562	-64.1143
26	-0.2176	-64.1274
27	-0.2779	-64.1447
28	-0.3369	-64.1662
29	-0.3942	-64.1917
30	-0.4496	-64.2211
31	-0.5029	-64.2544
32	-0.5537	-64.2913
33	-0.6017	-64.3316
34	-0.6469	-64.3753
35	-0.6889	-64.4219
36	-0.7276	-64.4714
37	-0.7627	-64.5234
38	-0.7940	-64.5778
39	-0.8216	-64.6342
40	-0.8451	-64.6924
41	-0.8645	-64.7521
42	-0.8797	-64.8130
43	-0.8906	-64.8748
44	-0.8971	-64.9373
45	-0.8993	-65.0000
46	-0.8971	-65.0627
47	-0.8906	-65.1252
48	-0.8797	-65.1870
49	-0.8645	-65.2479
50	-0.8451	-65.3076
51	-0.8216	-65.3658
52	-0.7940	-65.4222
53	-0.7627	-65.4766
54	-0.7276	-65.5286
55	-0.6889	-65.5781
56	-0.6469	-65.6247
57	-0.6017	-65.6684
58	-0.5537	-65.7087
59	-0.5029	-65.7456
60	-0.4496	-65.7789
61	-0.3942	-65.8083
62	-0.3369	-65.8338
63	-0.2779	-65.8553
64	-0.2176	-65.8726
65	-0.1562	-65.8857

Table B.4 Test 2.1: coordinates for Area 2 (continued).

Point	Latitude	Longitude
66	-0.0940	-65.8944
67	-0.0314	-65.8988
68	0.0314	-65.8988
69	0.0940	-65.8944
70	0.1562	-65.8857
71	0.2176	-65.8726
72	0.2779	-65.8553
73	0.3369	-65.8338
74	0.3942	-65.8083
75	0.4496	-65.7789
76	0.5029	-65.7456
77	0.5537	-65.7087
78	0.6017	-65.6684
79	0.6469	-65.6247
80	0.6889	-65.5781
81	0.7276	-65.5286
82	0.7627	-65.4766
83	0.7940	-65.4222
84	0.8216	-65.3658
85	0.8451	-65.3076
86	0.8645	-65.2479
87	0.8797	-65.1870
88	0.8906	-65.1252
89	0.8971	-65.0627
90	0.8993	-65.0000

Table B.5 Test 2.1: deaggregation tables.

Distance (km)	Magnitude	Epsilon*	Deaggregation results
0 – 20	5.0 – 5.1	< -1	
20 – 40	5.0 – 5.1	< -1	
↓	5.0 – 5.1	< -1	
80 – 100	5.0 – 5.1	< -1	
> 100	5.0 – 5.1	< -1	
0 – 20	5.1 – 5.2	< -1	
20 – 40	5.1 – 5.2	< -1	
↓	5.1 – 5.2	< -1	
80 – 100	5.1 – 5.2	< -1	
> 100	5.1 – 5.2	< -1	
	↓		
	6.9 – 7.0	< -1	
		↓	
		> 2	

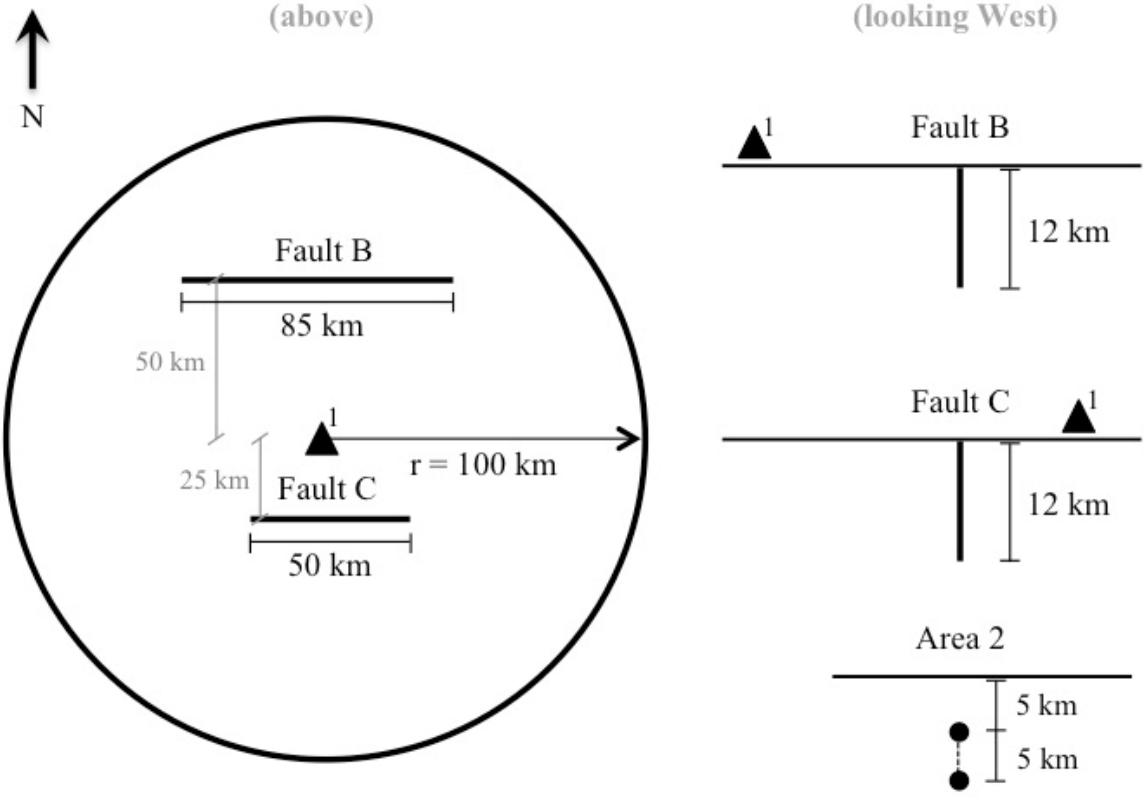

Figure B.1 Test 2.1: illustrations and dimensions of sources and site.

TEST 2.1 EXPLANATION: EPSILON* AND DEAGGREGATION MEANS

Epsilon*

The epsilon corresponding to a particular ground motion would just be epsilon, but in PSHA we calculate the probability of EXCEEDING a particular ground motion. Therefore, the epsilon (which we've denoted epsilon*) actually corresponds to any ground motion greater than the ground motion specified and can be thought of as the minimum epsilon needed to exceed that ground motion, as illustrated in Figure B.2.

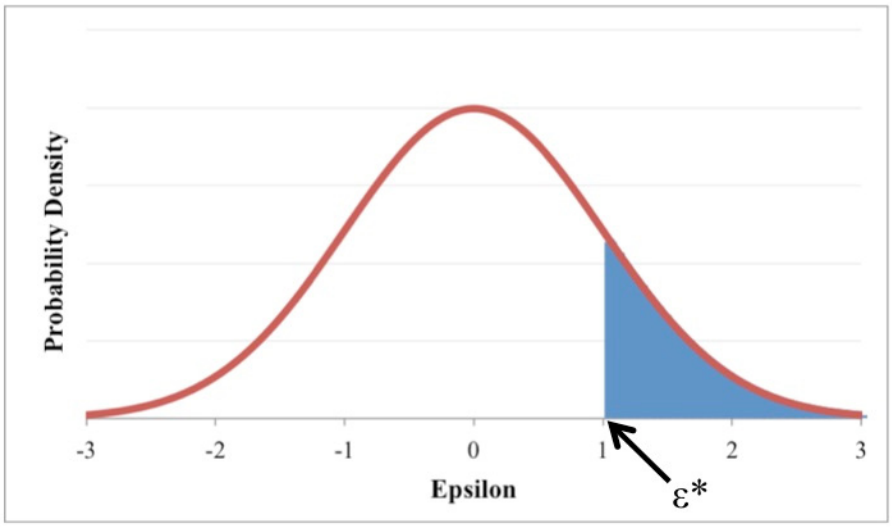

Figure B.2 **Illustration of ε^* (epsilon star), the minimum epsilon needed to exceed a ground motion.**

Mean deaggregaton values

Starting with the typical equation for a seismic hazard analysis, the total annual rate of events, v, with spectral accelerations, Sa, that exceed a specified value, z, is given by:

$$v(Sa > z) = \sum_{i=1}^{N_{source}} N_i(M_{\min}) \int_{r=0}^{\infty} \int_{m=M_{\min}}^{M_{\max}} f_{m_i}(m) f_{r_i}(r) P(Sa > z | m, r) \, dr \, dm$$

where N_i (M_{min}) is the annual rate of earthquakes with magnitude greater than or equal to M_{min}, r is the distance from the source to the site, m is earthquake magnitude, $f_m(m)$ and $f_r(r)$ are probability density functions for magnitude and distance, and $P(Sa>z|m,r)$ is the conditional probability of observing a spectral acceleration, Sa, greater than z for a given earthquake magnitude and distance.

The mean magnitude and mean distance values are the weighted averages with the weights given by the deaggregation. More specifically, the mean is the conditional mean given the exceedance of the specified ground motion. The equation for the mean magnitude is given by multiplying the magnitude inside the hazard integral (in other words multiplying the magnitude by the marginal hazard). Likewise, the equation for the mean distance is given by multiplying the distance inside the hazard integral:

$$\bar{M} = \frac{\sum_{i=1}^{N_{source}} N_i\left(M_{\min}\right) \int_{r=0}^{\infty} \int_{m=M_{\min}}^{M_{\max}} M\, f_{m_i}\left(m\right) f_{r_i}(r) P\left(Sa > z \middle| m, r\right) dr\, dm}{v\left(Sa > z\right)}$$

$$\bar{R} = \frac{\sum_{i=1}^{N_{source}} N_i\left(M_{\min}\right) \int_{r=0}^{\infty} \int_{m=M_{\min}}^{M_{\max}} R\, f_{m_i}\left(m\right) f_{r_i}(r) P\left(Sa > z \middle| m, r\right) dr\, dm}{v\left(Sa > z\right)}$$

The mean epsilon* is computed in exactly the same way, but for clarity, let's first rewrite the seismic hazard equation to replace the $P(Sa>z|m,r)$ term with an equation that explicitly shows ε^*:

$$P\left(Sa > z \middle| m, r\right) = 1 - \Phi(\varepsilon^*)$$

$$v\left(Sa > z\right) = \sum_{i=1}^{N_{source}} N_i\left(M_{\min}\right) \int_{r=0}^{\infty} \int_{m=M_{\min}}^{M_{\max}} f_{m_i}\left(m\right) f_{r_i}(r)[1 - \Phi(\varepsilon^*)] dr\, dm$$

where $\Phi(\ )$ is the standard normal cumulative distribution function, and ε^* is computed by:

$$\varepsilon^* = \frac{\ln z - \overline{\ln Sa}}{\sigma_{\ln Sa}}$$

Now the equation for the mean epsilon* is given by multiplying the epsilon* inside the hazard integral:

$$\overline{\varepsilon^*} = \frac{\sum_{i=1}^{N_{source}} N_i\left(M_{\min}\right) \int_{r=0}^{\infty} \int_{m=M_{\min}}^{M_{\max}} \varepsilon^* f_{m_i}\left(m\right) f_{r_i}(r)[1 - \Phi(\varepsilon^*)] dr\, dm}{v\left(Sa > z\right)}$$

TEST 2.2 INSTRUCTIONS

Description: Calculate the hazard for the six sites shown in Figure B.3 due to Fault 3 using the specified NGA-West2 ground-motion models. See Tables B.6 and B.7 for source and site coordinates.

Fault 3

Geometry: length 85 km, fault plane depths 0–12 km, strike–slip, dip 90°

Activity: slip rate 2 mm/yr

Mag-Density Function: truncated exponential, b-value = 0.9, M_{min} = 5, M_{max} = 7

Rupture dimension relationships

Log (A) = M – 4 $\sigma_A = 0$

Log (W) = 0.5*M – 2.15 $\sigma_W = 0$

Log (L) = 0.5*M – 1.85 $\sigma_L = 0$

The above equations are equivalent to an aspect ratio of 2

Uniform distribution along strike and down dip

Use a hypocenter depth location in the geometric center of the rupture plane

Ground-motion models

a. Abrahamson, Silva, and Kamai [2014], σ untruncated

b. Boore, Stewart, Seyhan, and Atkinson [2014], σ untruncated

c. Campbell and Bozorgnia [2014], σ untruncated

d. Chiou and Youngs [2014], σ untruncated

Damping ratio = 5%

V_{S30} = 760 m/sec

V_{S30} is measured

$Z_{1.0}$ = 0.048 km

$Z_{2.5}$ = 0.607 km

Region = California

Table B.6 Test 2.2: coordinates for Fault 3.

Latitude	Longitude	Comment
0.38221	-65.00000	North end of fault
-0.38221	-65.00000	South end of fault

Table B.7 Test 2.2: coordinates for Sites 1–6.

Site	Latitude	Longitude	Comment
1	0.00000	-64.91005	10 km east of fault, at midpoint along strike
2	0.00000	-65.04497	5 km west of fault, at midpoint along strike
3	0.00000	-65.08995	10 km west of fault, at midpoint along strike
4	0.00000	-65.13490	15 km west of fault, at midpoint along strike
5	0.00000	-65.22483	25 km west of fault, at midpoint along strike
6	-0.42718	-65.00900	5 km south of southern end, 1 km west

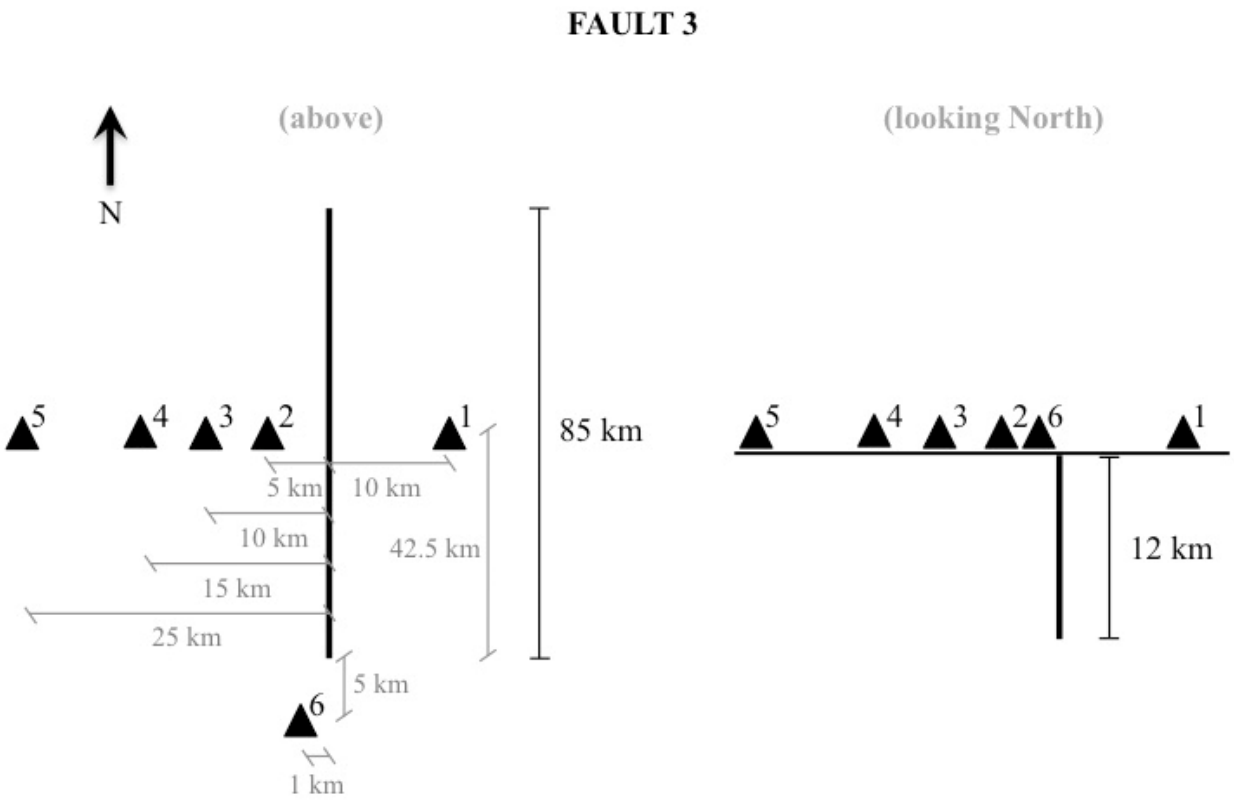

Figure B.3 Test 2.2: illustrations and dimensions of source and sites.

TEST 2.3 INSTRUCTIONS

Description: Calculate the hazard for the six sites shown in Figure B.4 due to a single-magnitude event on Fault 4 using the specified NGA-West2 ground-motion models. See Tables B.8 and B.9 for source and site coordinates.

Fault 4

Geometry: length 85 km, fault plane depths 1–12 km, reverse, dip 45°

Activity: slip rate 2 mm/yr

Mag-Density Function: delta function at M 7

Rupture dimension relationships

Log (A) = M – 4 $\sigma_A = 0$

Log (W) = 0.5*M – 2.15 $\sigma_W = 0$

Log (L) = 0.5*M – 1.85 $\sigma_L = 0$

The above equations are equivalent to an aspect ratio of 2

Uniform distribution along strike and down dip

Use a hypocenter depth location in the geometric center of the rupture plane

Ground-motion models

a. Abrahamson, Silva, and Kamai [2014], $\sigma = 0$

b. Boore, Stewart, Seyhan, and Atkinson [2014], $\sigma = 0$

c. Campbell and Bozorgnia [2014], $\sigma = 0$

d. Chiou and Youngs [2014], $\sigma = 0$

Damping ratio = 5%

V_{S30} = 760 m/sec

V_{S30} is measured

$Z_{1.0}$ = 0.048 km

$Z_{2.5}$ = 0.607 km

Region = California

Table B.8 Test 2.3: coordinates for Fault 4.

Latitude	Longitude	Comment
0.38221	-65.00000	North end of fault
-0.38221	-65.00000	South end of fault

Table B.9 Test 2.3: coordinates for Sites 1–6.

Site	Latitude	Longitude	Comment
1	0.00000	-64.91005	10 km east of fault, at midpoint along strike (FW)
2	0.00000	-65.04497	5 km west of fault, at midpoint along strike (HW)
3	0.00000	-65.08995	10 km west of fault, at midpoint along strike (HW)
4	0.00000	-65.13490	15 km west of fault, at midpoint along strike (HW)
5	0.00000	-65.22483	25 km west of fault, at midpoint along strike (HW)
6	-0.42718	-65.00900	5 km south of southern end, 1 km west (HW side)

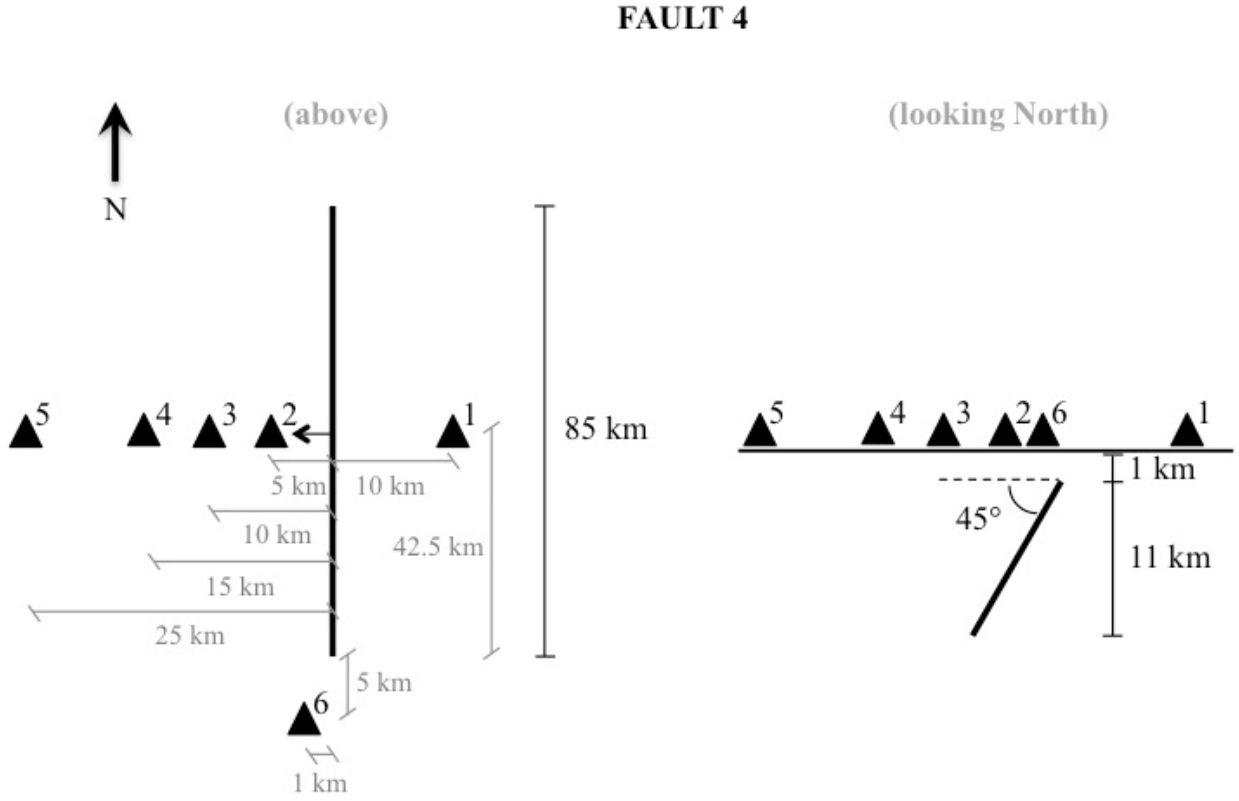

Figure B.4 Test 2.3: illustrations and dimensions of source and sites.

TEST 2.4 INSTRUCTIONS

a. Uniform Distribution Down Dip

Description: Calculate the hazard for the site shown in Figure B.5 due to a single-magnitude event on Fault 5 using the specified NGA-West2 ground-motion models. The purpose of this test is to have a comparison for the triangular distribution in part b. See Tables B.10 and B.11 for source and site coordinates.

Fault 5

Geometry: length 25 km, fault plane depths 0–30 km, strike-slip, dip 90°

Activity: slip rate 2 mm/yr

Mag-Density Function: delta function at M 6

Rupture dimension relationships

Log (A) = M – 4	$\sigma_A = 0$
Log (W) = 0.5*M – 2.15	$\sigma_W = 0$
Log (L) = 0.5*M – 1.85	$\sigma_L = 0$

The above equations are equivalent to an aspect ratio of 2

Uniform distribution along strike and down dip

Use a hypocenter depth location in the geometric center of the rupture plane

Ground-motion model: Chiou and Youngs [2014], σ = 0

Damping ratio = 5%

V_{S30} = 760 m/sec

V_{S30} is measured

$Z_{1.0}$ = 0.048 km

$Z_{2.5}$ = 0.607 km

Region = California

b. Triangular Distribution of Hypocenter Locations Down Dip

Description: Use the same specifications above, but replace the uniform distribution down dip with a triangular distribution of hypocenter locations down dip. The depths that define the triangular probability density function are 0 km, 10 km, and 30 km. A more detailed explanation on triangular depth distributions follows the tables and figures for this test.

Table B.10 Test 2.4: coordinates for Fault 5.

Latitude	Longitude	Comment
0.11240	-65.00000	North end of fault
-0.11240	-65.00000	South end of fault

Table B.11 Test 2.4: coordinates for Site 1.

Site	Latitude	Longitude	Comment
1	0.00000	-65.00900	1 km west of fault, at midpoint along strike

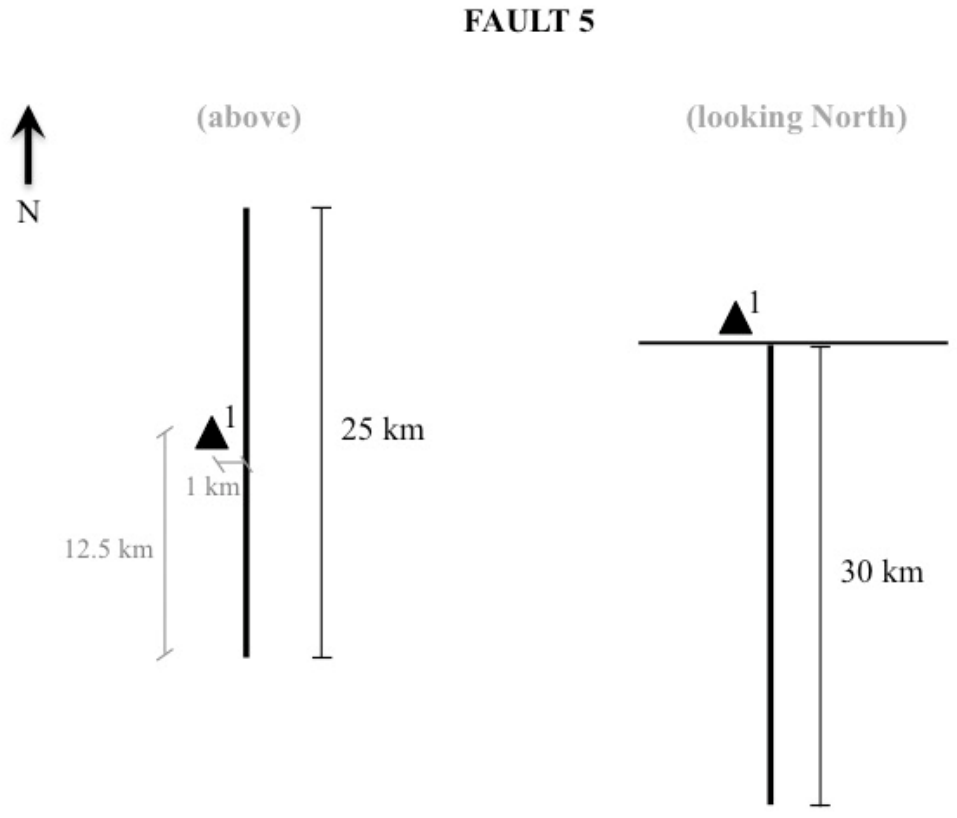

Figure B.5 Test 2.4: illustrations and dimensions of source and site.

TEST 2.4 EXPLANATION: TRIANGULAR DISTRIBUTION OF HYPOCENTER LOCATIONS DOWN DIP

The location of the rupture plane on the fault in the down dip direction is based on hypocenter observations. When source-characterization experts specify a triangular distribution, they are basing that on hypocenter locations on the fault plane. Therefore, it is not simply the rupture plane that follows the triangular distribution but specifically the hypocenter location on the rupture plane.

The distribution of the hypocenters down dip is specified as a triangle with z coordinates of 0, 10, and 30 km. The area of the triangle, which is a probability density function, must equal 1. With the given depth specifications, the probability density associated with the peak of the triangle, denoted here as y_2, is 0.0667. The triangular depth distribution of hypocenters with these specifications is illustrated in Figure B.6 in planar view.

The location of the hypocenter on the rupture plane itself can be modeled with a probability density function. For simplicity, this distribution is modeled as a delta function, with the hypocenter location always in the center of the rupture plane or at one half the rupture plane width. To sample the possible down-dip locations of the rupture on the fault, the rupture plane is moved down the dip of the fault. As ruptures are not allowed to go into the air, the first rupture plane's top edge is at a depth of zero, and i's hypocenter is at a depth of one-half the rupture width. As the rupture plane is moved down the dip of the fault, the location of the hypocenter corresponds to a probability density on the triangular distribution. Figure B.7 illustrates the resulting uniform distribution of rupture locations down dip with a triangular distribution on the hypocenter depths. Figure B.7 uses a relatively large step size for illustrative purposes, but participants should use a step size as small as necessary to reach stable results.

Note that in Figure B.7, the points on the triangle represent the portion of the pdf that was sampled. Because the entire pdf was not sampled, the probabilities will not sum to one and the pdf must be renormalized so that the probabilities sum to one. The pdf should be renormalized based on the hypocenter locations that were sampled.

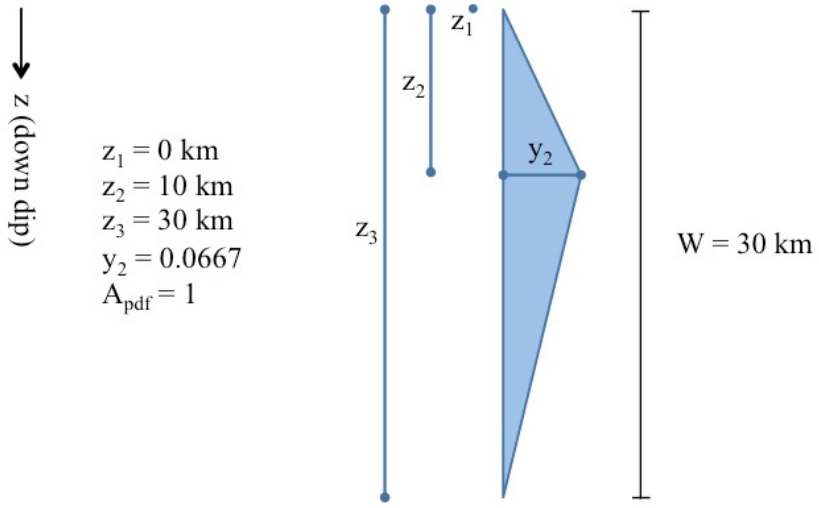

Figure B.6 **Test 2.4: illustration and specifications of triangular depth distribution of hypocenters; note that y_2 is not drawn to scale.**

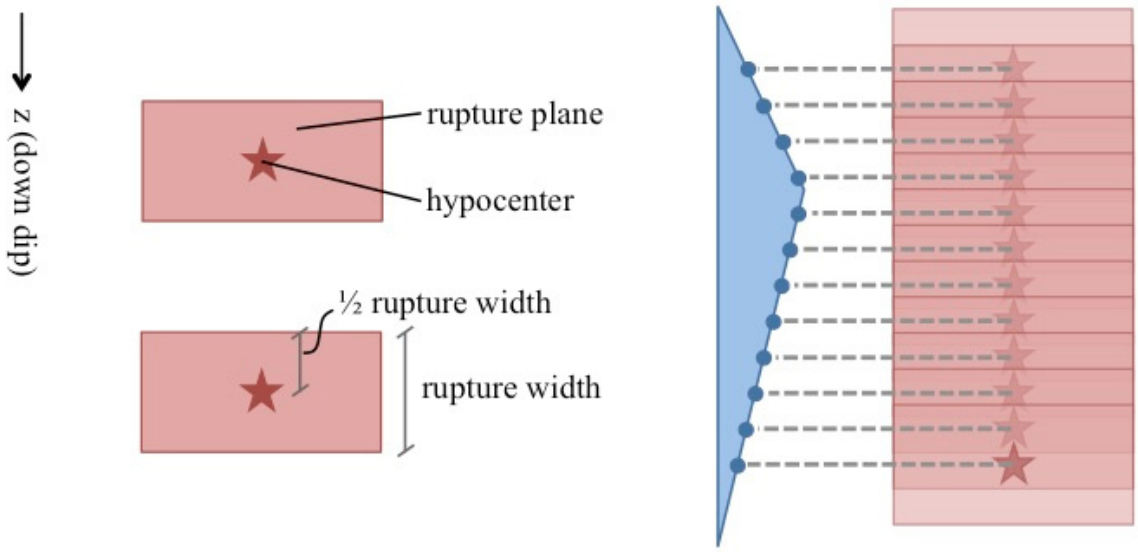

Figure B.7 **Test 2.4: illustration of uniform distribution of rupture locations down dip with triangular distribution of hypocenter depth locations.**

TEST 2.5 INSTRUCTIONS

a. Extreme Tails

Description: Calculate the hazard for the site shown in Figure B.8 due to a single-magnitude event on Fault 6 using the specified NGA-West2 ground-motion model. The purpose of this test is to test the ability to model a normal distribution out to high epsilon values. Because we are interested in the tails of the distribution, we need to change the PGA values. Please provide mean hazard results for PGA defined at 0.001, 0.01, 0.05, 0.1, 0.2, 0.4, 0.6, 0.8, 1.0, 1.25, 1.5, 2.0, 2.5, 3.0, 4.0, 5.0, 6.0, and 7.0*g*. See Tables B.12 and B.13 for source and site coordinates.

Fault 6

Geometry: length 25 km, fault plane depths 0–12 km, strike-slip, dip 90°

Activity: slip rate 2 mm/yr

Mag-Density Function: delta function at M 6

Rupture dimension relationships

Log (A) = M – 4 $\sigma_A = 0$

Log (W) = 0.5*M – 2.15 $\sigma_W = 0$

Log (L) = 0.5*M – 1.85 $\sigma_L = 0$

The above equations are equivalent to an aspect ratio of 2

Uniform distribution along strike and down dip

Ground-motion model: Chiou and Youngs [2014], use a fixed $\sigma = 0.65$, untruncated

Damping ratio = 5%

V_{S30} = 760 m/sec

V_{S30} is measured

$Z_{1.0}$ = 0.048 km

$Z_{2.5}$ = 0.607 km

Region = California

b. Mixture Model

Description: Use the same specifications above, but adjust the sigma (still fixed $\sigma = 0.65$) with the following mixture model specifications. A more detailed explanation on mixture models follows the tables and figures for this test.

Mixture model: two normal distributions

Distribution 1: weight $w_{Mix1} = 0.5$, sigma $\sigma_{Mix1} = 1.2\sigma$

Distribution 2: weight $w_{Mix2} = 0.5$, sigma $\sigma_{Mix2} = 0.8\sigma$

Table B.12 Test 2.5: coordinates for Fault 6.

Latitude	Longitude	Comment
0.11240	-65.00000	North end of fault
-0.11240	-65.00000	South end of fault

Table B.13 Test 2.5: coordinates for Site 1.

Site	Latitude	Longitude	Comment
1	0.00000	-65.13490	15 km west of fault, at midpoint along strike

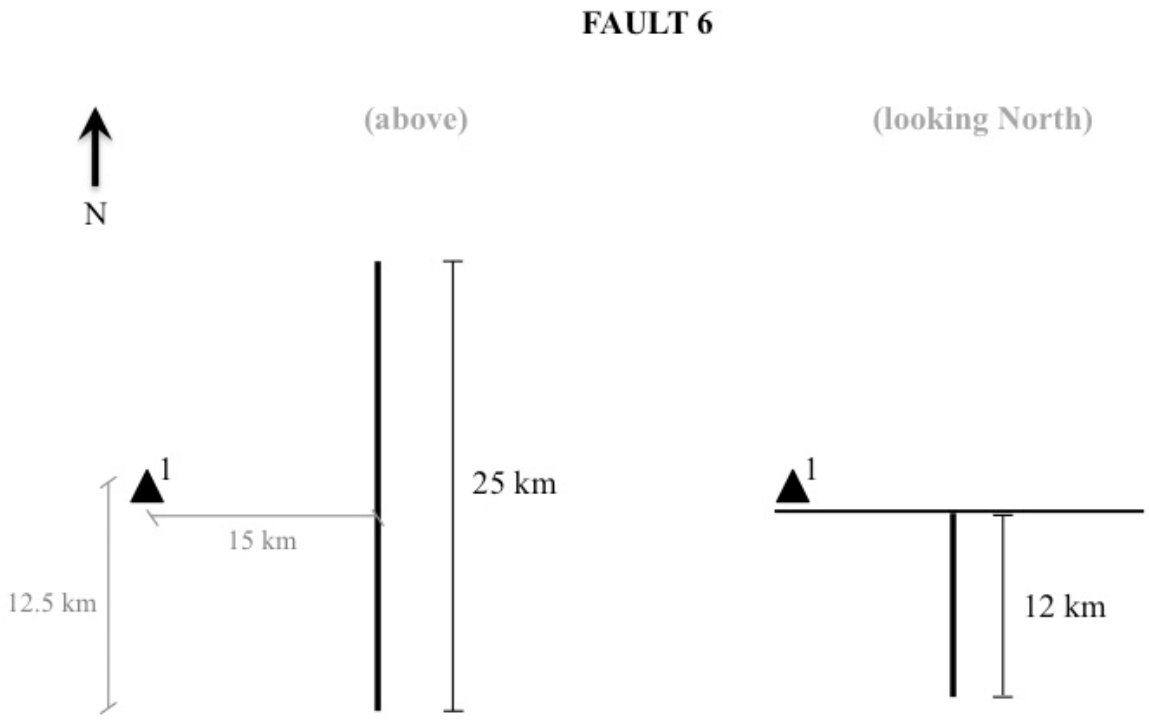

Figure B.8 Test 2.5: illustrations and dimensions of source and site.

TEST 2.5 EXPLANATION: MIXTURE MODEL

A mixture model is a combination of two distributions. In the case of ground motions, the mixture model is a combination of two log-normal distributions. The mixture model is used because ground-motion data do not exactly fit the standard log-normal distribution at high epsilons. For the case of shallow crustal earthquakes, the log-normal distribution is a good model for ground motions up until the tails of the distribution at about 2.5 epsilons, and then the data start to deviate from a log-normal distribution. The observed deviation is a higher probability of rare ground motions, sometimes referred to as "fat tails."

The typical approach to represent a heavy-tailed distribution for ground motions is to use a mixture model consisting of a weighted mixture of two log-normal distributions. The standard deviation for each distribution is specified as a ratio of the standard deviation for the standard log-normal distribution. The two distributions are combined with a specified weight to obtain the mixture model. For this test the standard deviation ratios are specified as 1.2 and 0.8 and the weight for each distribution is 50%. The conditional probability of exceeding a ground motion given a mixture model is calculated from the following equation:

$$P(Z > z) = w_{\text{mix1}}\left(1 - \Phi\frac{z-\mu}{\sigma_{\text{mix1}}}\right) + w_{\text{mix2}}\left(1 - \Phi\frac{z-\mu}{\sigma_{\text{mix2}}}\right)$$

The two log-normal distributions with standard deviations equal to 0.8σ and 1.2σ, where $\sigma = 0.65$, are illustrated in Figure B.9.

These two log-normal distributions are weighted and combined to produce the mixture model distribution. The resulting mixture model distribution is compared to the standard log-normal distribution in Figure B.10. As shown in Figure B.10(a), when the distributions are plotted with a linear scale on the *y*-axis, the difference is indistinguishable. Note that the misfit near the median in Figure B.10(a) is not significant. When plotted with a log scale on the *y*-axis, the higher probabilities of rare ground motions beyond epsilons of about 2.5 are evident, as shown in Figure B.10(b).

The standard log-normal distribution and mixture model distribution can also be compared on a quantile–quantile plot, where the standard log-normal distribution is considered the theoretical distribution and the mixture model distribution the observed. The mixture model distribution is compared to the standard log-normal distribution on a quantile–quantile plot in Figure B.11.

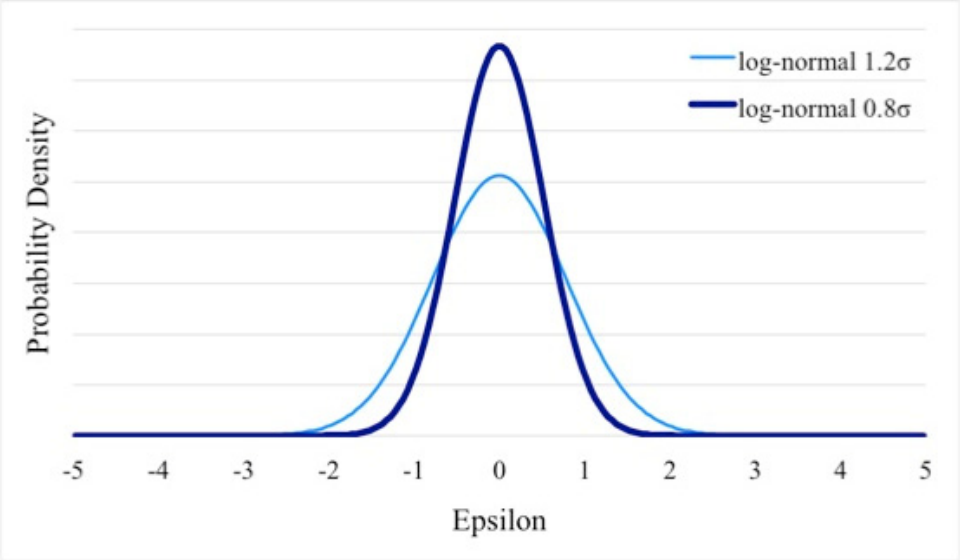

Figure B.9 Test 2.5b: two log-normal distributions used to create the mixture model.

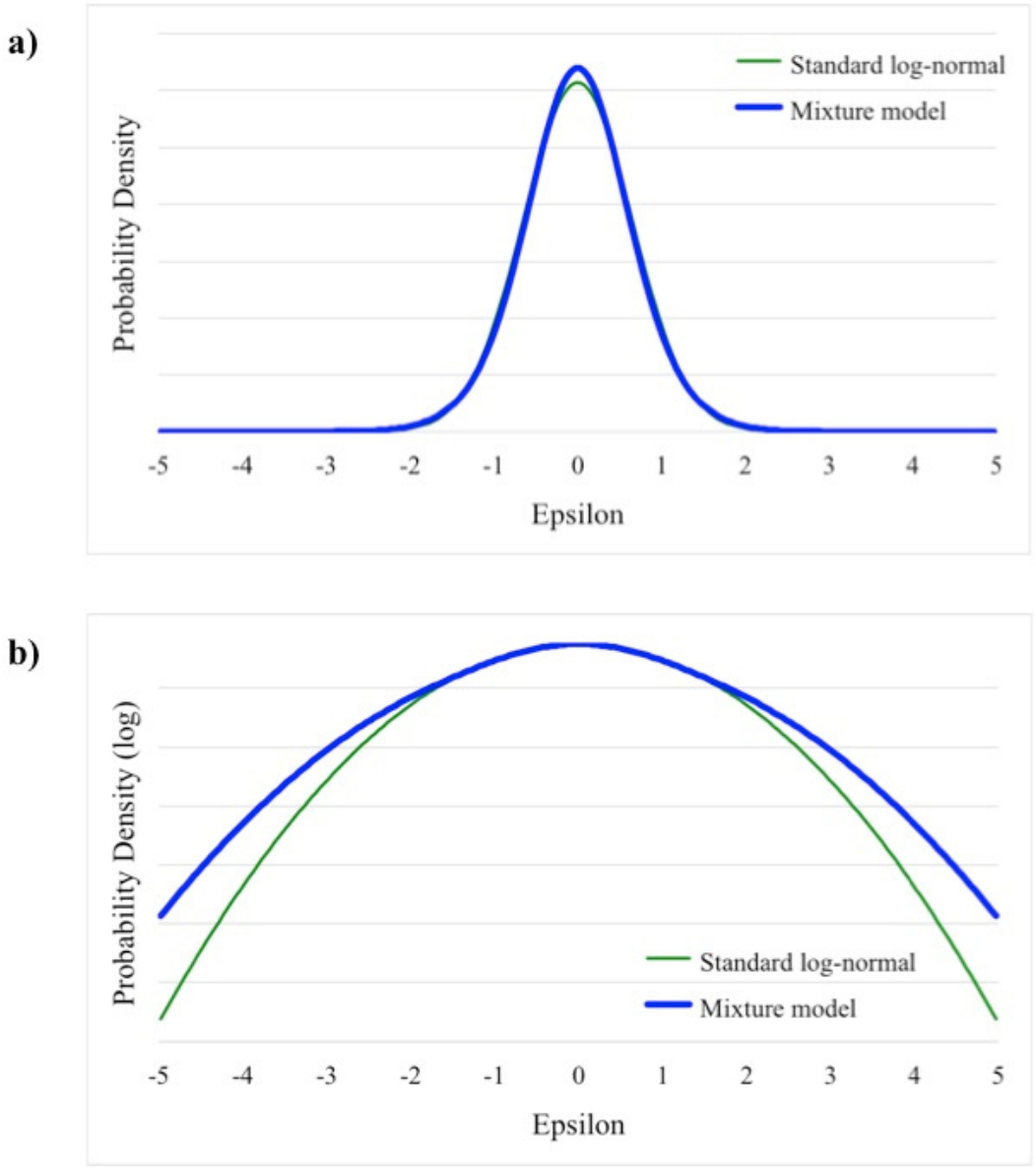

Figure B.10 **Test 2.5b: comparison of standard log-normal distribution and mixture model distribution with (a) linear scale on *y*-axis and (b) log scale on *y*-axis.**

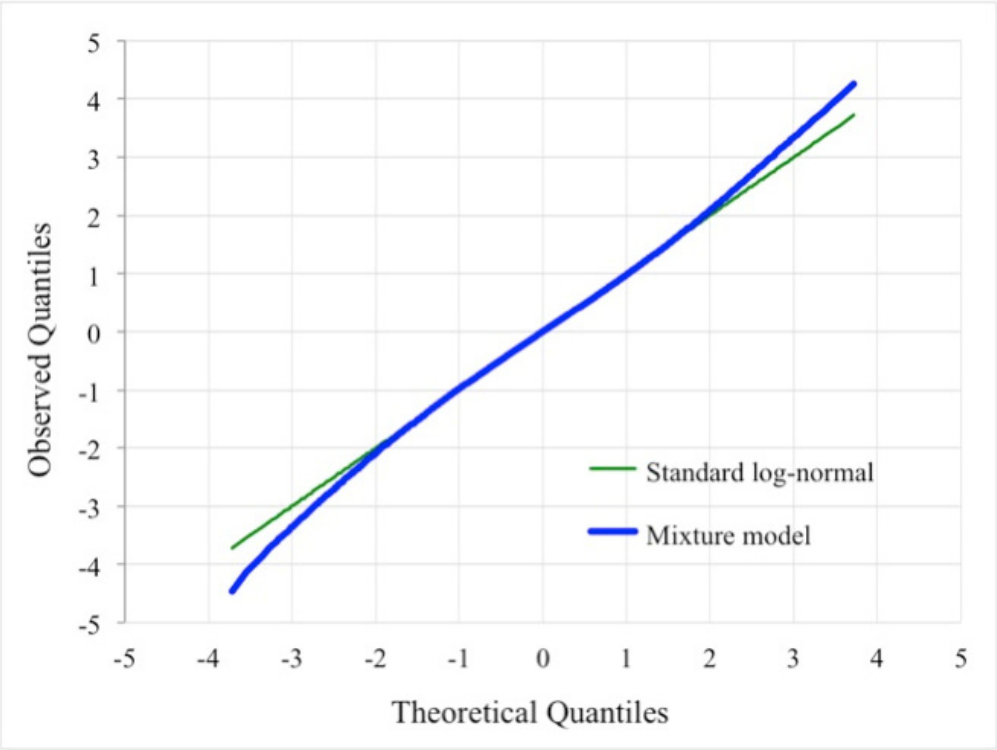

Figure B.11 **Test 2.5b: comparison of standard log-normal distribution and mixture model distribution on a quantile-quantile plot.**

APPENDIX C SET 3 INSTRUCTIONS

General instructions are the same as Set 1.

TEST 3.1 INSTRUCTIONS

a. Dipping East

Description: Calculate the hazard for Sites 1 and 2 shown in Figure C.1(a) due to Fault 7a. See Tables C.1 and C.2 for source and site coordinates. Note that in Figure C.1, the bottom edge of the fault plane (dashed grey line) is only meant to make it clear which direction the fault is dipping, and is not intended to indicate the correct way to model the fault geometry.

Fault 7a

Geometry: length 60 km, fault plane depths 0–12 km, reverse, dip 60°

Activity: slip rate 2 mm/yr

Mag-Density Function: delta function at M 6.75

Rupture dimension relationships

Log (A) = M – 4 $\sigma_A = 0$

Log (W) = 0.5*M – 2.15 $\sigma_W = 0$

Log (L) = 0.5*M – 1.85 $\sigma_L = 0$

The above equations are equivalent to an aspect ratio of 2

Uniform distribution along strike

Ground-motion model: Chiou and Youngs [2014], σ untruncated

Damping ratio = 5%

V_{S30} = 760 m/sec

V_{S30} is measured

$Z_{1.0}$ = 0.048 km

$Z_{2.5}$ = 0.607 km

Region = California

b. Dipping West

Description: Use the same specifications above, but with the fault dipping to the west. Calculate the hazard for Sites 3 and 4 shown in Figure C.1(b) due to Fault 7b. See Table C.3 for site coordinates.

Table C.1 Test 3.1a and 3.1b: coordinates for Fault 7a and 7b.

Latitude	Longitude	Comment
0.00000	-65.00000	North end of Segment 1
-0.16188	-65.00000	South end of Segment 1/North end of Segment 2
-0.36564	-64.90498	South end of Segment 2/North end of Segment 3
-0.45236	-64.80164	South end of Segment 3/West end of Segment 4
-0.45236	-64.78365	East end of Segment 4

Table C.2 Test 3.1a: coordinates for Site 1 and Site 2.

Site	Latitude	Longitude	Comment
1	-0.15738	-64.98651	1.5 km East, 0.5 km North of Seg 1/2 intersect
2	-0.45686	-64.77466	1 km East, 0.5 km South of Seg 4 East end

Table C.3 Test 3.1b: coordinates for Site 3 and Site 4.

Site	Latitude	Longitude	Comment
3	-0.38363	-64.92747	2.5 km West, 2 km South of Seg 3/4 intersect
4	-0.17088	-65.05396	6 km West, 1 km South of Seg 1/2 intersect

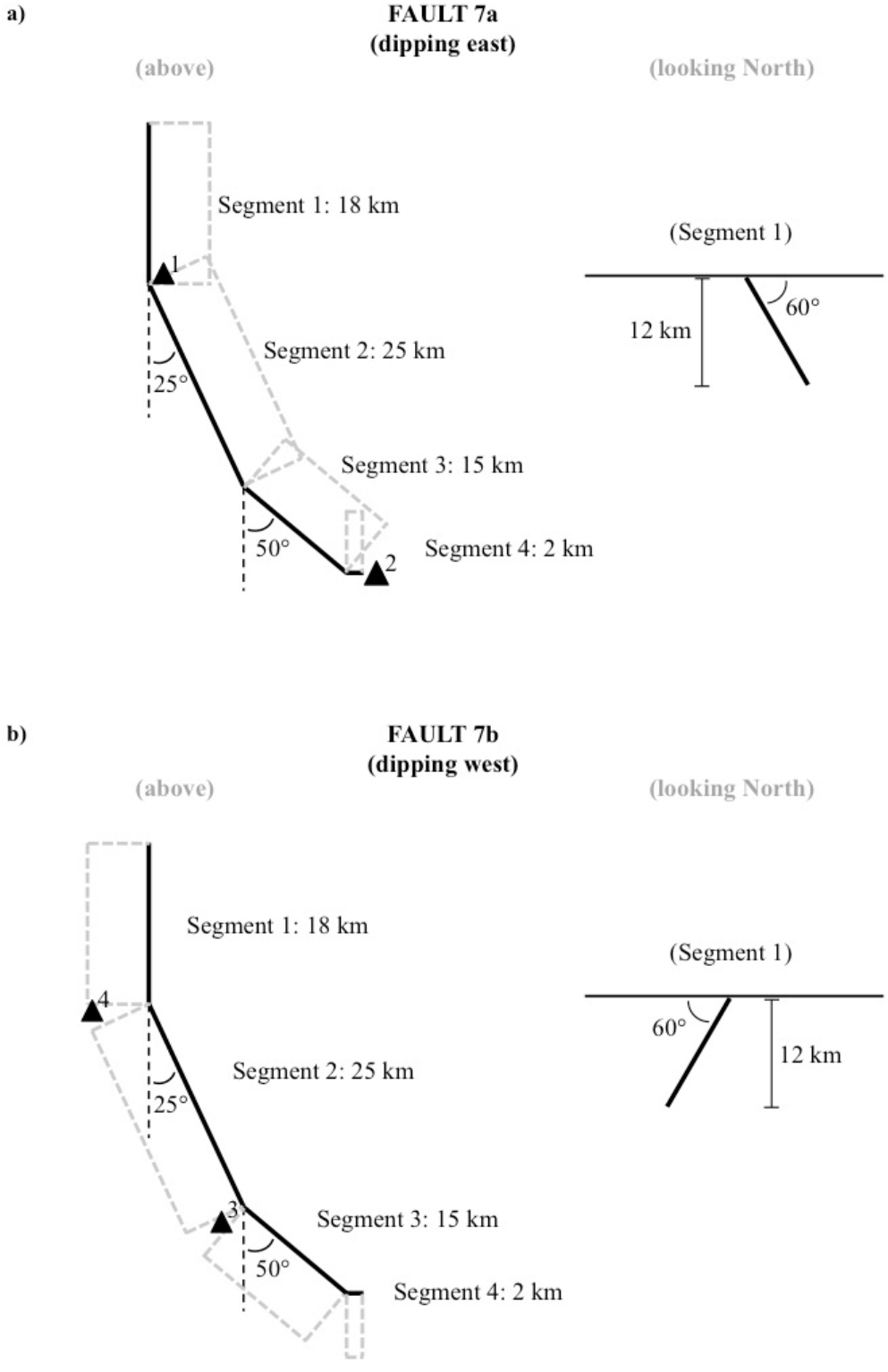

Figure C.1 Test 3.1a and Test 3.1b: illustrations and dimensions of source and sites.

TEST 3.2 INSTRUCTIONS

Description: Calculate the hazard for the site shown in Figure C.2 due to Fault 8 using the specifications below and logic tree in Figure C.3. Report mean hazard, 10^{th}, 50^{th} (median), and 90^{th} fractiles. See Tables C.4 and C.5 for source and site coordinates.

Fault 8

Geometry: length 85 km, fault plane depths 0–12 km, strike-slip, dip 90°

Activity: see logic tree

Mag-Density Functions:

Truncated exponential: *b*-value = 0.9, M_{min} = 5, M_{max} = see logic tree

Youngs and Coppersmith [1995]: *b*-value = 0.9, M_{min} = 5, M_{char} = see logic tree, $M_{max} = M_{char} + 0.25$

Rupture dimension relationships

Log (A) = M – 4 $\sigma_A = 0$

Log (W) = 0.5*M – 2.15 $\sigma_W = 0$

Log (L) = 0.5*M – 1.85 $\sigma_L = 0$

The above equations are equivalent to an aspect ratio of 2

Uniform distribution along strike and down dip

Ground-motion models

Sadigh [1997], rock, σ untruncated

Abrahamson, Silva, and Kamai [2014], σ untruncated

Damping ratio = 5%

V_{S30} = 760 m/sec

V_{S30} is measured

$Z_{1.0}$ = 0.048 km

$Z_{2.5}$ = 0.607 km

Region = California

Note there is no correlation between branches on the logic tree. Run every possible combination that will result in 36 alternative hazard curves.

Table C.4 Test 3.2: coordinates for Fault 8.

Latitude	Longitude	Comment
0.38221	-65.00000	North end of fault
-0.38221	-65.00000	South end of fault

Table C.5 Test 3.2: coordinates for Site 1.

Site	Latitude	Longitude	Comment
1	0.00000	-64.91005	10 km east of fault, at midpoint along strike

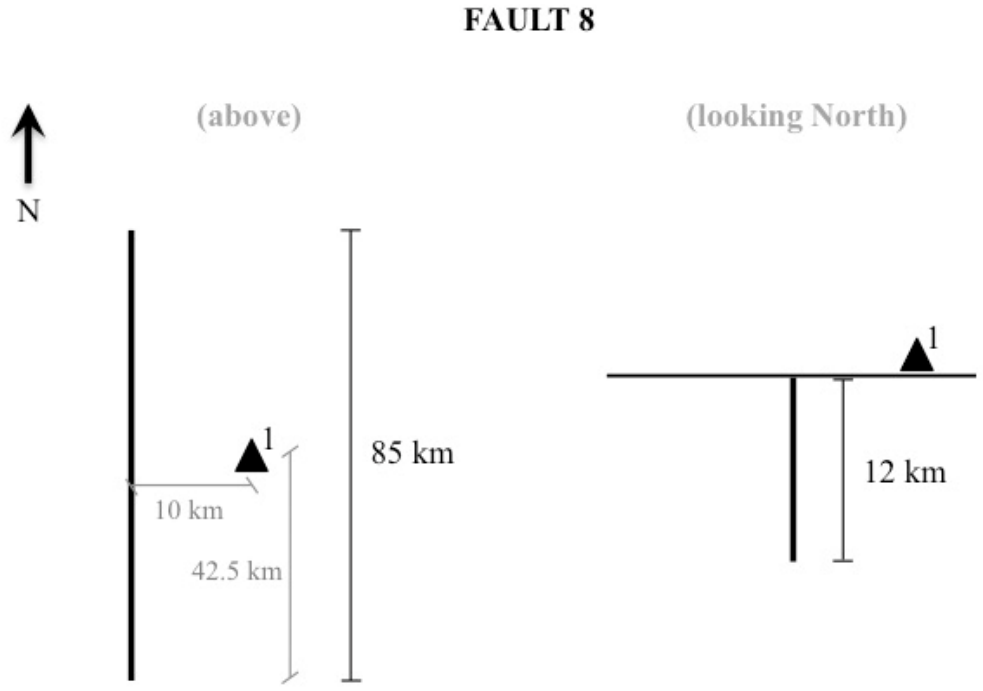

Figure C.2 Test 3.2: illustrations and dimensions of source and site.

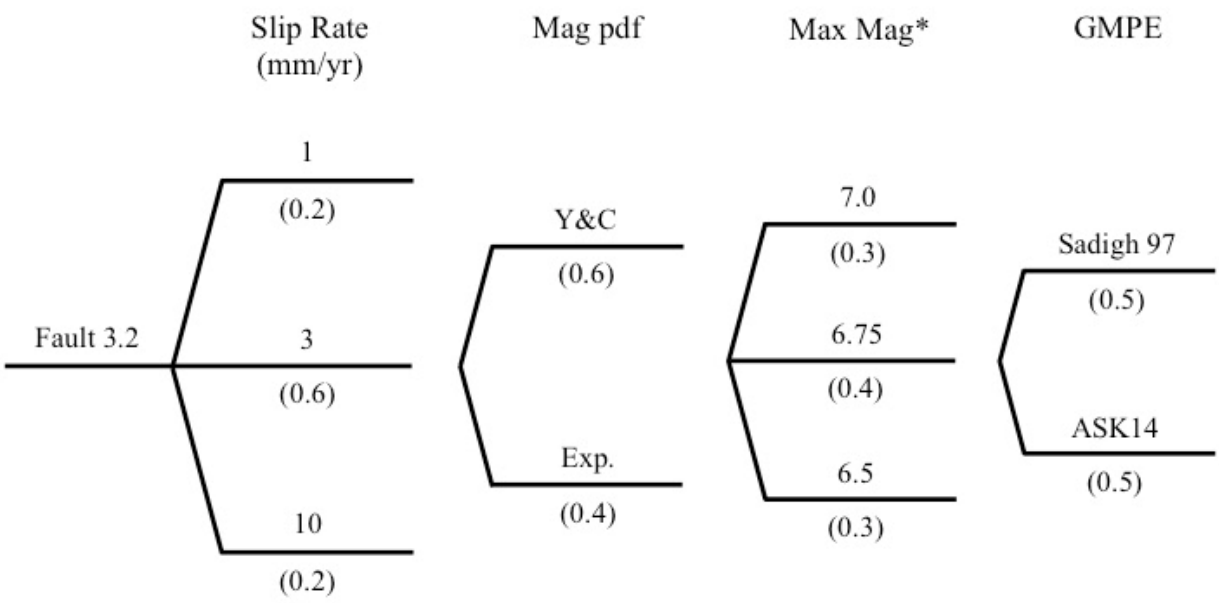

*For the truncated exponential magnitude pdf, the max magnitude in the logic tree is the max value at the high end where the pdf is truncated. For the Youngs and Coppersmith magnitude pdf, this max magnitude is the mean characteristic magnitude in the center of the box car. So for max magnitude = 7.0 on the logic tree, the Youngs and Coppersmith pdf would have $M_{char} = 7.0$, $M_{max} = 7.25$.

Figure C.3 Test 3.2: logic tree specifications.

TEST 3.3 INSTRUCTIONS

Description: Calculate the hazard for Sites 1 and 2 shown in Figure C.4(a) due to the instraslab zone. See Tables C.6 and C.7 for source and site coordinates. The six points defining the surface projection of the slab in Table C.6 are illustrated in Figure C.4(b).

Intraslab Zone

Geometry: see Figure C.4 for geometry specifications

Activity: $N(M_{min}>5) = 0.013$ eq/yr

Mag-Density Function: truncated exponential: b-value = 0.8, $M_{min} = 5$, $M_{max} = 7$

Ground-motion model: Zhao et al. [2006], Site Class I, Rock, σ untruncated

If you use an approach that models the ruptures within the volume of the slab with finite dimensions, use the following rupture dimension relationships and specifications:

Log (A) = M – 4 $\quad\quad$ $\sigma_A = 0$

Log (W) = 0.5*M – 2.15 $\quad\quad$ $\sigma_W = 0$

Log (L) = 0.5*M – 1.85 $\quad\quad$ $\sigma_L = 0$

The above equations are equivalent to an aspect ratio of 2

Uniform distribution throughout slab volume

Assume that the distance measure x in Zhao et al. [2006] was appropriately derived from rupture dimensions (i.e., $x = R_{RUP}$) even though x was derived from a combination of R_{RUP} and R_{HYP}.

Use a dip of 35° relative to the slab for the ruptures (absolute dip = 65° and 80°)

Table C.6 Test 3.3: coordinates for projection of top of intraslab zone.

Point	Latitude	Longitude	Comment
1	-0.44967	-65.50625	Southernmost point of western edge projection
2	-0.44967	-65.00000	Southernmost point where slope changes
3	-0.44967	-64.58666	Southernmost point of eastern edge projection
4	0.44967	-64.58666	Northernmost point of eastern edge projection
5	0.44967	-65.00000	Northernmost point where slope changes
6	0.44967	-65.50625	Northernmost point of western edge projection

Table C.7 Test 3.3: coordinates for Site 1 and Site 2.

Site	Latitude	Longitude	Comment
1	0.00000	-65.28146	25 km east of western edge projection
2	0.00000	-64.38200	125 km east of wetern edge projection

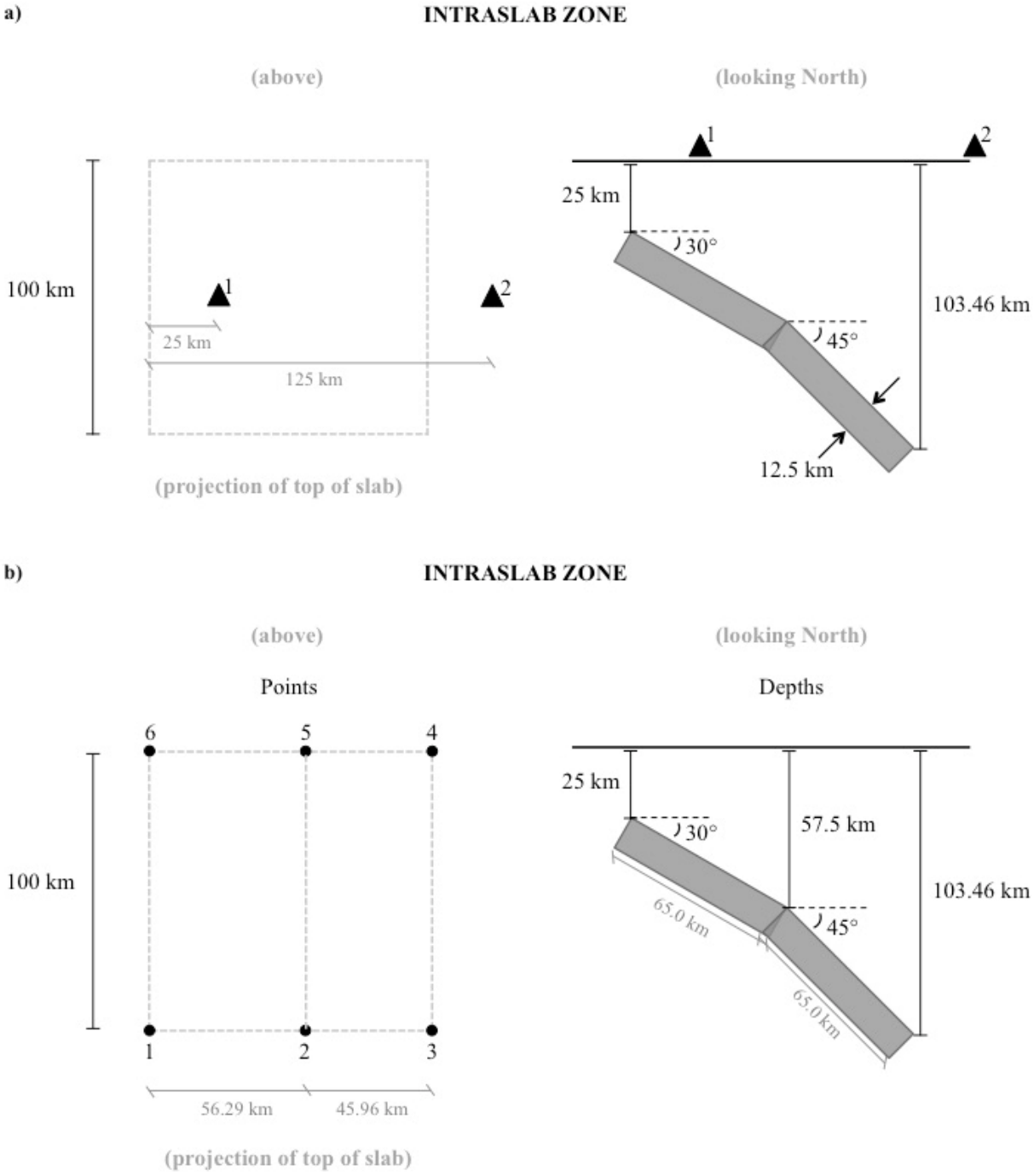

Figure C.4 Test 3.3: illustrations and dimensions of source and site.

TEST 3.4 INSTRUCTIONS

Description: Calculate the hazard for the four sites shown in Figure C.5 due to Area 3. Use virtual faults, virtual ruptures, or a point source correction to account for the rupture dimensions. The source coordinates for Area 3 are the same as Area 2, and are listed in Table B.4. See Table C.8 for site coordinates.

Area 3

Geometry: circle with r = 100 km, seismogenic zone is from 5–25 km

Activity: $N(M_{min}>5) = 0.0395$ eq/yr

Mag-Density Function: truncated exponential: b-value = 0.9, $M_{min} = 5$, $M_{max} = 6.5$

Ground-motion model: Chiou and Youngs [2014], σ untruncated

Damping ratio = 5%

V_{S30} = 760 m/sec

V_{S30} is measured

$Z_{1.0}$ = 0.048 km

$Z_{2.5}$ = 0.607 km

Region = California

Rupture dimension relationships

Log (A) = M – 4 $\sigma_A = 0$

Log (W) = 0.5*M – 2.15 $\sigma_W = 0$

Log (L) = 0.5*M – 1.85 $\sigma_L = 0$

The above equations are equivalent to an aspect ratio of 2

Uniform distribution throughout area zone (recommended spacing of 1 km on horizontal plane, 1 km spacing with depth, inclusive of 5 and 25 km)

Fault styles: strike-slip = 60%, normal = 20%, reverse = 20%

Dip angles: strike-slip = 90°, normal = 60°, reverse = 30°

Strike = 0.0 (fix the strike in the north direction)

Table C.8 Test 3.4: coordinates for Sites 1–4.

Site	Latitude	Longitude	Comment
1	0.0000	-65.0000	In center of area source
2	-0.4497	-65.0000	50 km from center (radially)
3	-0.8993	-65.0000	On area boundary
4	-1.1242	-65.0000	25 km from boundary

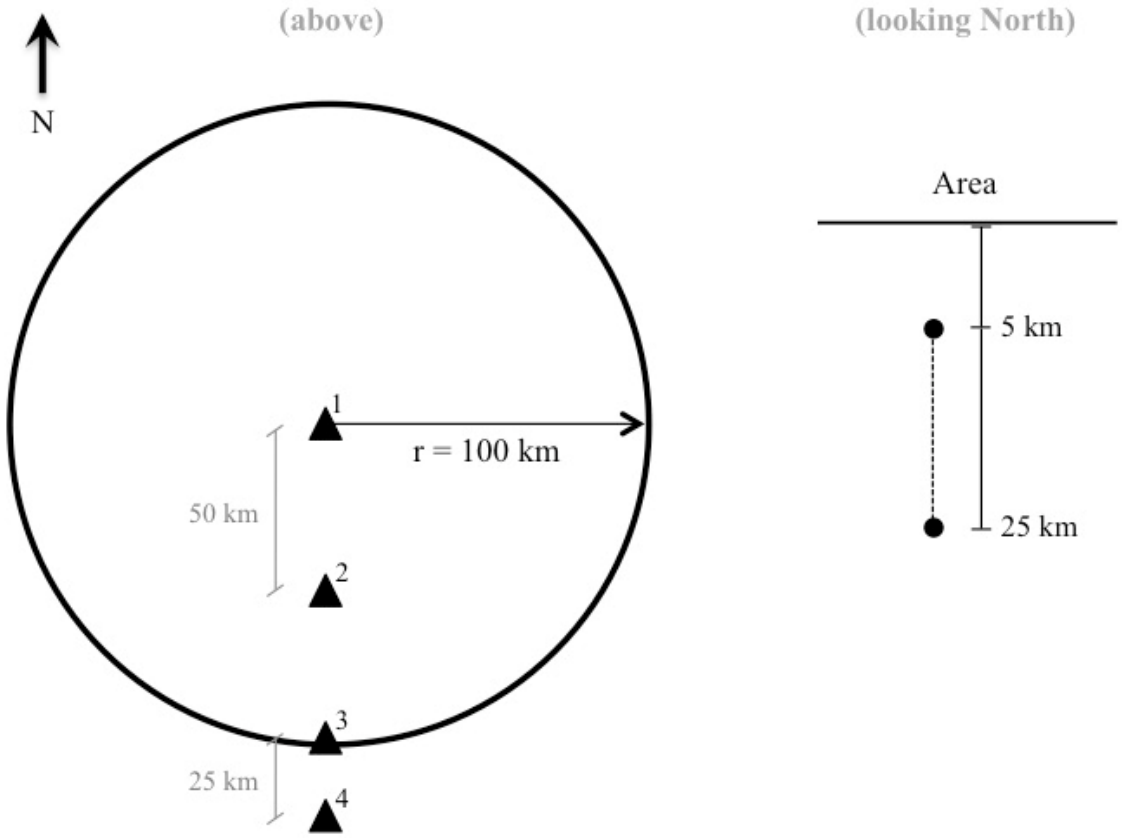

Figure C.5 Test 3.4: illustrations and dimensions of source and site.

APPENDIX D ELECTRONIC SUPPLEMENT

Final hazard results and available benchmark answers for the verification tests are provided as an electronic appendix to this report. There is one Excel workbook for each set of tests. Each workbook contains a tab for every test in that set, and within each tab there are tables for every site.

PEER REPORTS

PEER reports are available as a free PDF download from https://peer.berkeley.edu/peer-reports. Printed hard copies of PEER reports can be ordered directly from our printer by following the instructions also available at https://peer.berkeley.edu/peer-reports. For other related questions about the PEER Report Series, contact the Pacific Earthquake Engineering Research Center, 325 Davis Hall; Mail Code 1792, Berkeley, CA 94720. Tel.: (510) 642-3437; and Email: peer_center@berkeley.edu.

PEER 2018/02 *Update of the BCHydro Subduction Ground-Motion Model using the NGA-Subduction Dataset.* Norman Abrahamson, Nicolas Kuehn, Zeynep Gulerce, Nicholas Gregor, Yousef Bozorgnia, Grace Parker, Jonathan Stewart, Brian Chiou, I. M. Idriss, Kenneth Campbell, and Robert Youngs. June 2018.

PEER 2018/01 *PEER Annual Report 2017–2018*. Khalid Mosalam, Amarnath Kasalanati, and Selim Günay. June 2018.

PEER 2017/12 *Experimental Investigation of the Behavior of Vintage and Retrofit Concentrically Braced Steel Frames under Cyclic Loading*. Barbara G. Simpson, Stephen A. Mahin, and Jiun-Wei Lai. December 2017.

PEER 2017/11 *Preliminary Studies on the Dynamic Response of a Seismically Isolated Prototype Gen-IV Sodium-Cooled Fast Reactor* (*PGSFR*). Benshun Shao, Andreas H. Schellenberg, Matthew J. Schoettler, and Stephen A. Mahin. December 2017.

PEER 2017/10 *Development of Time Histories for IEEE693 Testing and Analysis (including Seismically Isolated Equipment).* Shakhzod M. Takhirov, Eric Fujisaki, Leon Kempner, Michael Riley, and Brian Low. December 2017.

PEER 2017/09 *""R" Package for Computation of Earthquake Ground-Motion Response Spectra.* Pengfei Wang, Jonathan P. Stewart, Yousef Bozorgnia, David M. Boore, and Tadahiro Kishida. December 2017.

PEER 2017/08 *Influence of Kinematic SSI on Foundation Input Motions for Bridges on Deep Foundations*. Benjamin J. Turner, Scott J. Brandenberg, and Jonathan P. Stewart. November 2017.

PEER 2017/07 *A Nonlinear Kinetic Model for Multi-Stage Friction Pendulum Systems*. Paul L. Drazin and Sanjay Govindjee, September 2017.

PEER 2017/06 *Guidelines for Performance-Based Seismic Design of Tall Buildings, Version 2.02*. TBI Working Group led by co-chairs Ron Hamburger and Jack Moehle: Jack Baker, Jonathan Bray, C.B. Crouse, Greg Deierlein, John Hooper, Marshall Lew, Joe Maffei, Stephen Mahin, James Malley, Farzad Naeim, Jonathan Stewart, and John Wallace. May 2017.

PEER 2017/05 *Recommendations for Ergodic Nonlinear Site Amplification in Central and Eastern North America*. Youssef M.A. Hashash, Joseph A. Harmon, Okan Ilhan, Grace A. Parker, and Jonathan P. Stewart. March 2017.

PEER 2017/04 *Expert Panel Recommendations for Ergodic Site Amplification in Central and Eastern North America*. Jonathan P. Stewart, Grace A Parker, Joseph P. Harmon, Gail M. Atkinson, David M. Boore, Robert B. Darragh, Walter J. Silva, and Youssef M.A. Hashash. March 2017.

PEER 2017/03 *NGA-East Ground-Motion Models for the U.S. Geological Survey National Seismic Hazard Maps*. Christine A. Goulet, Yousef Bozorgnia, Nicolas Kuehn, Linda Al Atik, Robert R. Youngs, Robert W. Graves, and Gail M. Atkinson. March 2017.

PEER 2017/02 *U.S.–New Zealand–Japan Workshop: Liquefaction-Induced Ground Movements Effects, University of California, Berkeley, California, 2–4 November 2016.* Jonathan D. Bray, Ross W. Boulanger, Misko Cubrinovski, Kohji Tokimatsu, Steven L. Kramer, Thomas O'Rourke, Ellen Rathje, Russell A. Green, Peter K. Robinson, and Christine Z. Beyzaei. March 2017.

PEER 2017/01 *2016 PEER Annual Report*. Khalid M. Mosalam, Amarnath Kasalanati, and Grace Kang. March 2017.

PEER 2016/10 *Performance-Based Robust Nonlinear Seismic Analysis with Application to Reinforced Concrete Bridge Systems*. Xiao Ling and Khalid M. Mosalam. December 2016.

PEER 2016/08 *Resilience of Critical Structures, Infrastructure, and Communities***.** Gian Paolo Cimellaro, Ali Zamani-Noori, Omar Kamouh, Vesna Terzic, and Stephen A. Mahin. December 2016.

PEER 2016/07 *Hybrid Simulation Theory for a Classical Nonlinear Dynamical System*. Paul L. Drazin and Sanjay Govindjee. September 2016.

PEER 2016/06 *California Earthquake Early Warning System Benefit Study*. Laurie A. Johnson, Sharyl Rabinovici, Grace S. Kang, and Stephen A. Mahin. July 2016.

PEER 2016/05 *Ground-Motion Prediction Equations for Arias Intensity Consistent with the NGA-West2 Ground-Motion Models.* Charlotte Abrahamson, Hao-Jun Michael Shi, and Brian Yang. July 2016.

PEER 2016/04 *The M_W 6.0 South Napa Earthquake of August 24, 2014: A Wake-Up Call for Renewed Investment in Seismic Resilience Across California.* Prepared for the California Seismic Safety Commission, Laurie A. Johnson and Stephen A. Mahin. May 2016.

PEER 2016/03 *Simulation Confidence in Tsunami-Driven Overland Flow.* Patrick Lynett. May 2016.

PEER 2016/02 *Semi-Automated Procedure for Windowing time Series and Computing Fourier Amplitude Spectra for the NGA-West2 Database.* Tadahiro Kishida, Olga-Joan Ktenidou, Robert B. Darragh, and Walter J. Silva. May 2016.

PEER 2016/01 *A Methodology for the Estimation of Kappa (κ) from Large Datasets: Example Application to Rock Sites in the NGA-East Database and Implications on Design Motions.* Olga-Joan Ktenidou, Norman A. Abrahamson, Robert B. Darragh, and Walter J. Silva. April 2016.

PEER 2015/13 *Self-Centering Precast Concrete Dual-Steel-Shell Columns for Accelerated Bridge Construction: Seismic Performance, Analysis, and Design*. Gabriele Guerrini, José I. Restrepo, Athanassios Vervelidis, and Milena Massari. December 2015.

PEER 2015/12 *Shear-Flexure Interaction Modeling for Reinforced Concrete Structural Walls and Columns under Reversed Cyclic Loading*. Kristijan Kolozvari, Kutay Orakcal, and John Wallace. December 2015.

PEER 2015/11 *Selection and Scaling of Ground Motions for Nonlinear Response History Analysis of Buildings in Performance-Based Earthquake Engineering*. N. Simon Kwong and Anil K. Chopra. December 2015.

PEER 2015/10 *Structural Behavior of Column-Bent Cap Beam-Box Girder Systems in Reinforced Concrete Bridges Subjected to Gravity and Seismic Loads. Part II: Hybrid Simulation and Post-Test Analysis*. Mohamed A. Moustafa and Khalid M. Mosalam. November 2015.

PEER 2015/09 *Structural Behavior of Column-Bent Cap Beam-Box Girder Systems in Reinforced Concrete Bridges Subjected to Gravity and Seismic Loads. Part I: Pre-Test Analysis and Quasi-Static Experiments*. Mohamed A. Moustafa and Khalid M. Mosalam. September 2015.

PEER 2015/08 *NGA-East: Adjustments to Median Ground-Motion Models for Center and Eastern North America*. August 2015.

PEER 2015/07 *NGA-East: Ground-Motion Standard-Deviation Models for Central and Eastern North America*. Linda Al Atik. June 2015.

PEER 2015/06 *Adjusting Ground-Motion Intensity Measures to a Reference Site for which V_{S30} = 3000 m/sec*. David M. Boore. May 2015.

PEER 2015/05 *Hybrid Simulation of Seismic Isolation Systems Applied to an APR-1400 Nuclear Power Plant.* Andreas H. Schellenberg, Alireza Sarebanha, Matthew J. Schoettler, Gilberto Mosqueda, Gianmario Benzoni, and Stephen A. Mahin. April 2015.

PEER 2015/04 *NGA-East: Median Ground-Motion Models for the Central and Eastern North America Region.* April 2015.

PEER 2015/03 *Single Series Solution for the Rectangular Fiber-Reinforced Elastomeric Isolator Compression Modulus*. James M. Kelly and Niel C. Van Engelen. March 2015.

PEER 2015/02 *A Full-Scale, Single-Column Bridge Bent Tested by Shake-Table Excitation.* Matthew J. Schoettler, José I. Restrepo, Gabriele Guerrini, David E. Duck, and Francesco Carrea. March 2015.

PEER 2015/01 *Concrete Column Blind Prediction Contest 2010: Outcomes and Observations.* Vesna Terzic, Matthew J. Schoettler, José I. Restrepo, and Stephen A Mahin. March 2015.

PEER 2014/20 *Stochastic Modeling and Simulation of Near-Fault Ground Motions for Performance-Based Earthquake Engineering*. Mayssa Dabaghi and Armen Der Kiureghian. December 2014.

PEER 2014/19 *Seismic Response of a Hybrid Fiber-Reinforced Concrete Bridge Column Detailed for Accelerated Bridge Construction*. Wilson Nguyen, William Trono, Marios Panagiotou, and Claudia P. Ostertag. December 2014.

PEER 2014/18 *Three-Dimensional Beam-Truss Model for Reinforced Concrete Walls and Slabs Subjected to Cyclic Static or Dynamic Loading*. Yuan Lu, Marios Panagiotou, and Ioannis Koutromanos. December 2014.

PEER 2014/17 *PEER NGA-East Database.* Christine A. Goulet, Tadahiro Kishida, Timothy D. Ancheta, Chris H. Cramer, Robert B. Darragh, Walter J. Silva, Youssef M.A. Hashash, Joseph Harmon, Jonathan P. Stewart, Katie E. Wooddell, and Robert R. Youngs. October 2014.

PEER 2014/16 *Guidelines for Performing Hazard-Consistent One-Dimensional Ground Response Analysis for Ground Motion Prediction*. Jonathan P. Stewart, Kioumars Afshari, and Youssef M.A. Hashash. October 2014.

PEER 2014/15 *NGA-East Regionalization Report: Comparison of Four Crustal Regions within Central and Eastern North America using Waveform Modeling and 5%-Damped Pseudo-Spectral Acceleration Response*. Jennifer Dreiling, Marius P. Isken, Walter D. Mooney, Martin C. Chapman, and Richard W. Godbee. October 2014.

PEER 2014/14 *Scaling Relations between Seismic Moment and Rupture Area of Earthquakes in Stable Continental Regions*. Paul Somerville. August 2014.

PEER 2014/13 *PEER Preliminary Notes and Observations on the August 24, 2014, South Napa Earthquake*. Grace S. Kang and Stephen A. Mahin, Editors. September 2014.

PEER 2014/12 *Reference-Rock Site Conditions for Central and Eastern North America: Part II – Attenuation (Kappa) Definition*. Kenneth W. Campbell, Youssef M.A. Hashash, Byungmin Kim, Albert R. Kottke, Ellen M. Rathje, Walter J. Silva, and Jonathan P. Stewart. August 2014.

PEER 2014/11 *Reference-Rock Site Conditions for Central and Eastern North America: Part I - Velocity Definition*. Youssef M.A. Hashash, Albert R. Kottke, Jonathan P. Stewart, Kenneth W. Campbell, Byungmin Kim, Ellen M. Rathje, Walter J. Silva, Sissy Nikolaou, and Cheryl Moss. August 2014.

PEER 2014/10 *Evaluation of Collapse and Non-Collapse of Parallel Bridges Affected by Liquefaction and Lateral Spreading*. Benjamin Turner, Scott J. Brandenberg, and Jonathan P. Stewart. August 2014.

PEER 2014/09 *PEER Arizona Strong-Motion Database and GMPEs Evaluation*. Tadahiro Kishida, Robert E. Kayen, Olga-Joan Ktenidou, Walter J. Silva, Robert B. Darragh, and Jennie Watson-Lamprey. June 2014.

PEER 2014/08 *Unbonded Pretensioned Bridge Columns with Rocking Detail*. Jeffrey A. Schaefer, Bryan Kennedy, Marc O. Eberhard, and John F. Stanton. June 2014.

PEER 2014/07 *Northridge 20 Symposium Summary Report: Impacts, Outcomes, and Next Steps*. May 2014.

PEER 2014/06 *Report of the Tenth Planning Meeting of NEES/E-Defense Collaborative Research on Earthquake Engineering*. December 2013.

PEER 2014/05 *Seismic Velocity Site Characterization of Thirty-One Chilean Seismometer Stations by Spectral Analysis of Surface Wave Dispersion*. Robert Kayen, Brad D. Carkin, Skye Corbet, Camilo Pinilla, Allan Ng, Edward Gorbis, and Christine Truong. April 2014.

PEER 2014/04 Effect of Vertical Acceleration on Shear Strength of Reinforced Concrete Columns. Hyerin Lee and Khalid M. Mosalam. April 2014.

PEER 2014/03 *Retest of Thirty-Year-Old Neoprene Isolation Bearings.* James M. Kelly and Niel C. Van Engelen. March 2014.

PEER 2014/02 *Theoretical Development of Hybrid Simulation Applied to Plate Structures.* Ahmed A. Bakhaty, Khalid M. Mosalam, and Sanjay Govindjee. January 2014.

PEER 2014/01 *Performance-Based Seismic Assessment of Skewed Bridges.* Peyman Kaviani, Farzin Zareian, and Ertugrul Taciroglu. January 2014.

PEER 2013/26 *Urban Earthquake Engineerin*g. Proceedings of the U.S.-Iran Seismic Workshop. December 2013.

PEER 2013/25 *Earthquake Engineering for Resilient Communities: 2013 PEER Internship Program Research Report Collection.* Heidi Tremayne (Editor), Stephen A. Mahin (Editor), Jorge Archbold Monterossa, Matt Brosman, Shelly Dean, Katherine deLaveaga, Curtis Fong, Donovan Holder, Rakeeb Khan, Elizabeth Jachens, David Lam, Daniela Martinez Lopez, Mara Minner, Geffen Oren, Julia Pavicic, Melissa Quinonez, Lorena Rodriguez, Sean Salazar, Kelli Slaven, Vivian Steyert, Jenny Taing, and Salvador Tena. December 2013.

PEER 2013/24 *NGA-West2 Ground Motion Prediction Equations for Vertical Ground Motions*. September 2013.

PEER 2013/23 *Coordinated Planning and Preparedness for Fire Following Major Earthquakes*. Charles Scawthorn. November 2013.

PEER 2013/22 *GEM-PEER Task 3 Project: Selection of a Global Set of Ground Motion Prediction Equations.* Jonathan P. Stewart, John Douglas, Mohammad B. Javanbarg, Carola Di Alessandro, Yousef Bozorgnia, Norman A. Abrahamson, David M. Boore, Kenneth W. Campbell, Elise Delavaud, Mustafa Erdik, and Peter J. Stafford. December 2013.

PEER 2013/21 *Seismic Design and Performance of Bridges with Columns on Rocking Foundations*. Grigorios Antonellis and Marios Panagiotou. September 2013.

PEER 2013/20 *Experimental and Analytical Studies on the Seismic Behavior of Conventional and Hybrid Braced Frames*. Jiun-Wei Lai and Stephen A. Mahin. September 2013.

PEER 2013/19 *Toward Resilient Communities: A Performance-Based Engineering Framework for Design and Evaluation of the Built Environment.* Michael William Mieler, Bozidar Stojadinovic, Robert J. Budnitz, Stephen A. Mahin, and Mary C. Comerio. September 2013.

PEER 2013/18 *Identification of Site Parameters that Improve Predictions of Site Amplification*. Ellen M. Rathje and Sara Navidi. July 2013.

PEER 2013/17 *Response Spectrum Analysis of Concrete Gravity Dams Including Dam-Water-Foundation Interaction*. Arnkjell Løkke and Anil K. Chopra. July 2013.

PEER 2013/16 *Effect of Hoop Reinforcement Spacing on the Cyclic Response of Large Reinforced Concrete Special Moment Frame Beams.* Marios Panagiotou, Tea Visnjic, Grigorios Antonellis, Panagiotis Galanis, and Jack P. Moehle. June 2013.

PEER 2013/15 *A Probabilistic Framework to Include the Effects of Near-Fault Directivity in Seismic Hazard Assessment*. Shrey Kumar Shahi, Jack W. Baker. October 2013.

PEER 2013/14 *Hanging-Wall Scaling using Finite-Fault Simulations.* Jennifer L. Donahue and Norman A. Abrahamson. September 2013.

PEER 2013/13 *Semi-Empirical Nonlinear Site Amplification and its Application in NEHRP Site Factors*. Jonathan P. Stewart and Emel Seyhan. November 2013.

PEER 2013/12 *Nonlinear Horizontal Site Response for the NGA-West2 Project.* Ronnie Kamai, Norman A. Abramson, Walter J. Silva. May 2013.

PEER 2013/11 *Epistemic Uncertainty for NGA-West2 Models.* Linda Al Atik and Robert R. Youngs. May 2013.

PEER 2013/10 *NGA-West 2 Models for Ground-Motion Directionality.* Shrey K. Shahi and Jack W. Baker. May 2013.

PEER 2013/09 *Final Report of the NGA-West2 Directivity Working Group.* Paul Spudich, Jeffrey R. Bayless, Jack W. Baker, Brian S.J. Chiou, Badie Rowshandel, Shrey Shahi, and Paul Somerville. May 2013.

PEER 2013/08 *NGA-West2 Model for Estimating Average Horizontal Values of Pseudo-Absolute Spectral Accelerations Generated by Crustal Earthquakes*. I. M. Idriss. May 2013.

PEER 2013/07 *Update of the Chiou and Youngs NGA Ground Motion Model for Average Horizontal Component of Peak Ground Motion and Response Spectra*. Brian Chiou and Robert Youngs. May 2013.

PEER 2013/06 *NGA-West2 Campbell-Bozorgnia Ground Motion Model for the Horizontal Components of PGA, PGV, and 5%-Damped Elastic Pseudo-Acceleration Response Spectra for Periods Ranging from 0.01 to 10 sec.* Kenneth W. Campbell and Yousef Bozorgnia. May 2013.

PEER 2013/05 *NGA-West 2 Equations for Predicting Response Spectral Accelerations for Shallow Crustal Earthquakes*. David M. Boore, Jonathan P. Stewart, Emel Seyhan, and Gail M. Atkinson. May 2013.

PEER 2013/04 *Update of the AS08 Ground-Motion Prediction Equations Based on the NGA-West2 Data Set*. Norman Abrahamson, Walter Silva, and Ronnie Kamai. May 2013.

PEER 2013/03 *PEER NGA-West2 Database.* Timothy D. Ancheta, Robert B. Darragh, Jonathan P. Stewart, Emel Seyhan, Walter J. Silva, Brian S.J. Chiou, Katie E. Wooddell, Robert W. Graves, Albert R. Kottke, David M. Boore, Tadahiro Kishida, and Jennifer L. Donahue. May 2013.

PEER 2013/02 *Hybrid Simulation of the Seismic Response of Squat Reinforced Concrete Shear Walls*. Catherine A. Whyte and Bozidar Stojadinovic. May 2013.

PEER 2013/01 *Housing Recovery in Chile: A Qualitative Mid-program Review*. Mary C. Comerio. February 2013.

PEER 2012/08 *Guidelines for Estimation of Shear Wave Velocity.* Bernard R. Wair, Jason T. DeJong, and Thomas Shantz. December 2012.

PEER 2012/07 *Earthquake Engineering for Resilient Communities: 2012 PEER Internship Program Research Report Collection.* Heidi Tremayne (Editor), Stephen A. Mahin (Editor), Collin Anderson, Dustin Cook, Michael Erceg, Carlos Esparza, Jose Jimenez, Dorian Krausz, Andrew Lo, Stephanie Lopez, Nicole McCurdy, Paul Shipman, Alexander Strum, Eduardo Vega. December 2012.

PEER 2012/06 *Fragilities for Precarious Rocks at Yucca Mountain.* Matthew D. Purvance, Rasool Anooshehpoor, and James N. Brune. December 2012.

PEER 2012/05 *Development of Simplified Analysis Procedure for Piles in Laterally Spreading Layered Soils.* Christopher R. McGann, Pedro Arduino, and Peter Mackenzie–Helnwein. December 2012.

PEER 2012/04 *Unbonded Pre-Tensioned Columns for Bridges in Seismic Regions.* Phillip M. Davis, Todd M. Janes, Marc O. Eberhard, and John F. Stanton. December 2012.

PEER 2012/03 *Experimental and Analytical Studies on Reinforced Concrete Buildings with Seismically Vulnerable Beam-Column Joints*. Sangjoon Park and Khalid M. Mosalam. October 2012.

PEER 2012/02 *Seismic Performance of Reinforced Concrete Bridges Allowed to Uplift during Multi-Directional Excitation*. Andres Oscar Espinoza and Stephen A. Mahin. July 2012.

PEER 2012/01 *Spectral Damping Scaling Factors for Shallow Crustal Earthquakes in Active Tectonic Regions.* Sanaz Rezaeian, Yousef Bozorgnia, I. M. Idriss, Kenneth Campbell, Norman Abrahamson, and Walter Silva. July 2012.

PEER 2011/10 *Earthquake Engineering for Resilient Communities: 2011 PEER Internship Program Research Report Collection*. Heidi Faison and Stephen A. Mahin, Editors. December 2011.

PEER 2011/09 *Calibration of Semi-Stochastic Procedure for Simulating High-Frequency Ground Motions*. Jonathan P. Stewart, Emel Seyhan, and Robert W. Graves. December 2011.

PEER 2011/08 *Water Supply in regard to Fire Following Earthquake*. Charles Scawthorn. November 2011.

PEER 2011/07 *Seismic Risk Management in Urban Areas*. Proceedings of a U.S.-Iran-Turkey Seismic Workshop. September 2011.

PEER 2011/06 *The Use of Base Isolation Systems to Achieve Complex Seismic Performance Objectives*. Troy A. Morgan and Stephen A. Mahin. July 2011.

PEER 2011/05 *Case Studies of the Seismic Performance of Tall Buildings Designed by Alternative Means.* Task 12 Report for the Tall Buildings Initiative. Jack Moehle, Yousef Bozorgnia, Nirmal Jayaram, Pierson Jones, Mohsen Rahnama, Nilesh Shome, Zeynep Tuna, John Wallace, Tony Yang, and Farzin Zareian. July 2011.

PEER 2011/04 *Recommended Design Practice for Pile Foundations in Laterally Spreading Ground.* Scott A. Ashford, Ross W. Boulanger, and Scott J. Brandenberg. June 2011.

PEER 2011/03 *New Ground Motion Selection Procedures and Selected Motions for the PEER Transportation Research Program*. Jack W. Baker, Ting Lin, Shrey K. Shahi, and Nirmal Jayaram. March 2011.

PEER 2011/02 *A Bayesian Network Methodology for Infrastructure Seismic Risk Assessment and Decision Support*. Michelle T. Bensi, Armen Der Kiureghian, and Daniel Straub. March 2011.

PEER 2011/01 *Demand Fragility Surfaces for Bridges in Liquefied and Laterally Spreading Ground.* Scott J. Brandenberg, Jian Zhang, Pirooz Kashighandi, Yili Huo, and Minxing Zhao. March 2011.

PEER 2010/05 *Guidelines for Performance-Based Seismic Design of Tall Buildings.* Developed by the Tall Buildings Initiative. November 2010.

PEER 2010/04 *Application Guide for the Design of Flexible and Rigid Bus Connections between Substation Equipment Subjected to Earthquakes.* Jean-Bernard Dastous and Armen Der Kiureghian. September 2010.

PEER 2010/03 *Shear Wave Velocity as a Statistical Function of Standard Penetration Test Resistance and Vertical Effective Stress at Caltrans Bridge Sites.* Scott J. Brandenberg, Naresh Bellana, and Thomas Shantz. June 2010.

PEER 2010/02 *Stochastic Modeling and Simulation of Ground Motions for Performance-Based Earthquake Engineering.* Sanaz Rezaeian and Armen Der Kiureghian. June 2010.

PEER 2010/01 *Structural Response and Cost Characterization of Bridge Construction Using Seismic Performance Enhancement Strategies.* Ady Aviram, Božidar Stojadinović, Gustavo J. Parra-Montesinos, and Kevin R. Mackie. March 2010.

PEER 2009/03 *The Integration of Experimental and Simulation Data in the Study of Reinforced Concrete Bridge Systems Including Soil-Foundation-Structure Interaction.* Matthew Dryden and Gregory L. Fenves. November 2009.

PEER 2009/02 *Improving Earthquake Mitigation through Innovations and Applications in Seismic Science, Engineering, Communication, and Response*. Proceedings of a U.S.-Iran Seismic Workshop. October 2009.

PEER 2009/01 *Evaluation of Ground Motion Selection and Modification Methods: Predicting Median Interstory Drift Response of Buildings*. Curt B. Haselton, Editor. June 2009.

PEER 2008/10 *Technical Manual for Strata.* Albert R. Kottke and Ellen M. Rathje. February 2009.

PEER 2008/09 *NGA Model for Average Horizontal Component of Peak Ground Motion and Response Spectra.* Brian S.-J. Chiou and Robert R. Youngs. November 2008.

PEER 2008/08 *Toward Earthquake-Resistant Design of Concentrically Braced Steel Structures*. Patxi Uriz and Stephen A. Mahin. November 2008.

PEER 2008/07 *Using OpenSees for Performance-Based Evaluation of Bridges on Liquefiable Soils*. Stephen L. Kramer, Pedro Arduino, and HyungSuk Shin. November 2008.

PEER 2008/06 *Shaking Table Tests and Numerical Investigation of Self-Centering Reinforced Concrete Bridge Columns*. Hyung IL Jeong, Junichi Sakai, and Stephen A. Mahin. September 2008.

PEER 2008/05 *Performance-Based Earthquake Engineering Design Evaluation Procedure for Bridge Foundations Undergoing Liquefaction-Induced Lateral Ground Displacement*. Christian A. Ledezma and Jonathan D. Bray. August 2008.

PEER 2008/04 *Benchmarking of Nonlinear Geotechnical Ground Response Analysis Procedures.* Jonathan P. Stewart, Annie On-Lei Kwok, Youssef M. A. Hashash, Neven Matasovic, Robert Pyke, Zhiliang Wang, and Zhaohui Yang. August 2008.

PEER 2008/03 *Guidelines for Nonlinear Analysis of Bridge Structures in California.* Ady Aviram, Kevin R. Mackie, and Božidar Stojadinović. August 2008.

PEER 2008/02 *Treatment of Uncertainties in Seismic-Risk Analysis of Transportation Systems*. Evangelos Stergiou and Anne S. Kiremidjian. July 2008.

PEER 2008/01 *Seismic Performance Objectives for Tall Buildings.* William T. Holmes, Charles Kircher, William Petak, and Nabih Youssef. August 2008.

PEER 2007/12 *An Assessment to Benchmark the Seismic Performance of a Code-Conforming Reinforced Concrete Moment-Frame Building.* Curt Haselton, Christine A. Goulet, Judith Mitrani-Reiser, James L. Beck, Gregory G. Deierlein, Keith A. Porter, Jonathan P. Stewart, and Ertugrul Taciroglu. August 2008.

PEER 2007/11 *Bar Buckling in Reinforced Concrete Bridge Columns.* Wayne A. Brown, Dawn E. Lehman, and John F. Stanton. February 2008.

PEER 2007/10 *Computational Modeling of Progressive Collapse in Reinforced Concrete Frame Structures*. Mohamed M. Talaat and Khalid M. Mosalam. May 2008.

PEER 2007/09 *Integrated Probabilistic Performance-Based Evaluation of Benchmark Reinforced Concrete Bridges*. Kevin R. Mackie, John-Michael Wong, and Božidar Stojadinović. January 2008.

PEER 2007/08 *Assessing Seismic Collapse Safety of Modern Reinforced Concrete Moment-Frame Buildings*. Curt B. Haselton and Gregory G. Deierlein. February 2008.

PEER 2007/07 *Performance Modeling Strategies for Modern Reinforced Concrete Bridge Columns*. Michael P. Berry and Marc O. Eberhard. April 2008.

PEER 2007/06 *Development of Improved Procedures for Seismic Design of Buried and Partially Buried Structures*. Linda Al Atik and Nicholas Sitar. June 2007.

PEER 2007/05 *Uncertainty and Correlation in Seismic Risk Assessment of Transportation Systems*. Renee G. Lee and Anne S. Kiremidjian. July 2007.

PEER 2007/04 *Numerical Models for Analysis and Performance-Based Design of Shallow Foundations Subjected to Seismic Loading.* Sivapalan Gajan, Tara C. Hutchinson, Bruce L. Kutter, Prishati Raychowdhury, José A. Ugalde, and Jonathan P. Stewart. May 2008.

PEER 2007/03 *Beam-Column Element Model Calibrated for Predicting Flexural Response Leading to Global Collapse of RC Frame Buildings*. Curt B. Haselton, Abbie B. Liel, Sarah Taylor Lange, and Gregory G. Deierlein. May 2008.

PEER 2007/02 *Campbell-Bozorgnia NGA Ground Motion Relations for the Geometric Mean Horizontal Component of Peak and Spectral Ground Motion Parameters*. Kenneth W. Campbell and Yousef Bozorgnia. May 2007.

PEER 2007/01 *Boore-Atkinson NGA Ground Motion Relations for the Geometric Mean Horizontal Component of Peak and Spectral Ground Motion Parameters*. David M. Boore and Gail M. Atkinson. May 2007.

PEER 2006/12 Societal Implications of Performance-Based Earthquake Engineering. Peter J. May. May 2007.

PEER 2006/11 *Probabilistic Seismic Demand Analysis Using Advanced Ground Motion Intensity Measures, Attenuation Relationships, and Near-Fault Effects*. Polsak Tothong and C. Allin Cornell. March 2007.

PEER 2006/10 *Application of the PEER PBEE Methodology to the I-880 Viaduct*. Sashi Kunnath. February 2007.

PEER 2006/09 *Quantifying Economic Losses from Travel Forgone Following a Large Metropolitan Earthquake*. James Moore, Sungbin Cho, Yue Yue Fan, and Stuart Werner. November 2006.

PEER 2006/08 *Vector-Valued Ground Motion Intensity Measures for Probabilistic Seismic Demand Analysis*. Jack W. Baker and C. Allin Cornell. October 2006.

PEER 2006/07 *Analytical Modeling of Reinforced Concrete Walls for Predicting Flexural and Coupled–Shear-Flexural Responses*. Kutay Orakcal, Leonardo M. Massone, and John W. Wallace. October 2006.

PEER 2006/06 *Nonlinear Analysis of a Soil-Drilled Pier System under Static and Dynamic Axial Loading*. Gang Wang and Nicholas Sitar. November 2006.

PEER 2006/05 *Advanced Seismic Assessment Guidelines.* Paolo Bazzurro, C. Allin Cornell, Charles Menun, Maziar Motahari, and Nicolas Luco. September 2006.

PEER 2006/04 *Probabilistic Seismic Evaluation of Reinforced Concrete Structural Components and Systems*. Tae Hyung Lee and Khalid M. Mosalam. August 2006.

PEER 2006/03 *Performance of Lifelines Subjected to Lateral Spreading.* Scott A. Ashford and Teerawut Juirnarongrit. July 2006.

PEER 2006/02 *Pacific Earthquake Engineering Research Center Highway Demonstration Project.* Anne Kiremidjian, James Moore, Yue Yue Fan, Nesrin Basoz, Ozgur Yazali, and Meredith Williams. April 2006.

PEER 2006/01 *Bracing Berkeley. A Guide to Seismic Safety on the UC Berkeley Campus.* Mary C. Comerio, Stephen Tobriner, and Ariane Fehrenkamp. January 2006.

PEER 2005/17 *Earthquake Simulation Tests on Reducing Residual Displacements of Reinforced Concrete Bridges.* Junichi Sakai, Stephen A Mahin, and Andres Espinoza. December 2005.

PEER 2005/16 *Seismic Response and Reliability of Electrical Substation Equipment and Systems.* Junho Song, Armen Der Kiureghian, and Jerome L. Sackman. April 2006.

PEER 2005/15 *CPT-Based Probabilistic Assessment of Seismic Soil Liquefaction Initiation.* R. E. S. Moss, R. B. Seed, R. E. Kayen, J. P. Stewart, and A. Der Kiureghian. April 2006.

PEER 2005/14 *Workshop on Modeling of Nonlinear Cyclic Load-Deformation Behavior of Shallow Foundations.* Bruce L. Kutter, Geoffrey Martin, Tara Hutchinson, Chad Harden, Sivapalan Gajan, and Justin Phalen. March 2006.

PEER 2005/13 *Stochastic Characterization and Decision Bases under Time-Dependent Aftershock Risk in Performance-Based Earthquake Engineering*. Gee Liek Yeo and C. Allin Cornell. July 2005.

PEER 2005/12 *PEER Testbed Study on a Laboratory Building: Exercising Seismic Performance Assessment.* Mary C. Comerio, Editor. November 2005.

PEER 2005/11 *Van Nuys Hotel Building Testbed Report: Exercising Seismic Performance Assessment.* Helmut Krawinkler, Editor. October 2005.

PEER 2005/10 *First NEES/E-Defense Workshop on Collapse Simulation of Reinforced Concrete Building Structures.* September 2005.

PEER 2005/09 *Test Applications of Advanced Seismic Assessment Guidelines.* Joe Maffei, Karl Telleen, Danya Mohr, William Holmes, and Yuki Nakayama. August 2006.

PEER 2005/08 *Damage Accumulation in Lightly Confined Reinforced Concrete Bridge Columns.* R. Tyler Ranf, Jared M. Nelson, Zach Price, Marc O. Eberhard, and John F. Stanton. April 2006.

PEER 2005/07 *Experimental and Analytical Studies on the Seismic Response of Freestanding and Anchored Laboratory Equipment.* Dimitrios Konstantinidis and Nicos Makris. January 2005.

PEER 2005/06 *Global Collapse of Frame Structures under Seismic Excitations*. Luis F. Ibarra and Helmut Krawinkler. September 2005.

PEER 2005//05 *Performance Characterization of Bench- and Shelf-Mounted Equipment.* Samit Ray Chaudhuri and Tara C. Hutchinson. May 2006.

PEER 2005/04 *Numerical Modeling of the Nonlinear Cyclic Response of Shallow Foundations.* Chad Harden, Tara Hutchinson, Geoffrey R. Martin, and Bruce L. Kutter. August 2005.

PEER 2005/03 *A Taxonomy of Building Components for Performance-Based Earthquake Engineering.* Keith A. Porter. September 2005.

PEER 2005/02 *Fragility Basis for California Highway Overpass Bridge Seismic Decision Making*. Kevin R. Mackie and Božidar Stojadinović. June 2005.

PEER 2005/01 *Empirical Characterization of Site Conditions on Strong Ground Motion.* Jonathan P. Stewart, Yoojoong Choi, and Robert W. Graves. June 2005.

PEER 2004/09 *Electrical Substation Equipment Interaction: Experimental Rigid Conductor Studies.* Christopher Stearns and André Filiatrault. February 2005.

PEER 2004/08 *Seismic Qualification and Fragility Testing of Line Break 550-kV Disconnect Switches.* Shakhzod M. Takhirov, Gregory L. Fenves, and Eric Fujisaki. January 2005.

PEER 2004/07 *Ground Motions for Earthquake Simulator Qualification of Electrical Substation Equipment.* Shakhzod M. Takhirov, Gregory L. Fenves, Eric Fujisaki, and Don Clyde. January 2005.

PEER 2004/06 *Performance-Based Regulation and Regulatory Regimes.* Peter J. May and Chris Koski. September 2004.

PEER 2004/05 *Performance-Based Seismic Design Concepts and Implementation: Proceedings of an International Workshop.* Peter Fajfar and Helmut Krawinkler, Editors. September 2004.

PEER 2004/04 *Seismic Performance of an Instrumented Tilt-up Wall Building.* James C. Anderson and Vitelmo V. Bertero. July 2004.

PEER 2004/03 *Evaluation and Application of Concrete Tilt-up Assessment Methodologies.* Timothy Graf and James O. Malley. October 2004.

PEER 2004/02 *Analytical Investigations of New Methods for Reducing Residual Displacements of Reinforced Concrete Bridge Columns.* Junichi Sakai and Stephen A. Mahin. August 2004.

PEER 2004/01 *Seismic Performance of Masonry Buildings and Design Implications.* Kerri Anne Taeko Tokoro, James C. Anderson, and Vitelmo V. Bertero. February 2004.

PEER 2003/18 *Performance Models for Flexural Damage in Reinforced Concrete Columns.* Michael Berry and Marc Eberhard. August 2003.

PEER 2003/17 *Predicting Earthquake Damage in Older Reinforced Concrete Beam-Column Joints.* Catherine Pagni and Laura Lowes. October 2004.

PEER 2003/16 *Seismic Demands for Performance-Based Design of Bridges.* Kevin Mackie and Božidar Stojadinović. August 2003.

PEER 2003/15 *Seismic Demands for Nondeteriorating Frame Structures and Their Dependence on Ground Motions.* Ricardo Antonio Medina and Helmut Krawinkler. May 2004.

PEER 2003/14 *Finite Element Reliability and Sensitivity Methods for Performance-Based Earthquake Engineering*. Terje Haukaas and Armen Der Kiureghian. April 2004.

PEER 2003/13 *Effects of Connection Hysteretic Degradation on the Seismic Behavior of Steel Moment-Resisting Frames.* Janise E. Rodgers and Stephen A. Mahin. March 2004.

PEER 2003/12 *Implementation Manual for the Seismic Protection of Laboratory Contents: Format and Case Studies*. William T. Holmes and Mary C. Comerio. October 2003.

PEER 2003/11 *Fifth U.S.-Japan Workshop on Performance-Based Earthquake Engineering Methodology for Reinforced Concrete Building Structures*. February 2004.

PEER 2003/10 *A Beam-Column Joint Model for Simulating the Earthquake Response of Reinforced Concrete Frames.* Laura N. Lowes, Nilanjan Mitra, and Arash Altoontash. February 2004.

PEER 2003/09 *Sequencing Repairs after an Earthquake: An Economic Approach.* Marco Casari and Simon J. Wilkie. April 2004.

PEER 2003/08 *A Technical Framework for Probability-Based Demand and Capacity Factor Design (DCFD) Seismic Formats*. Fatemeh Jalayer and C. Allin Cornell. November 2003.

PEER 2003/07 *Uncertainty Specification and Propagation for Loss Estimation Using FOSM Methods.* Jack W. Baker and C. Allin Cornell. September 2003.

PEER 2003/06 *Performance of Circular Reinforced Concrete Bridge Columns under Bidirectional Earthquake Loading*. Mahmoud M. Hachem, Stephen A. Mahin, and Jack P. Moehle. February 2003.

PEER 2003/05 *Response Assessment for Building-Specific Loss Estimation.* Eduardo Miranda and Shahram Taghavi. September 2003.

PEER 2003/04 *Experimental Assessment of Columns with Short Lap Splices Subjected to Cyclic Loads*. Murat Melek, John W. Wallace, and Joel Conte. April 2003.

PEER 2003/03 *Probabilistic Response Assessment for Building-Specific Loss Estimation*. Eduardo Miranda and Hesameddin Aslani. September 2003.

PEER 2003/02 *Software Framework for Collaborative Development of Nonlinear Dynamic Analysis Program*. Jun Peng and Kincho H. Law. September 2003.

PEER 2003/01 *Shake Table Tests and Analytical Studies on the Gravity Load Collapse of Reinforced Concrete Frames.* Kenneth John Elwood and Jack P. Moehle. November 2003.

PEER 2002/24 *Performance of Beam to Column Bridge Joints Subjected to a Large Velocity Pulse.* Natalie Gibson, André Filiatrault, and Scott A. Ashford. April 2002.

PEER 2002/23 *Effects of Large Velocity Pulses on Reinforced Concrete Bridge Columns.* Greg L. Orozco and Scott A. Ashford. April 2002.

PEER 2002/22 *Characterization of Large Velocity Pulses for Laboratory Testing.* Kenneth E. Cox and Scott A. Ashford. April 2002.

PEER 2002/21 *Fourth U.S.-Japan Workshop on Performance-Based Earthquake Engineering Methodology for Reinforced Concrete Building Structures*. December 2002.

PEER 2002/20 *Barriers to Adoption and Implementation of PBEE Innovations.* Peter J. May. August 2002.

PEER 2002/19 *Economic-Engineered Integrated Models for Earthquakes: Socioeconomic Impacts.* Peter Gordon, James E. Moore II, and Harry W. Richardson. July 2002.

PEER 2002/18 *Assessment of Reinforced Concrete Building Exterior Joints with Substandard Details.* Chris P. Pantelides, Jon Hansen, Justin Nadauld, and Lawrence D. Reaveley. May 2002.

PEER 2002/17 *Structural Characterization and Seismic Response Analysis of a Highway Overcrossing Equipped with Elastomeric Bearings and Fluid Dampers: A Case Study*. Nicos Makris and Jian Zhang. November 2002.

PEER 2002/16 *Estimation of Uncertainty in Geotechnical Properties for Performance-Based Earthquake Engineering*. Allen L. Jones, Steven L. Kramer, and Pedro Arduino. December 2002.

PEER 2002/15 *Seismic Behavior of Bridge Columns Subjected to Various Loading Patterns*. Asadollah Esmaeily-Gh. and Yan Xiao. December 2002.

PEER 2002/14 *Inelastic Seismic Response of Extended Pile Shaft Supported Bridge Structures.* T.C. Hutchinson, R.W. Boulanger, Y.H. Chai, and I.M. Idriss. December 2002.

PEER 2002/13 *Probabilistic Models and Fragility Estimates for Bridge Components and Systems.* Paolo Gardoni, Armen Der Kiureghian, and Khalid M. Mosalam. June 2002.

PEER 2002/12 *Effects of Fault Dip and Slip Rake on Near-Source Ground Motions: Why Chi-Chi Was a Relatively Mild M7.6 Earthquake*. Brad T. Aagaard, John F. Hall, and Thomas H. Heaton. December 2002.

PEER 2002/11 *Analytical and Experimental Study of Fiber-Reinforced Strip Isolators*. James M. Kelly and Shakhzod M. Takhirov. September 2002.

PEER 2002/10 *Centrifuge Modeling of Settlement and Lateral Spreading with Comparisons to Numerical Analyses***.** Sivapalan Gajan and Bruce L. Kutter. January 2003.

PEER 2002/09 *Documentation and Analysis of Field Case Histories of Seismic Compression during the 1994 Northridge, California, Earthquake*. Jonathan P. Stewart, Patrick M. Smith, Daniel H. Whang, and Jonathan D. Bray. October 2002.

PEER 2002/08 *Component Testing, Stability Analysis and Characterization of Buckling-Restrained Unbonded Braces™*. Cameron Black, Nicos Makris, and Ian Aiken. September 2002.

PEER 2002/07 *Seismic Performance of Pile-Wharf Connections.* Charles W. Roeder, Robert Graff, Jennifer Soderstrom, and Jun Han Yoo. December 2001.

PEER 2002/06 *The Use of Benefit-Cost Analysis for Evaluation of Performance-Based Earthquake Engineering Decisions*. Richard O. Zerbe and Anthony Falit-Baiamonte. September 2001.

PEER 2002/05 *Guidelines, Specifications, and Seismic Performance Characterization of Nonstructural Building Components and Equipment*. André Filiatrault, Constantin Christopoulos, and Christopher Stearns. September 2001.

PEER 2002/04 *Consortium of Organizations for Strong-Motion Observation Systems and the Pacific Earthquake Engineering Research Center Lifelines Program: Invited Workshop on Archiving and Web Dissemination of Geotechnical Data, 4–5 October 2001*. September 2002.

PEER 2002/03 *Investigation of Sensitivity of Building Loss Estimates to Major Uncertain Variables for the Van Nuys Testbed*. Keith A. Porter, James L. Beck, and Rustem V. Shaikhutdinov. August 2002.

PEER 2002/02 *The Third U.S.-Japan Workshop on Performance-Based Earthquake Engineering Methodology for Reinforced Concrete Building Structures*. July 2002.

PEER 2002/01 *Nonstructural Loss Estimation: The UC Berkeley Case Study.* Mary C. Comerio and John C. Stallmeyer. December 2001.

PEER 2001/16 *Statistics of SDF-System Estimate of Roof Displacement for Pushover Analysis of Buildings.* Anil K. Chopra, Rakesh K. Goel, and Chatpan Chintanapakdee. December 2001.

PEER 2001/15 *Damage to Bridges during the 2001 Nisqually Earthquake.* R. Tyler Ranf, Marc O. Eberhard, and Michael P. Berry. November 2001.

PEER 2001/14 *Rocking Response of Equipment Anchored to a Base Foundation.* Nicos Makris and Cameron J. Black. September 2001.

PEER 2001/13 *Modeling Soil Liquefaction Hazards for Performance-Based Earthquake Engineering*. Steven L. Kramer and Ahmed-W. Elgamal. February 2001.

PEER 2001/12 *Development of Geotechnical Capabilities in OpenSees*. Boris Jeremić. September 2001.

PEER 2001/11 *Analytical and Experimental Study of Fiber-Reinforced Elastomeric Isolators*. James M. Kelly and Shakhzod M. Takhirov. September 2001.

PEER 2001/10 *Amplification Factors for Spectral Acceleration in Active Regions.* Jonathan P. Stewart, Andrew H. Liu, Yoojoong Choi, and Mehmet B. Baturay. December 2001.

PEER 2001/09 *Ground Motion Evaluation Procedures for Performance-Based Design.* Jonathan P. Stewart, Shyh-Jeng Chiou, Jonathan D. Bray, Robert W. Graves, Paul G. Somerville, and Norman A. Abrahamson. September 2001.

PEER 2001/08 *Experimental and Computational Evaluation of Reinforced Concrete Bridge Beam-Column Connections for Seismic Performance*. Clay J. Naito, Jack P. Moehle, and Khalid M. Mosalam. November 2001.

PEER 2001/07 *The Rocking Spectrum and the Shortcomings of Design Guidelines.* Nicos Makris and Dimitrios Konstantinidis. August 2001.

PEER 2001/06 *Development of an Electrical Substation Equipment Performance Database for Evaluation of Equipment Fragilities*. Thalia Agnanos. April 1999.

PEER 2001/05 *Stiffness Analysis of Fiber-Reinforced Elastomeric Isolators.* Hsiang-Chuan Tsai and James M. Kelly. May 2001.

PEER 2001/04 *Organizational and Societal Considerations for Performance-Based Earthquake Engineering*. Peter J. May. April 2001.

PEER 2001/03 *A Modal Pushover Analysis Procedure to Estimate Seismic Demands for Buildings: Theory and Preliminary Evaluation*. Anil K. Chopra and Rakesh K. Goel. January 2001.

PEER 2001/02 *Seismic Response Analysis of Highway Overcrossings Including Soil-Structure Interaction*. Jian Zhang and Nicos Makris. March 2001.

PEER 2001/01 *Experimental Study of Large Seismic Steel Beam-to-Column Connections.* Egor P. Popov and Shakhzod M. Takhirov. November 2000.

PEER 2000/10 *The Second U.S.-Japan Workshop on Performance-Based Earthquake Engineering Methodology for Reinforced Concrete Building Structures*. March 2000.

PEER 2000/09 *Structural Engineering Reconnaissance of the August 17, 1999 Earthquake: Kocaeli (Izmit), Turkey.* Halil Sezen, Kenneth J. Elwood, Andrew S. Whittaker, Khalid Mosalam, John J. Wallace, and John F. Stanton. December 2000.

PEER 2000/08 *Behavior of Reinforced Concrete Bridge Columns Having Varying Aspect Ratios and Varying Lengths of Confinement*. Anthony J. Calderone, Dawn E. Lehman, and Jack P. Moehle. January 2001.

PEER 2000/07 *Cover-Plate and Flange-Plate Reinforced Steel Moment-Resisting Connections.* Taejin Kim, Andrew S. Whittaker, Amir S. Gilani, Vitelmo V. Bertero, and Shakhzod M. Takhirov. September 2000.

PEER 2000/06 *Seismic Evaluation and Analysis of 230-kV Disconnect Switches.* Amir S. J. Gilani, Andrew S. Whittaker, Gregory L. Fenves, Chun-Hao Chen, Henry Ho, and Eric Fujisaki. July 2000.

PEER 2000/05 *Performance-Based Evaluation of Exterior Reinforced Concrete Building Joints for Seismic Excitation*. Chandra Clyde, Chris P. Pantelides, and Lawrence D. Reaveley. July 2000.

PEER 2000/04 *An Evaluation of Seismic Energy Demand: An Attenuation Approach*. Chung-Che Chou and Chia-Ming Uang. July 1999.

PEER 2000/03 *Framing Earthquake Retrofitting Decisions: The Case of Hillside Homes in Los Angeles.* Detlof von Winterfeldt, Nels Roselund, and Alicia Kitsuse. March 2000.

PEER 2000/02 *U.S.-Japan Workshop on the Effects of Near-Field Earthquake Shaking*. Andrew Whittaker, Editor. July 2000.

PEER 2000/01 *Further Studies on Seismic Interaction in Interconnected Electrical Substation Equipment.* Armen Der Kiureghian, Kee-Jeung Hong, and Jerome L. Sackman. November 1999.

PEER 1999/14 *Seismic Evaluation and Retrofit of 230-kV Porcelain Transformer Bushings*. Amir S. Gilani, Andrew S. Whittaker, Gregory L. Fenves, and Eric Fujisaki. December 1999.

PEER 1999/13 *Building Vulnerability Studies: Modeling and Evaluation of Tilt-up and Steel Reinforced Concrete Buildings*. John W. Wallace, Jonathan P. Stewart, and Andrew S. Whittaker, Editors. December 1999.

PEER 1999/12 *Rehabilitation of Nonductile RC Frame Building Using Encasement Plates and Energy-Dissipating Devices*. Mehrdad Sasani, Vitelmo V. Bertero, James C. Anderson. December 1999.

PEER 1999/11 *Performance Evaluation Database for Concrete Bridge Components and Systems under Simulated Seismic Loads*. Yael D. Hose and Frieder Seible. November 1999.

PEER 1999/10 *U.S.-Japan Workshop on Performance-Based Earthquake Engineering Methodology for Reinforced Concrete Building Structures*. December 1999.

PEER 1999/09 *Performance Improvement of Long Period Building Structures Subjected to Severe Pulse-Type Ground Motions*. James C. Anderson, Vitelmo V. Bertero, and Raul Bertero. October 1999.

PEER 1999/08 *Envelopes for Seismic Response Vectors.* Charles Menun and Armen Der Kiureghian. July 1999.

PEER 1999/07 *Documentation of Strengths and Weaknesses of Current Computer Analysis Methods for Seismic Performance of Reinforced Concrete Members*. William F. Cofer. November 1999.

PEER 1999/06 *Rocking Response and Overturning of Anchored Equipment under Seismic Excitations*. Nicos Makris and Jian Zhang. November 1999.

PEER 1999/05 *Seismic Evaluation of 550 kV Porcelain Transformer Bushings.* Amir S. Gilani, Andrew S. Whittaker, Gregory L. Fenves, and Eric Fujisaki. October 1999.

PEER 1999/04 *Adoption and Enforcement of Earthquake Risk-Reduction Measures.* Peter J. May, Raymond J. Burby, T. Jens Feeley, and Robert Wood. August 1999.

PEER 1999/03 *Task 3 Characterization of Site Response General Site Categories*. Adrian Rodriguez-Marek, Jonathan D. Bray and Norman Abrahamson. February 1999.

PEER 1999/02 *Capacity-Demand-Diagram Methods for Estimating Seismic Deformation of Inelastic Structures: SDF Systems*. Anil K. Chopra and Rakesh Goel. April 1999.

PEER 1999/01 *Interaction in Interconnected Electrical Substation Equipment Subjected to Earthquake Ground Motions*. Armen Der Kiureghian, Jerome L. Sackman, and Kee-Jeung Hong. February 1999.

PEER 1998/08 *Behavior and Failure Analysis of a Multiple-Frame Highway Bridge in the 1994 Northridge Earthquake*. Gregory L. Fenves and Michael Ellery. December 1998.

PEER 1998/07 *Empirical Evaluation of Inertial Soil-Structure Interaction Effects.* Jonathan P. Stewart, Raymond B. Seed, and Gregory L. Fenves. November 1998.

PEER 1998/06 *Effect of Damping Mechanisms on the Response of Seismic Isolated Structures*. Nicos Makris and Shih-Po Chang. November 1998.

PEER 1998/05 *Rocking Response and Overturning of Equipment under Horizontal Pulse-Type Motions*. Nicos Makris and Yiannis Roussos. October 1998.

PEER 1998/04 *Pacific Earthquake Engineering Research Invitational Workshop Proceedings, May 14–15, 1998: Defining the Links between Planning, Policy Analysis, Economics and Earthquake Engineering*. Mary Comerio and Peter Gordon. September 1998.

PEER 1998/03 *Repair/Upgrade Procedures for Welded Beam to Column Connections*. James C. Anderson and Xiaojing Duan. May 1998.

PEER 1998/02 *Seismic Evaluation of 196 kV Porcelain Transformer Bushings.* Amir S. Gilani, Juan W. Chavez, Gregory L. Fenves, and Andrew S. Whittaker. May 1998.

PEER 1998/01 *Seismic Performance of Well-Confined Concrete Bridge Columns.* Dawn E. Lehman and Jack P. Moehle. December 2000.

PEER REPORTS: ONE HUNDRED SERIES

PEER 2012/103 *Performance-Based Seismic Demand Assessment of Concentrically Braced Steel Frame Buildings.* Chui-Hsin Chen and Stephen A. Mahin. December 2012.

PEER 2012/102 *Procedure to Restart an Interrupted Hybrid Simulation: Addendum to PEER Report 2010/103.* Vesna Terzic and Bozidar Stojadinovic. October 2012.

PEER 2012/101 *Mechanics of Fiber Reinforced Bearings.* James M. Kelly and Andrea Calabrese. February 2012.

PEER 2011/107 *Nonlinear Site Response and Seismic Compression at Vertical Array Strongly Shaken by 2007 Niigata-ken Chuetsu-oki Earthquake.* Eric Yee, Jonathan P. Stewart, and Kohji Tokimatsu. December 2011.

PEER 2011/106 *Self Compacting Hybrid Fiber Reinforced Concrete Composites for Bridge Columns.* Pardeep Kumar, Gabriel Jen, William Trono, Marios Panagiotou, and Claudia Ostertag. September 2011.

PEER 2011/105 *Stochastic Dynamic Analysis of Bridges Subjected to Spacially Varying Ground Motions.* Katerina Konakli and Armen Der Kiureghian. August 2011.

PEER 2011/104 *Design and Instrumentation of the 2010 E-Defense Four-Story Reinforced Concrete and Post-Tensioned Concrete Buildings.* Takuya Nagae, Kenichi Tahara, Taizo Matsumori, Hitoshi Shiohara, Toshimi Kabeyasawa, Susumu Kono, Minehiro Nishiyama (Japanese Research Team) and John Wallace, Wassim Ghannoum, Jack Moehle, Richard Sause, Wesley Keller, Zeynep Tuna (U.S. Research Team). June 2011.

PEER 2011/103 *In-Situ Monitoring of the Force Output of Fluid Dampers: Experimental Investigation.* Dimitrios Konstantinidis, James M. Kelly, and Nicos Makris. April 2011.

PEER 2011/102 *Ground-Motion Prediction Equations 1964–2010.* John Douglas. April 2011.

PEER 2011/101 *Report of the Eighth Planning Meeting of NEES/E-Defense Collaborative Research on Earthquake Engineering.* Convened by the Hyogo Earthquake Engineering Research Center (NIED), NEES Consortium, Inc. February 2011.

PEER 2010/111 *Modeling and Acceptance Criteria for Seismic Design and Analysis of Tall Buildings.* Task 7 Report for the Tall Buildings Initiative - Published jointly by the Applied Technology Council. October 2010.

PEER 2010/110 *Seismic Performance Assessment and Probabilistic Repair Cost Analysis of Precast Concrete Cladding Systems for Multistory Buildlings.* Jeffrey P. Hunt and Božidar Stojadinovic. November 2010.

PEER 2010/109 *Report of the Seventh Joint Planning Meeting of NEES/E-Defense Collaboration on Earthquake Engineering. Held at the E-Defense, Miki, and Shin-Kobe, Japan, September 18–19, 2009.* August 2010.

PEER 2010/108 *Probabilistic Tsunami Hazard in California.* Hong Kie Thio, Paul Somerville, and Jascha Polet, preparers. October 2010.

PEER 2010/107 *Performance and Reliability of Exposed Column Base Plate Connections for Steel Moment-Resisting Frames.* Ady Aviram, Božidar Stojadinovic, and Armen Der Kiureghian. August 2010.

PEER 2010/106 *Verification of Probabilistic Seismic Hazard Analysis Computer Programs.* Patricia Thomas, Ivan Wong, and Norman Abrahamson. May 2010.

PEER 2010/105 *Structural Engineering Reconnaissance of the April 6, 2009, Abruzzo, Italy, Earthquake, and Lessons Learned.* M. Selim Günay and Khalid M. Mosalam. April 2010.

PEER 2010/104 *Simulating the Inelastic Seismic Behavior of Steel Braced Frames, Including the Effects of Low-Cycle Fatigue.* Yuli Huang and Stephen A. Mahin. April 2010.

PEER 2010/103 *Post-Earthquake Traffic Capacity of Modern Bridges in California.* Vesna Terzic and Božidar Stojadinović. March 2010.

PEER 2010/102 *Analysis of Cumulative Absolute Velocity (CAV) and JMA Instrumental Seismic Intensity (I_{JMA}) Using the PEER–NGA Strong Motion Database.* Kenneth W. Campbell and Yousef Bozorgnia. February 2010.

PEER 2010/101 *Rocking Response of Bridges on Shallow Foundations.* Jose A. Ugalde, Bruce L. Kutter, and Boris Jeremic. April 2010.

PEER 2009/109 *Simulation and Performance-Based Earthquake Engineering Assessment of Self-Centering Post-Tensioned Concrete Bridge Systems.* Won K. Lee and Sarah L. Billington. December 2009.

PEER 2009/108 *PEER Lifelines Geotechnical Virtual Data Center.* J. Carl Stepp, Daniel J. Ponti, Loren L. Turner, Jennifer N. Swift, Sean Devlin, Yang Zhu, Jean Benoit, and John Bobbitt. September 2009.

PEER 2009/107 *Experimental and Computational Evaluation of Current and Innovative In-Span Hinge Details in Reinforced Concrete Box-Girder Bridges: Part 2: Post-Test Analysis and Design Recommendations.* Matias A. Hube and Khalid M. Mosalam. December 2009.

PEER 2009/106 *Shear Strength Models of Exterior Beam-Column Joints without Transverse Reinforcement.* Sangjoon Park and Khalid M. Mosalam. November 2009.

PEER 2009/105 *Reduced Uncertainty of Ground Motion Prediction Equations through Bayesian Variance Analysis.* Robb Eric S. Moss. November 2009.

PEER 2009/104 *Advanced Implementation of Hybrid Simulation.* Andreas H. Schellenberg, Stephen A. Mahin, Gregory L. Fenves. November 2009.

PEER 2009/103 *Performance Evaluation of Innovative Steel Braced Frames.* T. Y. Yang, Jack P. Moehle, and Božidar Stojadinovic. August 2009.

PEER 2009/102 *Reinvestigation of Liquefaction and Nonliquefaction Case Histories from the 1976 Tangshan Earthquake.* Robb Eric Moss, Robert E. Kayen, Liyuan Tong, Songyu Liu, Guojun Cai, and Jiaer Wu. August 2009.

PEER 2009/101 *Report of the First Joint Planning Meeting for the Second Phase of NEES/E-Defense Collaborative Research on Earthquake Engineering.* Stephen A. Mahin et al. July 2009.

PEER 2008/104 *Experimental and Analytical Study of the Seismic Performance of Retaining Structures.* Linda Al Atik and Nicholas Sitar. January 2009.

PEER 2008/103 *Experimental and Computational Evaluation of Current and Innovative In-Span Hinge Details in Reinforced Concrete Box-Girder Bridges. Part 1: Experimental Findings and Pre-Test Analysis.* Matias A. Hube and Khalid M. Mosalam. January 2009.

PEER 2008/102 *Modeling of Unreinforced Masonry Infill Walls Considering In-Plane and Out-of-Plane Interaction.* Stephen Kadysiewski and Khalid M. Mosalam. January 2009.

PEER 2008/101 *Seismic Performance Objectives for Tall Buildings.* William T. Holmes, Charles Kircher, William Petak, and Nabih Youssef. August 2008.

PEER 2007/101 *Generalized Hybrid Simulation Framework for Structural Systems Subjected to Seismic Loading*. Tarek Elkhoraibi and Khalid M. Mosalam. July 2007.

PEER 2007/100 *Seismic Evaluation of Reinforced Concrete Buildings Including Effects of Masonry Infill Walls*. Alidad Hashemi and Khalid M. Mosalam. July 2007.

The Pacifi c Earthquake Engineering Research Center (PEER) is a multi-institutional research and education center with headquarters at the University of California, Berkeley. Investigators from over 20 universities, several consulting companies, and researchers at various state and federal government agencies contribute to research programs focused on performance-based earthquake engineering.

These research programs aim to identify and reduce the risks from major earthquakes to life safety and to the economy by including research in a wide variety of disciplines including structural and geotechnical engineering, geology/seismology, lifelines, transportation, architecture, economics, risk management, and public policy.

PEER is supported by federal, state, local, and regional agencies, together with industry partners.

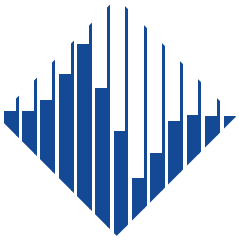

PEER Core Institutions

University of California, Berkeley (Lead Institution)
California Institute of Technology
Oregon State University
Stanford University
University of California, Davis
University of California, Irvine
University of California, Los Angeles
University of California, San Diego
University of Nevada, Reno
University of Southern California
University of Washington

PEER reports can be ordered at https://peer.berkeley.edu/peer-reports or by contacting

Pacific Earthquake Engineering Research Center
University of California, Berkeley
325 Davis Hall, Mail Code 1792
Berkeley, CA 94720-1792
Tel: 510-642-3437
Email: peer_center@berkeley.edu

ISSN 2770-8314
https://doi.org/10.55461/KJZH2652